Universidade de Aveiro Departamento de Engenharia Mecânica
2013

Saeed Tamimi

Laminação assimétrica de liga de alumínio 5182 e chapas de aço sem intersticiais

Asymmetric rolling of 5182 aluminium alloy and interstitial free steel sheets

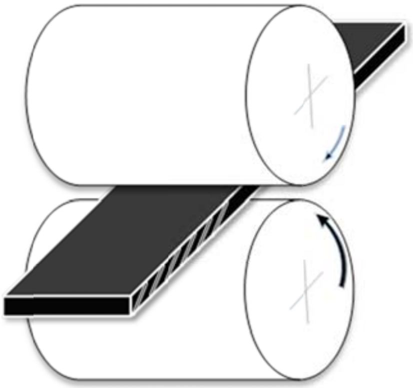

Universidade de Aveiro Departamento de Engenharia Mecânica
2013

Saeed Tamimi

Laminação assimétrica de liga de alumínio 5182 e chapas de aço sem intersticiais

Asymmetric rolling of 5182 aluminium alloy and interstitial free steel sheets

Tese apresentada à Universidade de Aveiro para cumprimento dos requisitos necessários à obtenção do grau de Doutor em Engenharia Mecanica, realizada sob a orientação científica do Professor Jose Joaquim de Almeida Gracio, Professor Catedrático do Departamento de Engenharia Mecânica da Universidade de Aveiro.

Dissertation submitted to the University of Aveiro, as the fulfilment of necessary requirements for obtaining the Ph.D. degree in Mechanical Engineering was carried out under the supervision of Professor Jose Joaquim de Almeida Gracio, full professor of the Mechanical Engineering Department of the University of Aveiro. This work has given me the opportunity to work on asymmetric rolling process as a new field of materials technology and has been very educational. Hopefully, the initiation of this work will result in new insights in the field of metal forming in coming years.

FCT Fundação para a Ciência e a Tecnologia
MINISTÉRIO DA CIÊNCIA, TECNOLOGIA E ENSINO SUPERIOR Portugal

Bolsa de Doutoramento concedida pela Fundação para a Ciencia e a Tecnologia (FCT), referência SFRH/BD/45835/2008

Ph.D. scholarship granted by Fundacao para a Ciencia e a Tecnologia (FCT), reference SFRH/BD/45835/2008

To my parents Iran and Ali, and my wife Ensieh;
with admiration, gratitude and love.

o júri

presidente

Prof. Doutor António Carlos Matias Correia
Professor Catedrático da Universidade de Aveiro

Prof. Doutor José Joaquim de Almeida Grácio
Professor Catedrático do Departamento de Engenharia Mecânica da Universidade de Aveiro

Prof. Doutora Marta Cristina Cardoso de Oliveira
Professora Auxiliar do departamento de Engenharia Mecânica da Faculdade de Ciências e Tecnologia da Universidade de Coimbra

Prof. Doutor Abel Dias dos Santos
Professor Associado do Departamento de Engenharia Mecânica da Faculdade de Engenharia da Universidade do Porto

Prof. Doutor António Manuel de Bastos Pereira
Professor Auxiliar de Departamento de Engenharia Mecânica da Universidade de Aveiro

Prof. Doutor Fábio Jorge Pereira Simões
Professor adjunto da Escola Superior de Tecnologia e Gestão do Instituto Politécnico de Leiria

Prof. Doutora Gabriela Tamara Vincze
Professora Auxiliar Convidada do Departamento de Engenharia Mecânica da Universidade de Aveiro

agradecimentos

I would like to express the deepest appreciation to my supervisor, Professor Jose Gracio for his valuable advice and the fruitful discussions during the development of the work, and for providing me with innumerable lessons and insights into the workings of academic research in general. He continually and convincingly conveyed a spirit of adventure in regard to research. Without his guidance and persistent help this dissertation would not have been possible.

I would like to thank to Dr. Edgar Rauch of the Center National de la Recherche Scientifique (CNRS) in Grenoble and Professor Frederic Barlat for their valuable advices and suggestions throughout the work. In addition, it is with immense gratitude that I acknowledge the support and help of Professor Said Ahzi of the University of Strasbourg who introduced me to crystal plastic approaches. Also I wish to voice my appreciation for Professor Carlos Tome of Los Alamos National Lab for the knowledge and experience in crystal plasticity he brought to the group.

The contribution of Dr. Augusto L.B.Lopes is gratefully acknowledged for his assistance during materials characterization. His knowledge and expertise in the field made me more comfortable dealing with this topic. In addition, a special thanks goes to Dr. Joao P.M. Correia of the University of Strasbourg for his helps during this work.

I wish to thank the members of our research group, who have each in different ways been valuable resources of time and advice during this process. I would like to thank especially to Dr. Gabriela T.Vincze and Dr. Zohreh R.Hesabi for all their assistances.

Last but not least I would like to thank my family membres; without their love and labour I could not achieve what I have achieved. A special vote of gratitude goes to my parents, Iran and Ali whose words of encouragement and push for tenacity ring in my ears; and my wife, Ensieh who absolutely supported me every step of the way. I will always appreciate all they have done.

palavras-chave laminagem assimétrica, textura cristalográfica, microestrutura, comportamento mecânico, AA-5182, aço IF

resumo

A presente tese de doutoramento foi dedicada ao estudo da laminagem assimétrica (ASR) como técnica alternativa para a melhoria das propriedades mecânicas das ligas de alumínio-magnésio e aço IF durante processos industriais de conformação plástica.

As ligas de alumínio são bastante atrativas devido às suas propriedades específicas, nomeadamente baixa densidade e resistência à corrosão. No entanto, a sua baixa formabilidade limita o seu campo de aplicação. A formabilidade das ligas de alumínio pode ser melhorada através da alteração da textura cristalográfica. Assim, parte desta dissertação é dedicada ao desenvolvimento de uma textura compatível com formabilidade acrescida, através da técnica ASR. A ASR foi conduzida de duas formas distintas designadas ASR – contínua e ASR – com trajetória invertida. O impacto da deformação de corte imposta pela ASR no desenvolvimento da textura e comportamento mecânico pretendidos foi analisado em detalhe. A textura cristalográfica desenvolvida produz o aumento da anisotropia planar. A evolução da textura cristalográfica foi simulada com recurso aos modelos “self-consistent” e Taylor.

O aço IF foi o segundo material estudado. Dada a sua vasta utilização na indústria automóvel pretende-se investigar o efeito da deformação de corte desenvolvida durante a ASR nas suas propriedades micro e macro com o intuito de melhorar a resposta a solicitações mecânicas. No aço IF foram também estudadas as duas condições de ASR anteriormente referidas. De acordo com as observações realizadas por microscopia ótica e microscopia de força de atómica as morfologias dos grãos obtidas durante o processo ASR e laminagem convencional são semelhantes. As observações realizadas por microscopia eletrónica de transmissão revelaram que durante a ASR se formam nano células de deslocações com forma equiaxial. A estrutura desenvolvida deverá estar associada à deformação de corte imposta durante a ASR. O comportamento mecânico do aço recozido e deformado foi avaliado através de ensaios de tração uniaxial. Para valores de redução de espessura da ordem dos 18% os provetes pré-deformados por ASR apresentam valores de tensão mais elevados do que os provetes pré-deformados em laminagem convencional. Para reduções de espessura da ordem dos 60% verificaram-se resultados opostos. A análise de textura indicou que o componente de laminagem se desenvolve de forma intensa para reduções de 60%, pelo contrário, a estrutura refinada resultante da ASR parece estar na origem do valor elevado de tensão observado após pré-deformação de 18%.

keywords Asymmetric rolling, crystallographic texture, microstructure, mechanical behaviour, AA-5182, IF steel

abstract

This Ph.D. research focuses on asymmetric rolling (ASR), as an alternative method for improving mechanical responses of aluminium-magnesium alloy and interstitial free (IF) steel regarding industrial requirements.

Aluminium alloys are attractive materials in various industries due to their appropriate properties such as low density and corrosion resistance; however, their low formability has limited their applications. As formability of aluminium alloys can be improved through texture development, part of this dissertation is dedicated to producing the desired crystallographic texture with the ASR process. Two types of ASR (i.e. reverse and continuous asymmetric rolling) were investigated. The impact of shear deformation imposed by ASR processes on developing the desirable texture and consequently on mechanical behaviours was observed. The developed shear texture increased the normal and also planar anisotropy. Texture evolution during plastic deformation as well as induced mechanical behaviour were simulated using the “self-consistent” and Taylor models.

Interstitial free (IF) steel was the second material selected in this dissertation. Since IF steel is one of the most often used materials in automotive industries it was chosen to investigate the effect of shear deformation through ASR on its properties. Two types of reverse and continuous asymmetric rolling were carried out to deform IF steel sheets. The results of optical microscopy and atomic force microscopy observations showed no significant difference between the grains’ morphology of asymmetric and conventionally rolled samples, whereas the obtained results of transmission electron microscopy indicated that fine and equiaxed dislocation cells were formed through the asymmetric rolling process. This structure is due to imposed shear deformation during the ASR process. Furthermore, the mechanical behaviour of deformed and annealed sheets was evaluated through uniaxial tensile tests. Results showed that at low thickness reductions (18%) the asymmetric rolled sample presented higher stress than that of the conventionally rolled sheet; while for higher thickness reductions (60%) the trend was reversed. The texture analyses indicated that intense rolling texture components which developed through 60% thickness reduction of conventional rolling cause a relatively higher stress; on the contrary the fine structure resulting from ASR appears to be the source of higher stress observed after pre-deformation of 18%.

Table of Contents

Chapter 1

Chapter 2

Chapter 4

Chapter 5

List of figures

List of tables

Chapter 1

Introduction

Nowadays, automotive, aerospace, structural and food packaging industries are the main fields of metal forming industries. Generally with a view to meeting environmental and economic concerns, engineers and manufacturers need to design lighter and safer products, and also with more complex shapes. This requires producing materials with extra ordinary properties.

About 90% of all metal production starts off as cast. However, a very large proportion of this is then processed by metal forming processes, either to improve the structure and properties and/or to give the desired final shape (or close to that) required. The rolling process can be regarded as the principal metal forming process, in which the metallic sheets are compressed and squeezed by working-rolls. Currently, millions of tons of rolled steel and aluminium alloys are produced annually in the world. Hence this is a field of manufacturing where improving mechanical properties through optimizing the parameters could translate into considerable economic benefits.

The rolling process often introduces anisotropy to metallic sheets. Anisotropy is the state of a material possessing properties depending on directionality of the material. Anisotropic mechanical behaviour of rolled materials which are associated with the texture developed in the rolling process is not desirable for some applications such as deep drawing industries. This results in thinning and earing problems during the process. The asymmetric rolling process, as a derivation of the rolling process, seems to have the potential to develop appropriate textures in metallic sheets to solve these problems. Furthermore in the literature it has been shown that the asymmetric rolling process is capable of refining the microstructure and changing its morphology. The prominent factor of asymmetric rolling which distinguishes it from the rolling process is its potential to distribute uniform shear deformation throughout the sample thickness. This shear strain promotes the development of shear texture and microstructure refinement.

The main objective of this thesis is to study the effect of asymmetric rolling on the mechanical behaviours of aluminium alloys and steel sheets and evaluate the impact of shear deformation on texture evolution and microstructure changes. The study of the influence of shear deformation imposed by asymmetric rolling on samples with two different crystallographic structures (i.e. face centre cubic of aluminium alloy and body centre cubic of IF steel) may give us a more comprehensive view of this process which makes it possible to improve the mechanical properties of the materials.

The current thesis is structured into four chapters, the introduction being the first. Subsequently, the asymmetric rolling process as a severe plastic deformation method is presented in the second chapter. Additionally, the basic concepts of plastic deformation mechanisms of cubic materials are discussed. Furthermore, the main crystal plasticity theories including their benefits and deficiencies are briefly introduced. Chapter 3 deals with the materials observed in this work and also experimental methodologies. In addition to characterizing the received materials, preliminary results are presented in this chapter. Chapter 4 is dedicated to the results and discussion of both materials in the process. A list of conclusions is also given chapter 5.

Chapter 2

Bibliography review

In this chapter, a general introduction to sheet metal forming is provided, with a focus on microstructure and crystallographic texture evolution during plastic deformation. Additionally, the asymmetric rolling (ASR) process as a new severe plastic deformation (SPD) method is introduced. It is shown that shear strain is a significant feature of SPD processes. Likewise the impact of shear deformation provided by ASR on microstructure and crystallographic texture is discussed. Due to the great practical interest in a deformation polycrystalline theory, a large number of studies have been devoted to various theories. In this chapter, a short review of crystal plasticity models that have been used to predict texture evolution and its resulting mechanical responses is presented.

2-1 severe plastic deformation techniques

Materials processing by severe plastic deformation (SPD) have been under intense focus in the research community the last decade due to the unique mechanical properties obtainable by SPD processing. The process of SPD is based on intense plastic deformation of a work-piece, resulting in alteration of the microstructure and texture. Thanks to these new techniques, a new horizon has opened for processing metallic materials.

Several SPD processes have been proposed in order to optimize the microstructure and crystallographic texture and present better mechanical properties, such as equal channel angular pressing and accumulative roll bonding. Also, some other developed techniques which originated from ECAP are suggested.

2-1-1 traditional SPD processes

Equal channel angular pressing: The equal channel angular pressing (ECAP) process was first developed by Segal [Segal 1981]. In this technique shear plastic deformation is applied to the sample through an angle in the ECAP die while retaining its dimension [Kim 2001]. The ECAP tool is a die with two intersecting channels of identical cross-section. A well lubricated specimen of the same cross-section is placed into one of the channels, and a plunger then presses it into the second channel. Under these circumstances the specimen will move as a rigid body, and deformation is achieved ideally by a simple shear in the sample at the crossing plane of the channels. Fig. 2.1 illustrates the principle for the ECAP technique. In the presence of a hydrostatic compressive stress field in ECAP, in spite of the high level of plastic deformation, specimen fracture does not occur.

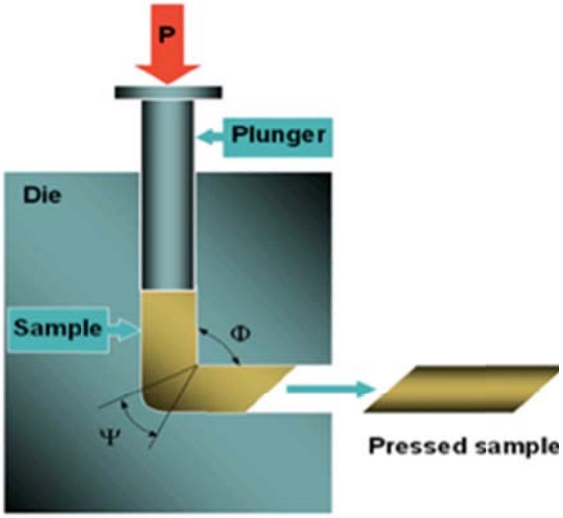

Figure 2.1: schematic sketch of the ECAP technique

The die geometry is defined by the cross section area and the angles Φ (the angle of intersection between the two channels) and ψ (the arc of curvature at the outer point of intersection). These parameters determine the shear strain introduced into the sample during the process. The shear strain which is the responsible for forming the ultra-fine structure and also developing the texture can be modified by repeating the process and changing the sample direction after each pass of ECAP [Iwahashi 1998].

As mentioned above, the deformation in ECAP is mainly a simple shear acting at the crossing plane of the channels. This circumstance leads to form the shear component texture in the processed sample. Toth et al. showed the similarity between introduced plastic strain in the ECAP process and the simple shear test. They reported that the texture obtained by ECAP is similar to that obtained during the shear test [Toth 2004]. Similar results were also observed by other studies [e.g. Werenskiold 2005, Skrozki 2008 and Jining 2004]. The initial massive reduction in grain size is achieved during shear deformation in the first pass through the die because the original grains break up into bands of sub grains. These sub-boundaries subsequently evolve with more shear strain in further pressings into high-angle grain boundaries, ultimately giving a reasonable equiaxed microstructure. In other words, one pass of ECAP results in a microstructure consisting of bands of elongated sub-grains and further pressing leads to form arrays of equiaxed grains.

It is thought that the ECAP can certainly fabricate bulk materials, but the typical size of the sample is still small. From a viewpoint of practical application, one of the greatest disadvantages of ECAP is that it is not a continuous process but a batch process; trials for developing ECAP to a continuous process have been done, like the Conshearing process [Saito 2000] and equal channel angular rolling (ECAR) [Lee 2002a]. Fig. 2.2 schematically illustrates the Conshearing and ECAR processes.

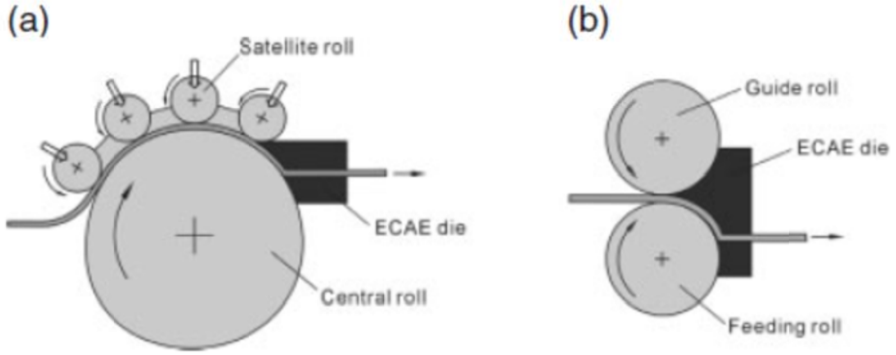

Figure 2.2: schematic sketches of a) the Conshearing and b) the ECAR technique

Accumulative roll bonding: Accumulative roll bonding (ARB) is a continuous SPD process which produces the ultra-fine grain (UFG) structure in sheet samples. Saito and co-workers developed the ARB process for the first time in which SPD strategies are applied in a simple rolling process [Saito 1998]. In this technique, the surfaces of two sheet samples are carefully degreased and wire brushed in order to form appropriate bonds between the sheet pieces. Two sheets were stacked such that brushed surfaces were in contact. Subsequently, rolling of 50% reduction was conducted which leads to forming new bonds between the sheet specimens. For the second pass of the process, the rolled sample is cut and stacked with a treatment described for the first pass. This procedure is repeated several times. The principal of ARB is schematically illustrated in Fig. 2.3.

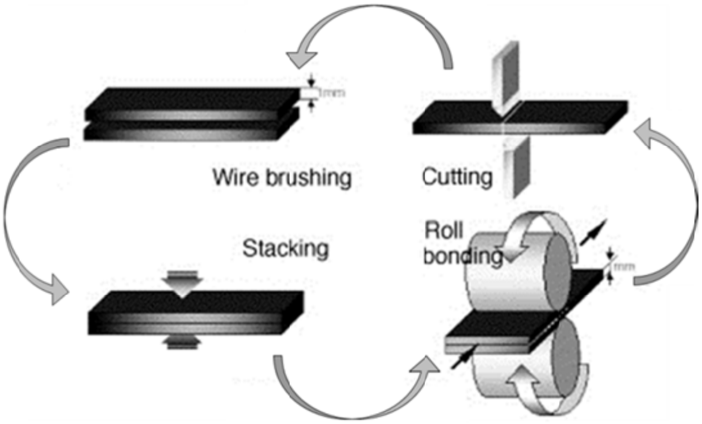

Figure 2.3: schematic sketch of the ARB technique

Since the ARB process is carried out without lubrication, a large amount of shear deformation is introduced in the surface regions in every single pass of the process. Subsequently, half of the surface regions come to the centre in the next pass and this procedure is repeated. As a result, the sheared regions do not localize only on subsurface layers but are complexly distributed through the thickness of the sheets as the ARB cycle proceeds. Lee et al. [Lee 2002b] obtained the distribution of shear strain from the thickness of the sample in the ARB process. He measured the shear strain from the thickness of the sample after the first pass and then predicted the shear strain distribution after several ARB cycles on the basis of the measurement (Fig. 2.4).

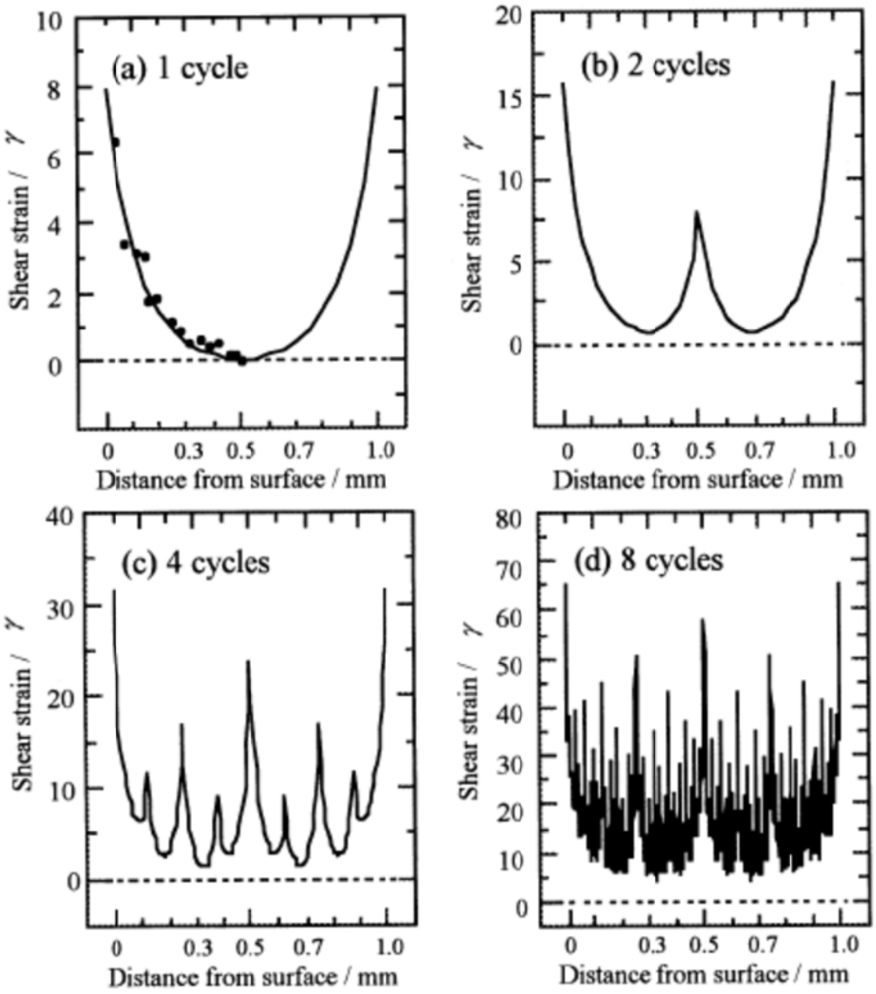

Figure 2.4: the distribution of shear deformation through thickness of the sample severely ARB processed by a) 1, b) 2, c) 4 and d) 8 cycles [Lee 2002b]

A similar distribution has also been reported in the previous works [Costa 2005 and Kamikava 2007]. Like other SPD techniques, the ARB process changes the microstructure and crystallographic texture of the samples. The amount of total strain is important but the produced shear strain throughout the thickness of the sheet during the process is a key factor which distinguishes the ARB process from cold-rolling. Studies show that heavy cold-rolling may lead to pronounced ultrafine structures in metallic materials. But the formation of the ultrafine structure during the ARB process is much faster than that in cold-rolling with the same total deformation [Yan 2011]; i.e. the distributed shear strain in the thickness of the sheet introduced during this process, presented in Fig. 2.4, is the cause for fast forming the UFG structure.

In terms of crystallographic orientation evolution during the ARB process, it was reported that the samples deformed by this technique possess large difference between the centre and surface regions. Despite of shear texture detected in the surface regions of the sheet, the texture in the thickness centre seems relatively random which is somewhat surprising because of severe plastic deformation applied on the sample [Huang 2003]. Since the final surface has been surface throughout the ARB process and the shear strain has been accumulated, this area presents the maximum shear strain. Consequently, a strong shear texture in the surface is expected. But the texture evolution in the centre area is different; the sharp shear texture developed by severe shear deformation in the previous passes is destroyed by the subsequent rolling (plane-strain) deformation in the following pass.

Other techniques: Recently, new SPD processes which seem hopeful for continuous production of bulky UFG materials has been suggested. Groove pressing is introduced which contains a grooving and a flattening die (Fig. 2.5). The geometry of the grooving die leads to developing a shear deformation in the orthogonal plane to the sheet plane. Groove pressing is not a continuous process and the thickness of the sheet sample is unaltered [Park 2005].

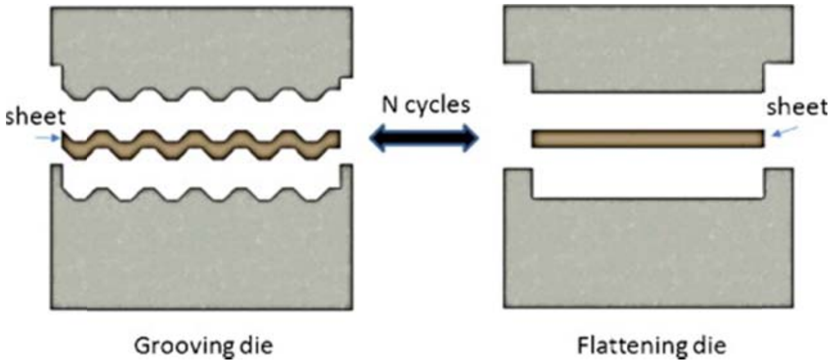

Figure 2.5: schematic sketch of the groove pressing

Repetitive corrugation and straightening (RCS) process has been also carried out which is the repetition of bending and bending-back without change in the sample size [Huang 2001]. This technique seems to be continuous to the groove process in terms of the strain mode. The schematic sketch of the process is shown in Fig. 2.6.

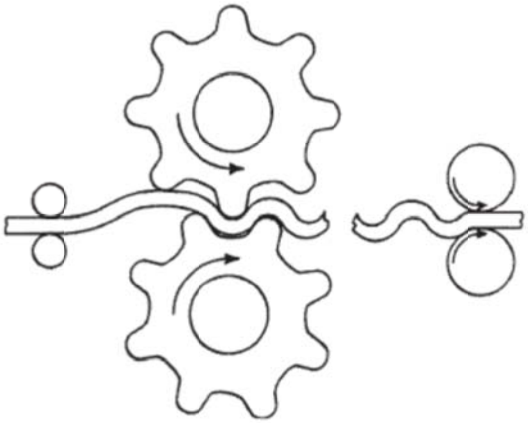

Figure 2.6: schematic sketch of the RCS techniques [Huang 2001]

The RCS and groove pressing processes are based on repeating the bending in the passes, but the difference between them is the amount of plastic deformation per pass which depends on the tolls dimensions.

2-1-2 asymmetric rolling process

It has been shown that SPD techniques were proposed in order to improve the mechanical behaviour. However, a weakness of these methods is still the fact that they are conducted on samples with limited dimensions, which greatly affects their potential for industrial applications. The modified SPD techniques presented in the previous section were attempts to solve this deficiency, but they still have limitations such as extra ordinary equipment and also sample sizes. Recently, the asymmetric rolling (ASR) process, a novel continuous SPD process has been introduced, which is able to produce ultrafine grain materials and also modify crystallographic texture with enhanced performance. The principal base of ASR is a disturbance of the symmetry of the conventional rolling process which causes a shear deformation through the metallic sheet, i.e. the ASR is a kind of rolling process with no symmetry about the centre line of the sheet. The schematic illustration of the ASR process is provided in Fig. 2.7.

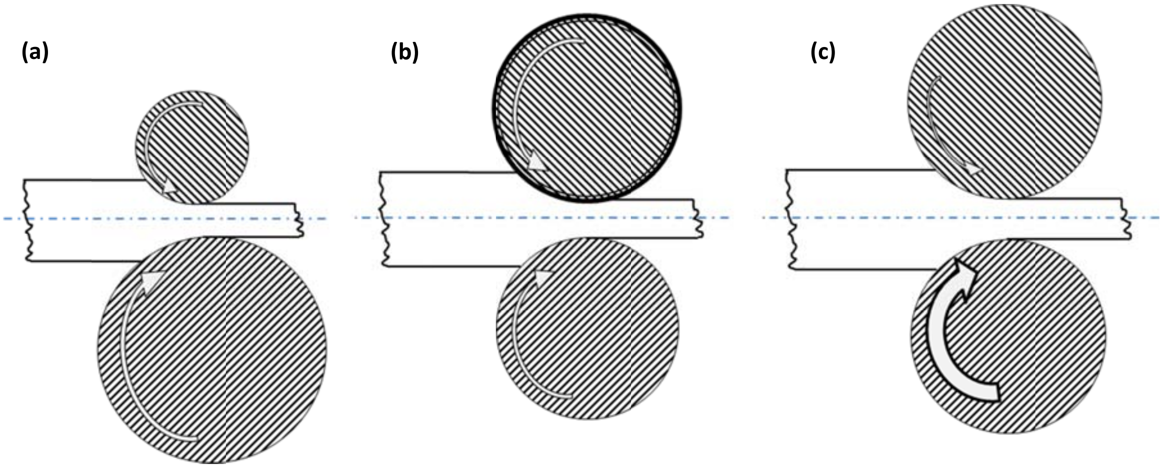

Figure 2.7: the schematics of asymmetric rolling processes using different methods: a) working-rolls diameter, b) friction conditions and c) rotation speeds

In this process, the symmetry disturbance is due to the variance of roll parameters in upper the work-roll and lower one; such as either circumferential velocities of rolls or friction conditions on the sheet faces. Under these circumstances, the metallic sheet is subjected to an extra shear strain in addition to compression deformation. This extra shear strain causes grain rotation during deformation which is responsible for grain refinement and also for forming desirable textures. The level of symmetry disturbance of the ASR determines the amount of shear strain imposed through the thickness of the sample.

Those kinds of ASR processes in which the circumferential velocities of upper and lower working-rolls are different can be gained by either varying the diameter of rolls at the same rotation speed or varying the rotation speed of rolls of the same diameter. In the works of K.H.Kim and D.N.Lee [Kim 2001a] and also S.H.Kim et al. [Kim 2002] different working-rolls diameters are considered to impose shear strain through the aluminium sheet samples. In addition, Jin and Lioyd [Jin 2005] and F.Simoes et al. [Simoes 2008] applied various rotation speeds of working rolls in order to achieve the desirable shear strain in the sheet samples.

Fig. 2.8 shows the FEM analysis of the influence of difference in roll diameter and rotation velocity ratio during the ASR on the shear deformation distribution through thickness of the steel sheet [Lee 2001]. The deformed meshes indicate that the shear deformation penetrates into the centre with change in circumferential velocities. This work also shows that applying a single roll drive results in a shear distribution through the thickness.

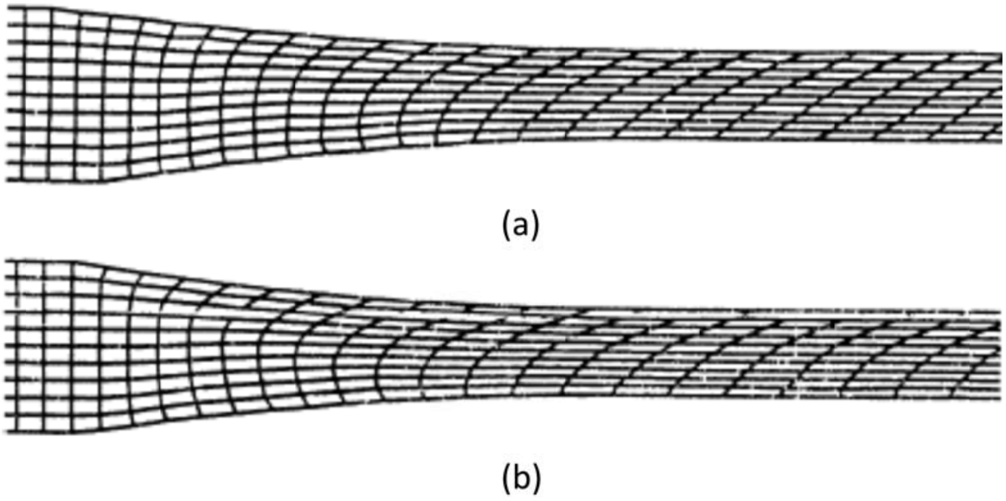

Figure 2.8: FEM calculation of deformed steel sheets with the ASR: a) at roll radius ratio of 1.5 and b) at roll rotation speed ratio of 1.5 [Lee 2001]

Usually in ASR technique, a high value of friction is demanded to impose shear deformation in the metallic sheet Nevertheless, it can still be a factor of this process if the frictions of two surfaces are not equal. The roughness difference of two sheet surfaces was experimentally observed by Utsunomiya et al. [Utsunomiya 2007] and also analysed using the FE method by Ji and Park [Ji 2009].

Like the other types of SPD techniques, ASR is based on repeating of different passes. This raises the idea that rotating the sheet sample between the passes leads to imposing larger shear strain throughout the thickness of the sample. The possible routs of sample rotations between the passes through ASR are shown in Fig. 2.9 [Lee 2001]. Furthermore Sidor et al. applied complex strain paths including conventional rolling and ASR in order to promote shear strain throughout thickness of the sheet specimen [Sidor 2008].

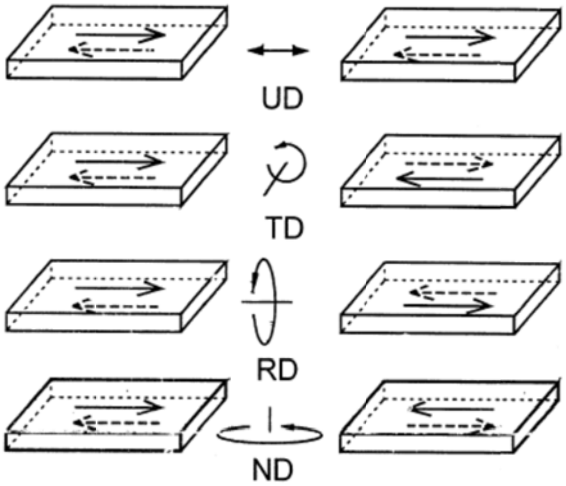

Figure 2.9: possible sample rotations between the ASR passes [Lee 2001]

2-2 sheet rolling

Rolling is a metal forming operation in which metal is passed between a set of cylindrical rolls rotating in opposite directions in order to reduce the initial thickness of the metal. The primary objectives of the flat rolling process are to reduce the cross-section of the incoming material while improving its properties.

2-2-1 basic concepts of conventional and asymmetric rolling

Since in sheet rolling, the length of contact between rolls and work piece, L, is usually much smaller than the width of the sheet, w, it is essentially a plane strain compression (Fig. 2.10).

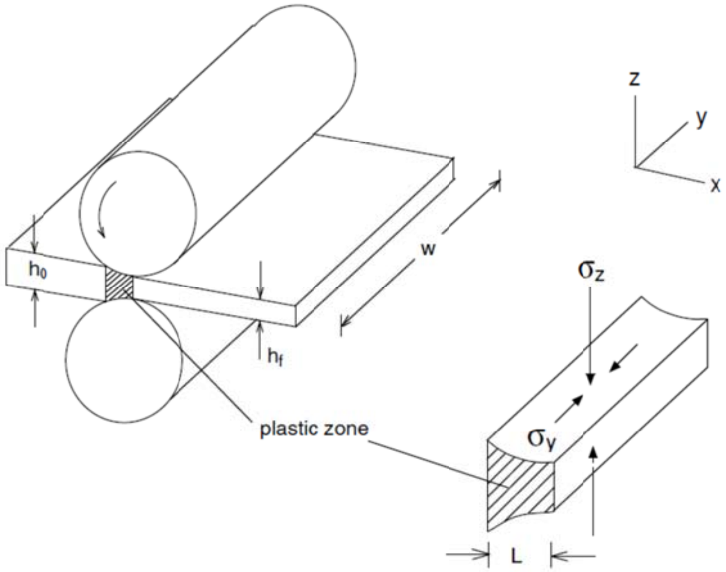

Figure 2.10: schematic of the deformation zone in flat rolling

The plastic zone which is thinned by the compressive stress is free to expand in the rolling direction, x. But lateral expansion in the y-direction is limited by the undeforming material on both sides of the roll gap except at the edges which leads to such a plane strain.

Neutral point: The rolls make contact with the surface of the sample over the length of contact depicted by an arc (see Fig. 2.11). At a certain point of contact, the surface of the material and the roll move with the same speed which is called the neutral point N in Fig. 2.11.

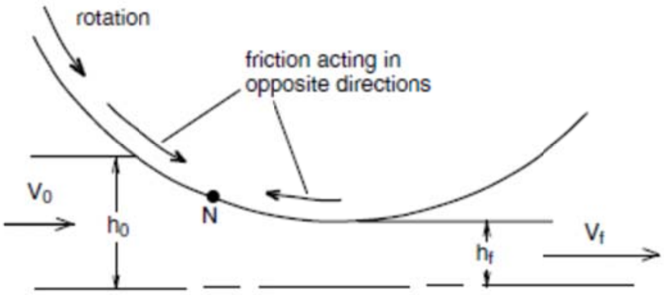

Figure 2.11: the friction direction on the inlet and outlet side of the sample

From N to the exit, the metal moves faster than the roll surface. In this region, the friction between work-piece and roll opposes motion. The metal moves slower than the rolls between N and the inlet point. The friction in this part acts in the direction of rolling, aiding the process. This friction force over the contact arc draws the metal into the roll gap. The position of neutral point in the contact arc depends on the amount of reduction, the diameters of the rolls and the coefficient of friction and also on applying the front and back tensions to the sheet. The neutral point tends to move to outlet as the amount of reduction increases.

There exists the A’B’ arc with the N’ point as a neutral point on the other face of the sheet in contact with the second work-roll (Fig. 2.12). It can be discussed in two different ways; ideal conventional rolling in which assumes symmetry about the strip centre-line and asymmetric rolling which the symmetry of the process is disturbed as mentioned in the previous section (§ 2-1-2). In the rolling process, the thickness of the sheet is reduced and the sample speed increased from inlet to outlet and roll speeds have some intermediate values between these entry and exit speeds. As mentioned above, where the sheet and the roll surface speed are equal we have a neutral point. Due to symmetry in conventional rolling, the horizontal position of the neutral point on the upper roll is equal to that on the lower roll. But in asymmetric rolling, since the speeds of the upper and lower roll are different, the location of the neutral point of the upper roll is different from that of the lower roll (Fig. 2.12b).

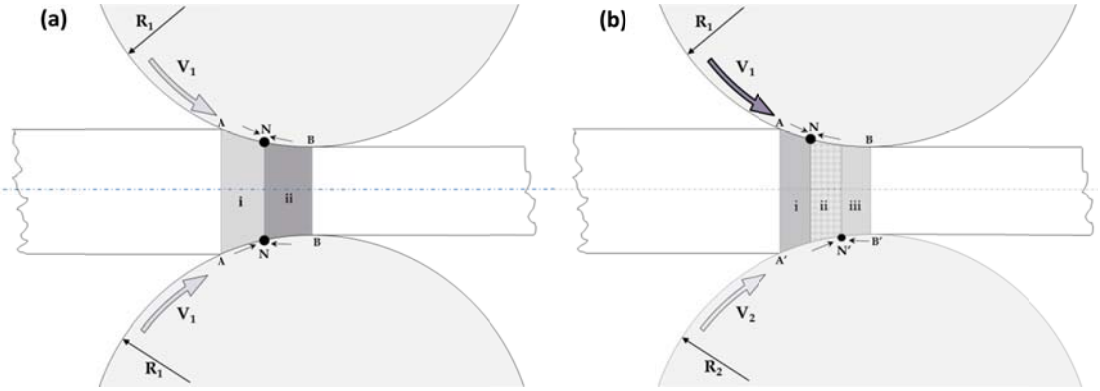

Figure 2.12: schematic illustrations of a) conventional rolling and b) asymmetric rolling

Figure 2.12 also shows the plastic deformation regions in two conventional and asymmetric rolling processes. In conventional rolling the region at the roll gap is divided into backward and forward-slip zones according to the friction directions exerted on the sheet from the work-rolls. In asymmetric rolling a third cross shear deformation zone is formed between the backward-slip zone and the forward-slip zone. Both compressive and shear stresses occur simultaneously in the cross shear deformation zone.

2-2-2 forces and torque

The rolling power is applied to a rolling mill by applying a torque to the rolls. This power is expended principally in different ways; the necessary energy for deforming the specimen and the necessary energy to overcome frictional forces. The rolling load is distributed over the arc of contact in the typical friction hill pressure distribution which describes the profile of the rolling pressure across the contact arc. Numerous works have been carried out developing the analysis of treatments of rolling. Slab method, slip line field theory and finite element method are the main theoretical methods to attain rolling force and rolling torque. Slab method is the simplest method which is aimed at expressing the rolling force and rolling torque in terms of geometry of the deformation and the strength properties of the material. In this method, a differentially thick slab of the material is selected perpendicular to the rolling direction in the deformation region. Force balance for the slab results in a differential equation, which is solved either by close form analytical methods or numerical methods. The constants of integration are obtained by applying the appropriate boundary conditions [e.g. Dieter 1988 and Hosford 1993]. In the following section the rolling force and torque in both conventional and asymmetric rolling processes will be analysed.

The assumptions for slab analysis of rolling pressure and torque are:

- The rolls are rigid
- The material is elastic-plastic
- There is no width expansion during the process- plane strain condition
- The stresses are uniform in the contact area
- The friction conditions are uniform along the contact length, although the upper and lower coefficient friction can be different (in the ASR process).
- The plastic flow at the entrance and exit are assumed to be horizontal.
- The principal axes are in the directions of the applied loads.

In the conventional sheet rolling process the rolling loads are derived as a function of rolling geometrical parameters. The rolling load, P, is given by the roll pressure, p, times the contact area (L). The pressure is the yield stress of the material, σ_0, and the contact area is the projected area of the arc of the contact of sheet in the rolling gap:

$$P = pL = \sigma_0\sqrt{R\Delta h} \tag{2.1}$$

Where Δh and R are the thickness reduction and the roll radius respectively. The friction effects are similar to those in plane strain compression. As concerns to the plane strain condition in the sheet rolling process, the pressure, P_{av}, has been derived as below [Hosford 1993]:

$$P_{av} = \frac{h}{\mu L}(exp\frac{\mu L}{h} - 1)\sigma_0 \tag{2.2}$$

where h and μ are the thickness of the sample and the average of friction coefficient between the surfaces respectively. The equation shows that rolling load increases as the initial sheet sample becomes thinner. Eventually, a point is reached where the deformation resistance of the sheet is greater than the roll pressure. Figure 2.13 depicts the distribution of roll pressure along the contact. The roll pressure rises to a maximum at the neutral point and then falls off.

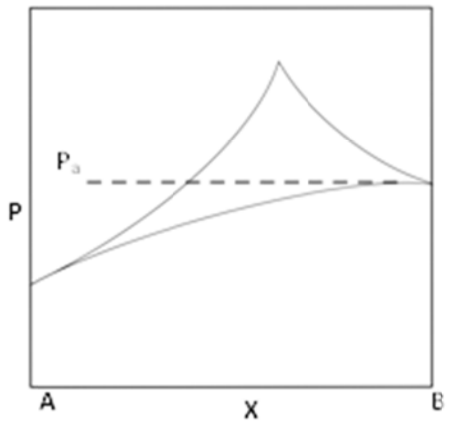

Figure 2.13: distribution of roll pressure along the contact [Hosford 1993]

The area under the curve is proportional to the rolling load which for purposes of calculation acts at the centre of gravity of the pressure distribution. Therefore, the shape of the pressure distribution is important because the location of the rolling load with respect to the roll centre determines the torque and the power required to produce the reduction.

Since the neutral point in the rolling process is not really a line on the roll surface but an area, the pressure distribution does not present a sharp maximum at the neutral point (see Fig. 2.14).

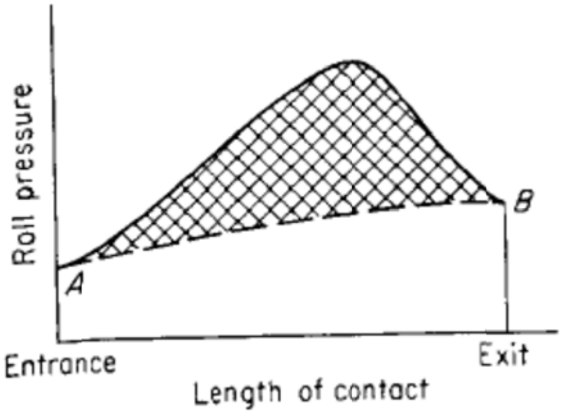

Figure 2.14: distribution of roll pressure along the contact [Dieter 1988]

In the asymmetric rolling process due to the positions of upper and lower neutral points, there are three deformation regions in the asymmetric rolling process (Fig. 2.12) which should be analysed separately. Figure 2.15 illustrates the stress states of the slab element in each deformation zone [Yong 2009].

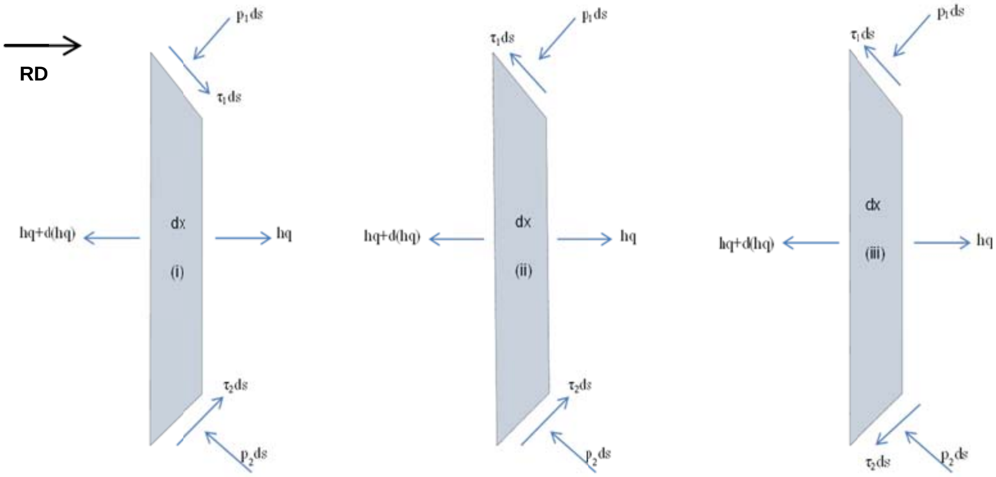

Figure 2.15: slab element of different deformation zones

The balance of forces along *x* and *y* directions in three different zones and the boundary conditions make it possible to describe the roll pressure *p* when the sheet passes through the roll gap. Here, q_0 is the front-tension force and q_i is the back-tension force. Using equilibrium conditions of the deformation zones and also with the Von Mises yielding criterion:

$$p + q = 2k \qquad (2.3),$$

where k is the yield strength in shear. The general equation of rolling pressure equation was obtained by Gao et al. [Gao 2002]:

$$\bar{p} = Ce^{-\bar{\mu}\,\bar{x}} + (\frac{\bar{x}^3}{3\bar{\mu}} - \frac{\bar{x}^2}{\bar{\mu}^2} + \left(\frac{1}{\bar{\mu}} + \frac{1}{\bar{\mu}^3}\right)\bar{x} - \left(\frac{1}{\bar{\mu}^2} + \frac{1}{\bar{\mu}^4}\right)) \qquad (2.4)$$

where

$$\bar{p} = \frac{p}{2k}, \qquad \bar{\mu} = \mu_e\sqrt{\frac{R}{h_0}}, \qquad \bar{x} = arctan\frac{x}{\sqrt{Rh_0}}$$

where R is roll mill diameter, μ_e is the effective friction coefficient and x is the distance from the vertical line through the centres of the working-rolls. The constant C is related to the boundary condition which can be obtained.

The boundary condition for zone iii:

$$\mu_e = \mu_1 + \mu_2\,, \qquad \bar{p}_0 = 1 - \frac{q_0}{2k}\ (at\ x = 0) \qquad (0 \le x \le x_{n2})$$

And in zone i:

$$\mu_e = -\mu_1 - \mu_2\,, \qquad \bar{p}_0 = 1 - \frac{q_i}{2k}\ (at\ x = L) \qquad (x_{n2} \le x \le L)$$

And in zone ii, shear region:

$$\mu_e = \mu_1 - \mu_2\,, \qquad \bar{p}_s = \bar{p}_f\ (at\ x = x_{n2}),\ \ \bar{p}_s = \bar{p}_b\ (at\ x = x_{n1}) \qquad (x_{n2} \le x \le x_{n1})$$

where x_{n1} and x_{n2} are the positions of neutral points which can be determined using the boundary conditions of p_s=p_b at x_{n1} and also p_s=p_f at x_{n2}.

Figure 2.16 shows the specific rolling pressure distributions for various friction coefficients [Gao 2002]. In the conventional rolling curve, where the friction coefficient ratio equals 1, there is no shear region in the deformation zone. The peak of the curve indicates the neutral point of the process. Increasing the ratio results in the appearance of an area like a plateau in the deformation region that shows the shear zone with the neutral points at the sides. The length of the shear zone increases when the friction coefficient ratio goes up.

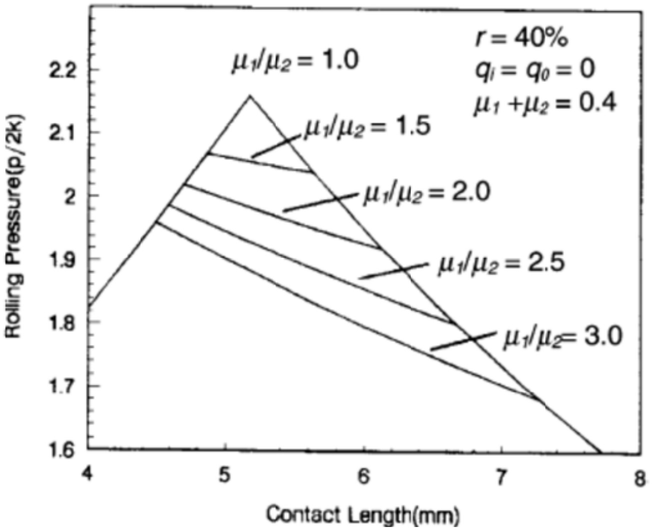

Figure 2.16: the specific rolling pressure distributions for different friction factors [Gao 2002]

The same trend has been detected when asymmetric rolling was due to the variance of roll velocities and roll diameters [Hwang 1997, Salimi 2002 and Yong 2009]. When the ratio of circumferential velocities of upper and lower rolls increases, the shear zone expands and also the average rolling pressure decreases.

The total rolling force is the sum of the pressures in three different deformation zones:

$$P = p_b + p_s + p_f \qquad (2.5)$$

The rolling torque is a parameter that determines the energy consumption of the rolling mill. Generally, the rolling torque of upper and lower rolls, T_1 and T_2, can be obtained by integrating the moment of the friction stress along the contact length of each roll [Gao 2002].

$$T_1 = \mu_1 R_1 (P_b - P_s - P_f) \qquad (2.6)$$

$$T_2 = \mu_2 R_2 (P_b - P_s - P_f) \tag{2.7}$$

Figure 2.17 illustrates the influence of the friction coefficient ratio on rolling torque in the rolls with higher and lower friction coefficient. In both working rolls, the friction force acts to enhance not to resist rolling. This effect is even higher in the roll with the higher friction coefficient.

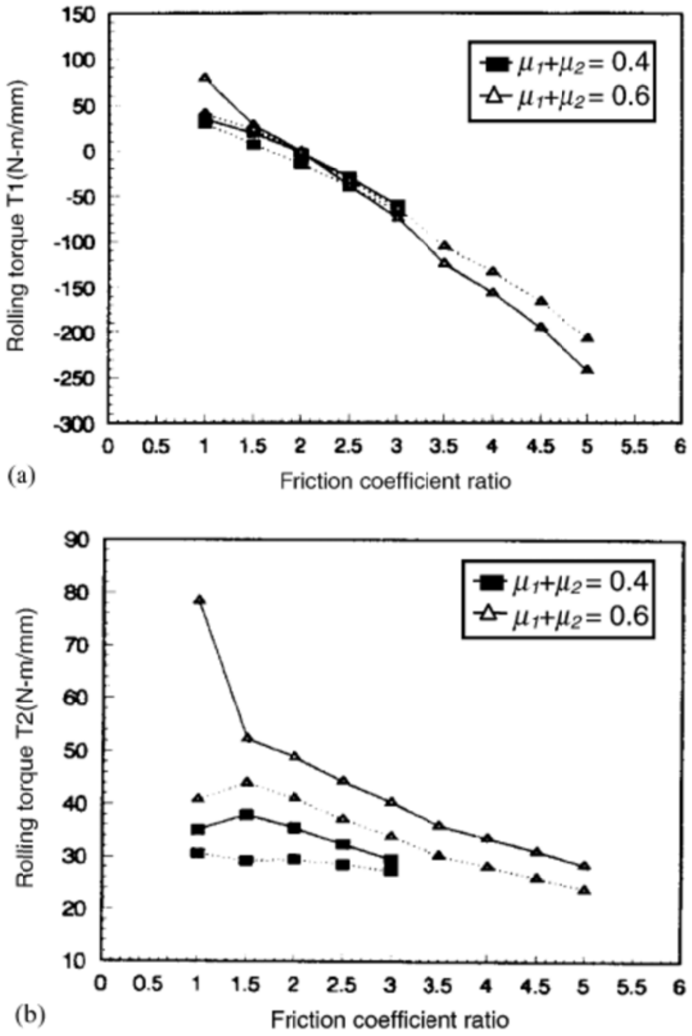

Figure 2.17: variation of rolling torque with change in friction coefficient ratio [Gao 2002]: a) the roll with higher friction coefficient and b) the roll with lower friction coefficient

2-3 slip system: a plastic deformation mechanism

Plastic deformation occurs by sliding of one part of a crystal relative to another along the certain planes. Unlike elastic deformation involving only the stretching of interatomic bonds, slip requires the breaking and re-forming of interatomic bonds and the motion of one plane of atoms relative to another.

In order for plastic deformation to take place, dislocations move through the grains. They do not move with the same degree of ease on all crystallographic planes in all crystallographic directions. Observations show that slip tends to occur preferentially on certain crystal planes and in certain specific crystal directions. These planes are known to the slip planes and the direction of the dislocation movement is called the slip direction. The combination of the slip plane and the slip direction is termed the slip system. The slip system depends on the crystal structure and is such that the atomic distortion that accompanies the motion of a dislocation is minimal. Usually in the crystals, slip plane is the plane with the most dense atomic packing. The slip direction corresponds to the direction in this plane that is the most closely packed with atoms. As shown in Fig. 2.18 the dominant slip systems vary with the material's crystal lattice. In the case of face centre cubic (FCC) crystals, slip occurs mostly on {111} octahedral planes and in <110> directions which are parallel to cube face diagonals. In all, there are 12 such slip systems (four unique {111} planes, and within each plane three independent <110> directions) [Kocks 1998]. In body centre cubic (BCC) crystals, slip occurs in the <111> cube diagonal direction and on {110} dodecahedral planes. In this structure, dislocations also slip on other planes such as {112} and {123} under various conditions, and sometimes the behaviour can be adequately described by pencil glide with a <111>slip direction. There are 48 possible slip systems, which are the combinations of these three planes and pencil glide direction [Kocks 1998].

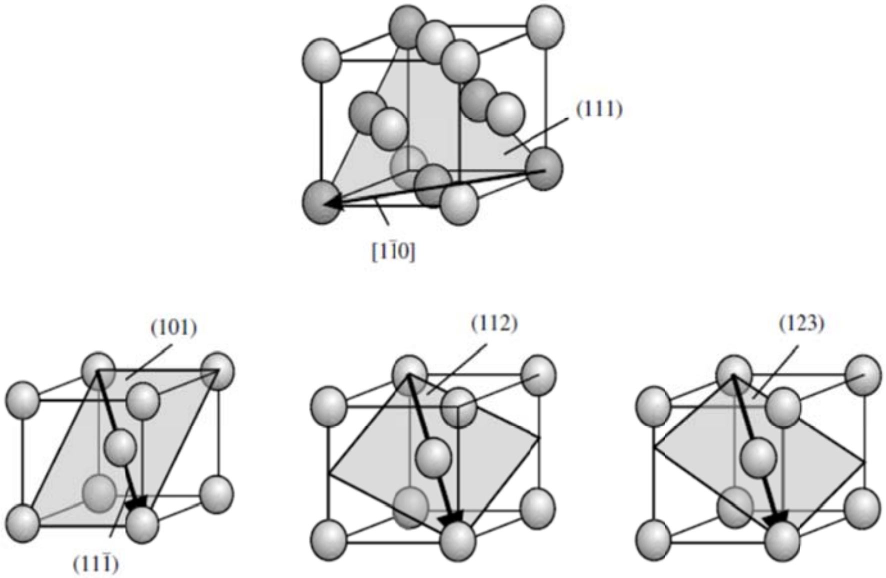

Figure 2.18: slip systems in FCC and BCC materials

Plastic slip is a shearing process; dislocations move in response to shear stresses applied in a slip plane and along a slip direction. Even though an applied stress may be purely tensile, the shear component exists to force dislocations moving in the slip plane. Hydrostatic stress can often be assumed not to influence slip.

As can be seen in Fig. 2.19 the movement of dislocations in the slip plane leads to the formation of small steps on the surface of the sample that are parallel to one another and loop around its circumference.

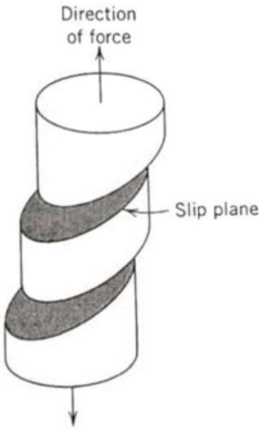

Figure 2.19: macroscopic slip in a single crystal

2-3-1 Plastic deformation of single crystals

Assuming that a single crystal in the shape of a rod is tested in tension; as shown in Fig. 2.20 ϕ represents the angle between the normal to the slip plane and the applied stress direction; and λ indicates the angle between the slip and stress directions. When the sample is loaded with tensile stress σ, the shear stress acting on the slip plane and in the slip direction is τ. As shown in Fig. 2.20, if the cross section area of sample is A, the force in the slip direction is A.σ.cosλ, which acts on slip area A/cosφ. Hence the resolved shear stress on the slip plane and in the slip direction is:

$$\tau = \sigma \cos\lambda \cos\phi \qquad (2.8)$$

where cosλcosϕ represents an orientation factor (often referred to as the Schmid factor). In response to the applied stress, slip in the mentioned slip system will occur when the resolved shear stress reaches a critical value, termed the critical resolved shear stress, τ_{crss} [e.g. Hertzberg 1937 and Calister 1999]. There are a number of slip systems in a single crystal, each of them having a different Schmid's factor. The yielding will occur on the slip system possessing the greatest Schmid's factor. Consequently, if only a few systems are available, the necessary load for yielding can vary dramatically with the relative orientation of the slip systems.

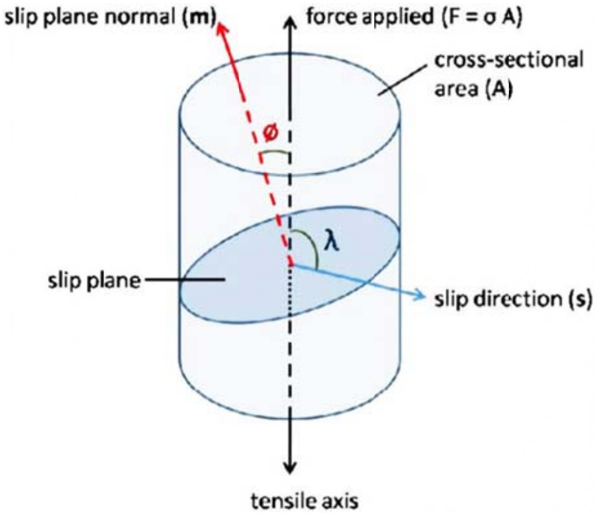

Figure 2.20: geometrical relationships between the tensile axis, slip plane and slip direction

2-3-2 plastic deformation of polycrystals

Since polycrystal materials are formed of a significant number of crystals with different orientations, plastic deformation of these materials is quite complex. Due to the random orientation of grains, the direction of dislocation slip varies from one grain to another. With the purpose of studying the plastic deformation of polycrystal materials one needs to know detailed information about crystallographic orientation and dislocation structure of polycrystals.

2-3-2-1 crystallographic orientation

2-3-2-1-1 basic concepts

Generally, the grains of a polycrystal material possess different crystallographic orientation from that of their neighbours. To describe the orientation of a crystal relative to macroscopic reference, one often specifies the Miller indices of two directions: the normal of the plane {hkl}, and a line in it, <uvw>. For instance in the case of sheet rolling, the orientation {hkl}<uvw>, means that a {hkl} plane is parallel to the rolling plane, and a <uvw> direction is parallel to the rolling direction.

In order to introduce an orientation, terms of reference are required, which are called a coordinate system [Kocks 1998 and Bunge 1982]. Two Cartesian systems are necessary:

1. **The sample coordinate system S= {s_1 s_2 s_3}:** The axes of the sample are chosen according to important surfaces and directions associated with the external shape of the sample. The sample coordinate systems in sheet metal rolling are the rolling direction (RD); the transverse direction (TD); and the normal direction (ND).
2. **The crystal coordinate systems C= {c_1 c_2 c_3}:** The axes of the crystal are specified by the directions in the crystal which usually are adapted to the crystal symmetries. For instance, in cubic crystals, the axes [100], [010] and [001] are usually assumed as the crystal coordinates.

The crystal coordinate system (C_c) can be transformed to the sample coordinate system (C_s) with the orientation matrix (g) which contains the rotations of the sample coordinates onto the crystal coordinates.

$$C_c = g \, . \, C_s \tag{2.9}$$

where the orientation matrix is a matrix including cosines of the angles between the crystal and sample axes. The Euler angles refer to three rotations that transform the sample coordinate system onto the crystal coordinate system [Bunge 1982]. The rotations are as follows:

1. φ_1 about the normal direction ND, transforming the transverse direction TD into TD' and the rolling direction RD into RD'
2. Φ about the axis RD' (in the new orientation)
3. φ_2 about ND'' (in the new orientation)

where φ_1, Φ and φ_2 are the Euler angles (Bunge definition). Figure 2.21 shows how rotation through the Euler angles describes the rotation between sample and crystal axes.

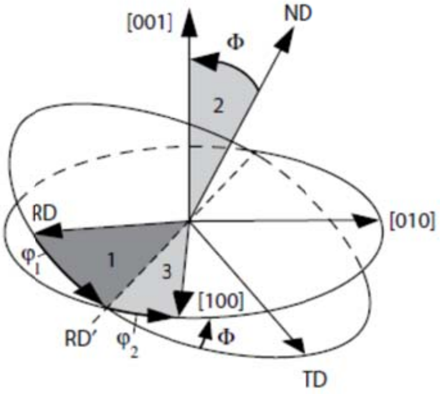

Figure 2.21: the Euler angles φ_1, Φ and φ_2 describing the rotation between the sample and macroscopic axis

The rotations through Euler angles about ND, RD' and ND'' can be analytically expressed as three matrices:

$$g\varphi_1 = \begin{bmatrix} \cos\varphi_1 & \sin\varphi_1 & 0 \\ -\sin\varphi_1 & \cos\varphi_1 & 0 \\ 0 & 0 & 1 \end{bmatrix};$$

$$g\Phi = \begin{bmatrix} 1 & 0 & 0 \\ 0 & \cos\Phi & \sin\Phi \\ 0 & -\sin\Phi & \cos\Phi \end{bmatrix} \text{ and}$$

$$g\varphi_2 = \begin{bmatrix} \cos\varphi_2 & \sin\varphi_2 & 0 \\ -\sin\varphi_2 & \cos\varphi_2 & 0 \\ 0 & 0 & 1 \end{bmatrix}$$

Matrix g, introduced in equation 2.9, can be obtained by multiplication of the three above matrices:

$$g = g\varphi_2 \cdot g\Phi \cdot g\varphi_1 \qquad (2.10)$$

Any orientation can be identified as three Euler angles (φ_1, Φ, φ_2) represented as a point in a 3-D frame with the axes φ_1, Φ and φ_2 (Fig. 2.22). The resulting space which is called Euler space can also be used to represent the orientation distribution in a polycrystal sample.

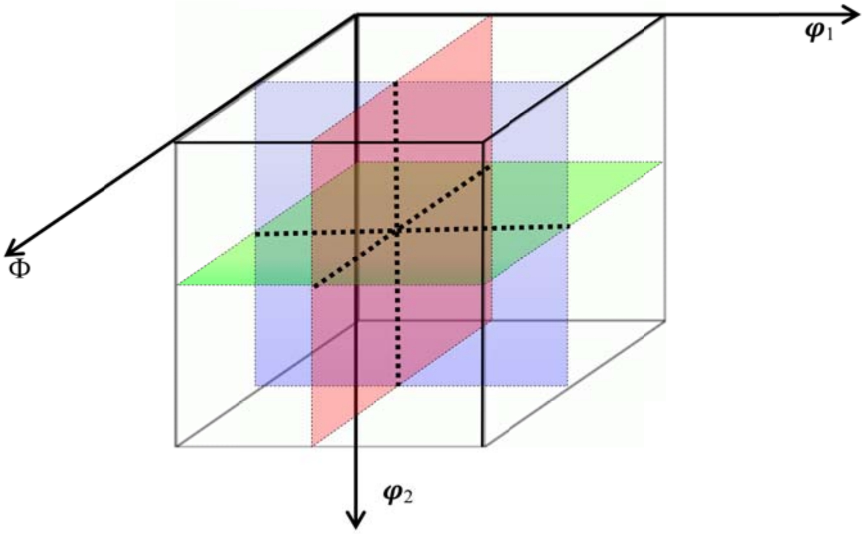

Figure 2.22: three dimensional orientation space of Euler angles

In the most general case of triclinic crystal symmetry and no sample symmetry, the Euler angles are defined in the range $0° \leq \varphi_1, \varphi_2 \leq 360°$, and $0° \leq \Phi \leq 180°$, which in turn defines the maximum size of the Euler angle space. However, various sample symmetries reduce the size of Euler space by affecting the range of the angle φ_1 and also crystal symmetries reduce the range of the angles Φ and φ_2 (for instance in cubic crystals $\Phi, \varphi_2=90°$).

The orientations of all the grains may be randomly distributed in relation to the reference which causes them to possess isotropic properties. However, the orientation may tend to cluster to a greater degree about a particular orientation. This is called preferred orientation, or texture and leads to present directional properties. Preferred orientation forms during deformation and is modified through plastic deformation and heat treatment processes.

2-3-2-1-2 pole figure and ODF

The normal of any plane in a crystal can be indicated as a point on the unit reference sphere which is a sphere with radius 1 notionally residing around the crystal. The first point of the vector coincides with the centre of the sphere, and the second point lies on the surface of the sphere. Here, a similar concept can be used for a crystallographic direction which needs two points for each direction.

The orientation of a single crystal located in the centre of a unit sphere can be obtained if the sphere reference system is set as the macroscopic reference system (RD, TD, and ND). Also, if a polycrystal is located in the centre of the unit sphere, the distribution of orientation of the crystals relatively to the sample reference system can be obtained.

Due to difficulty of representation of a 3-D orientation on the unit sphere and also measuring angular distances between them, a 2-D representation is required. The pole figure which is based on the stereographic projection is a method of 2-D representation.

The position of a given pole on the sphere is commonly characterized in terms of two angles (Hansen 1978): The angle α describes the azimuth of the pole, where $\alpha = 0°$ is the north pole of the unit sphere, and the angle β characterizes the rotation of the pole around the polar axis, starting from a specified reference direction (Fig. 2.23).

As mentioned above, in order to characterize the crystallographic orientation of a crystal, the spatial arrangement of the corresponding poles in terms of the angles α and β has to be determined with respect to the sample coordinate system S. In a sheet rolling study, the rolling direction RD is usually chosen to be the north-pole and the rotation angle β is 0° for the transverse direction TD.

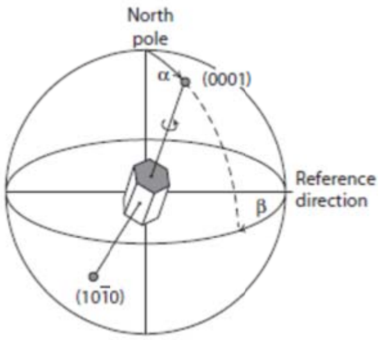

Figure 2.23: orientation of (0001) plane in a hexagonal crystal described by the two angles α and β

The pole figures usually are only capable of determining the distribution of the normal of specific crystallographic planes and not directions on the planes. Since the texture of polycrystals contains many components including the normal planes and the directions, the reasonable way to interpret their texture is by using pole figures to compute the orientation distribution function (ODF). In the ODF representation, a given orientation is determined relative to the random texture as the reference. The ODF is defined as the volume fraction of grains possessing a certain orientation g:

$$\frac{dV(g)}{V} = ODF(g).d_g \qquad (2.11)$$

As an ODF representation is a function of three Euler angles, a 3-D plot is required. However, it is usually represented in 2-D by keeping one Euler angle (φ_2) and two other Euler angles are plotted on a Cartesian frame (Fig. 2.24).

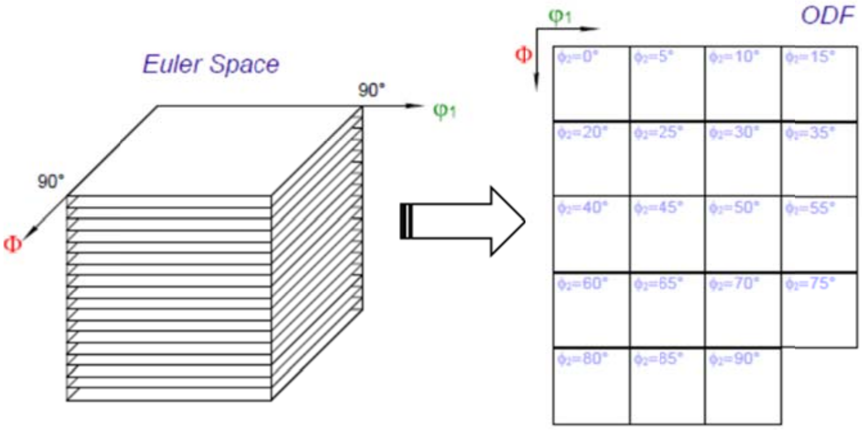

Figure 2.24: the 3-D and 2-D ODF presentation [www]

2-3-2-1-3 important texture types in FCC and BCC materials

A considerable number of investigations have been carried out in the characterization of sheet metal textures and among those FCC and BCC materials receive much attention in this work, since the research is focused on the study of these crystallographic textures. The majority of texture researchers investigate conditions leading to favourable texture for particular applications. Here there is a list of significant texture components of FCC and BCC materials.

- **FCC materials**

The main slip system in FCC materials are {111} <110>, consisting of 12 symmetrically equivalent variants. Activity of these slip systems establishes various textures during different processes. Table 2.1 summarizes the main FCC texture components. In the following section, the main components of aluminium in different states will be discussed.

Table 2.1: the texture components of FCC material

Label	Miller indices {h,k,l}<u,v,w>	Euler angles			texture type
		φ_1	Φ	φ_2	
cube	{001}<100>	0	0	0	Recrystallization texture components
Goss	{110}<001>	0	45	0	
Copper	{112}<111>	90	35	45	Rolling texture components
Brass	{011}<211>	35	45	0	
Dillamore	{4 4 11}<11 11 8>	90	27	45	
E	{111}<110>	60	54.7	45	shear texture components
F	{111}<112>	90	54.7	45	
H	{001}<111>	0	0	45	

Figure 2.25 depicts the presented FCC components in ODF sections in order to simplify studying the texture evolution.

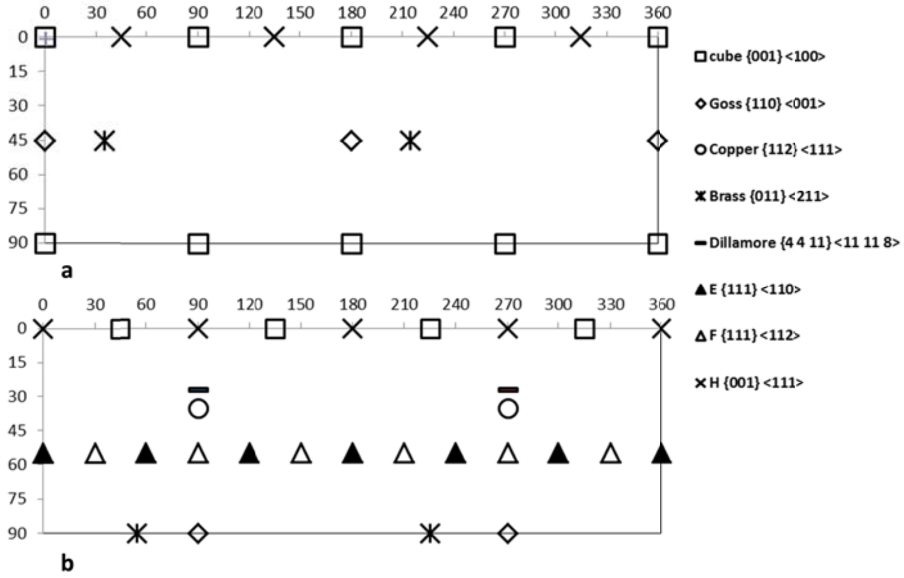

Figure 2.25: the texture components of FCC material: a) φ_2= 0 and b) φ_2=45°

FCC- rolling texture: As mentioned, various activated slip systems, which are controlled by deformation mechanisms, form different orientations. The influence of the materials' stacking fault energy on the rolling texture can be understood in terms of its impact on the deformation mechanism. Hence, according to this parameter the deformation texture in FCC materials is introduced in two categories, namely, textures of pure metals-type possessing low SFE (such as Aluminium and copper), and alloy-type texture owning a higher value of SFE (such as brass). Figure 2.26 shows the texture of pure metal rolling texture.

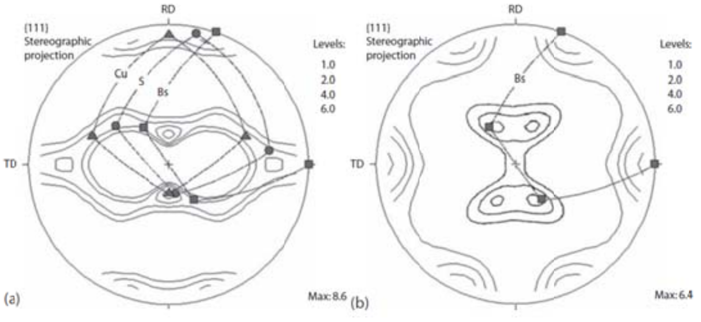

Figure 2.26: rolling texture {111} pole figure of a) pure copper and b) brass

More refined idealized descriptions have been introduced, such as texture fibres, corresponding to scattering a line in Euler space. Figure 2.27 shows the schematic representation of the rolling texture in orientation space. There exist two main fibres. In these materials, the most important fibres are α which is the observed fibre at low deformation levels and β fibres which exist at higher deformation degrees. α fibre is detected with {001}//RD, which runs from the orientation to Bs. In the other side, β fibre runs from the Cu orientation through the E-F orientation to the Bs component where it meets α fibre.

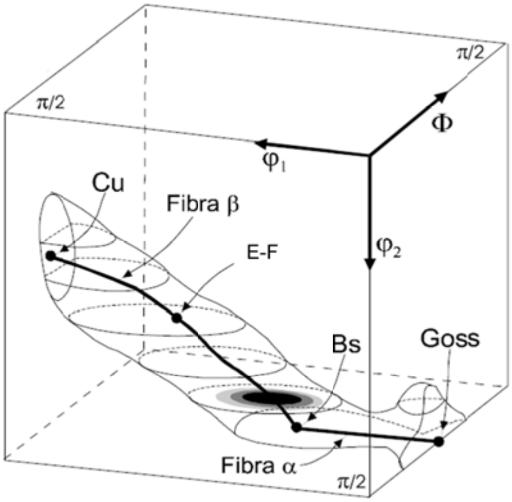

Figure 2.27: α and β fibres in Euler space

FCC- Recrystallization texture: The orientation of deformed materials is established by nucleation of new grains and growth into the deformed one. This phenomenon is characterized by the formation and movement of high-angle grain boundaries. Therefore, these evaluations cause a change in the orientation of the grains and crystallographic texture as well. In the other words, nucleation and growth are two fundamental steps of recrystallization. The evaluations of crystallographic texture of the deformed material during recrystallization are interpreted in terms of the two rival theories of oriented nucleation and oriented growth [Sha 2007]. Hence, the cube and Goss are formed from rolling texture of deformed FCC materials.

- **BCC materials**

The formability of BCC materials depends on the texture of the sheets. Due to the large number of activated slip systems in BCC materials, there is no very intense peak in the

XRD test and these materials tend to form fibre textures. Some components and fibres are identified in BCC structure material (see table 2.2).

Table 2.2: list of texture components and fibres of BCC materials

components	{hkl}<uvw>	φ_1	ϕ	φ_2
Cube	{001}<100>	45	0	45
H	{001}<110>	0	0	45
E_1	{111}<110>	0	54.7	45
E_2	{111}<110>	60	54.7	45
F_1	{111}<11-2>	30	54.7	45
F_2	{111}<11-2>	90	54.7	45
i	{112}<-110>	0	35	45
goss	{110}<001>	90	90	45

fibres	fiber axes	Euler angles
α	<011>//RD	0,0,45 _ 0,90,45°
γ	<111>//ND	60,55,45 _ 90, 55,45°
ε	<110>//TD	90,0,45 _ 90,90,45°

Figure 2.28 also presents the some fibres and texture components which can be found in ODF section of φ_2=45° of in BCC materials.

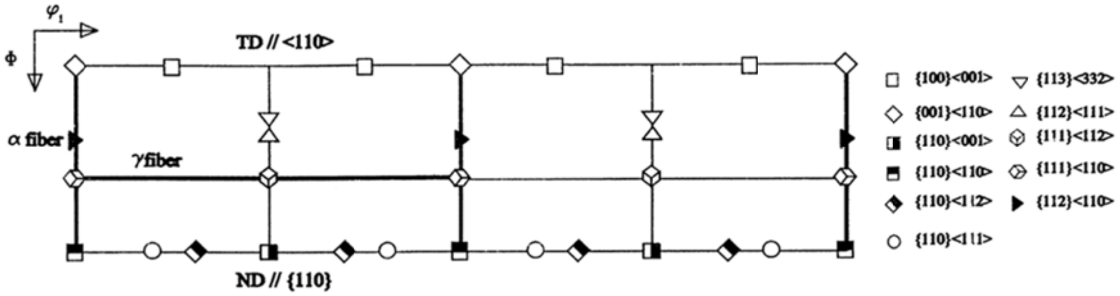

Figure 2.28: fiber texture in a BCC material; φ_2=45° [Lee 2001]

BCC- rolling texture: A strong α-fibre texture with the i component and weaker γ-fibre texture with the E component were developed during the rolling of BCC materials. The mostly partial, α fibre comprises the orientations with a common ⟨110⟩ crystal axis parallel to the RD, that is, the orientations {hkl}⟨110⟩, which include the orientations H, i, and E. Also, the γ fibre comprises the orientations with {111} parallel to the ND, that is, the orientations {111}⟨uvw⟩, including the E and F textures. Figure 2.29 represents the texture of rolled IF steel in the φ_2 = 45° section.

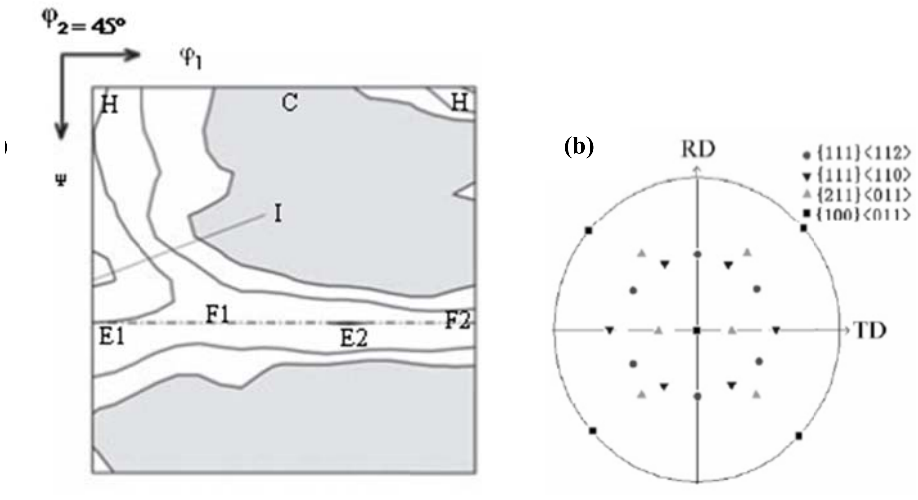

Figure 2.29: important texture of BCC material a) ODF in φ_2=45° and b) {200} pole figure

Figure 2.30 illustrates the texture evolution through cold rolling of a low-carbon steel in the form of the intensity along the α and γ fibres [Holscher 1991]. Due to the cubic crystal symmetry, the α fibre is shown in the range 0°≤ Φ ≤90° and the range 60° ≤ φ_1 ≤90° is sufficient for a representation of the full γ fibre.

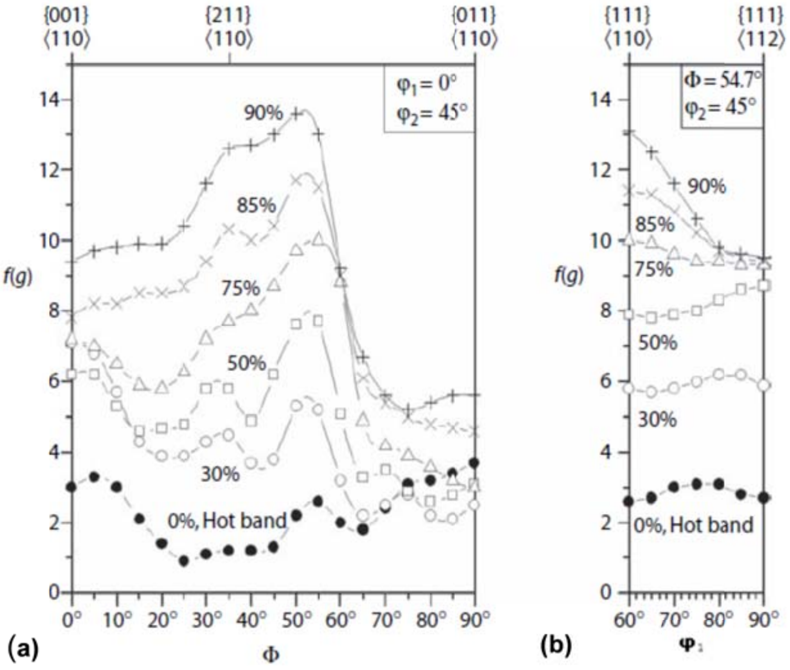

Figure 2.30: evolution of the rolling texture: a) α and b) γ of low-carbon steel of different total deformations [Holscher 1991]

Increasing rolling deformation tends to shift the texture maxima from H along the α fibre over i toward E and F in the γ fibre. Also it should be noted that unlike in FCC metals, the rolling texture evolution in iron and low-carbon steels is largely independent of composition and processing.

BCC- recrystallization texture: As shown in Fig. 2.30 representative α and γ fiber texture components are strongly developed in the fully deformed state. Figure 2.31 shows the variation of the volume fraction of each texture component of deformed sample with the annealing time in IF steel. The i component starts to decrease and the F component starts to increase after the mid-stage of recrystallization. As can be seen, the volume fraction of the E component increases only at the end of recrystallization and the H component also remains for a long time and decreases rapidly at the late stage of recrystallization. Due to these results, many scientists have reported that the transformation of the i to F components determines the final recrystallization texture.

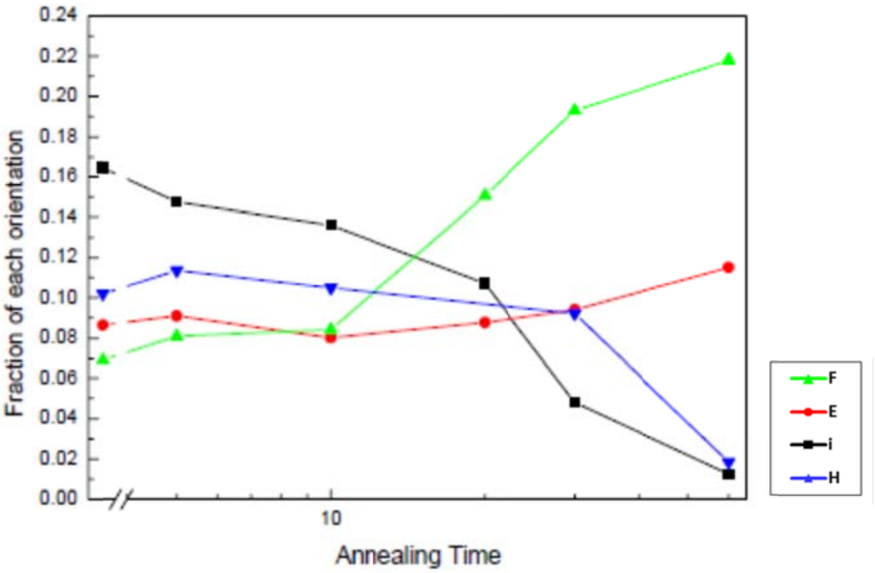

Figure 2.31: the variation of the volume fraction of BCC texture with annealing time [Kang 2007]

2-3-2-1-4 polycrystal models of plastic deformation

There are several reasons why it is important to simulate the development of texture and mechanical properties during deformation. For an engineering application an important consideration is the cost of experiments compared to simulations to obtain information on properties after particular processes. Also, if simulations with a physical theory can satisfactorily explain experimental results, it is likely that the underlying processes are understood and can be generalized. Through the plastic deformation of materials in addition to a plastic deformation of each grain, they tend to rotate in order to gain appropriate orientations. Since a grain in a polycrystal bulk is in the contact with its neighbours, it is not free to deform plastically as if it was a single crystal. So, in order to keep the contact of grains, they should accommodate the shape changes of their neighbours through deformation. A lot of effort has been devoted to different approximate theories in order to explain the plastic deformation of polycrystals with this condition. In the following section, a review of crystal plasticity models is given. These models are generally classified into lower bound (Sachs), upper bound (Taylor) and self-consistent models. Advantages and disadvantages of these models in texture predictions are also discussed.

Sachs-Type Model: The Sachs model [Sachs 1928] is the first ever crystal plasticity model. According to this model, it is assumed that the resolved shear stress on the principal slip system is the same for all crystallographic grains, and is identical to the critical resolved shear stress. This hypothesis implies that the stress tensor in each grain is proportional to the macroscopic stress tensor. It is also assumed that each grain deforms by single slip system (s) with the highest resolved shear stress and there is no kinematical constraint due to grain interactions. Under these assumptions, grains having distinct crystallographic orientations are deformed by different activated slip systems leading to unlikely overlaps and gaps at grain boundaries [Gmabin 1997]. Under these circumstances and according to Schmid’s law (Eq. 2.8), the behaviour of a polycrystal is given by:

$$\tau_c = < m > . \sigma \qquad (2.12)$$

Here < m > is the average value of the Schmid factors and τ_c is the critical resolved shear stress which is considered the same for all the grains.

There are at least two objections to Sachs’ approach. Firstly, it is not possible to maintain compatibility among the grains when all the grains are assumed to deform by single slip. Secondly, it is assumed that the equilibrium of stresses is valid inside grains; however, it cannot be established across grain boundaries. To overcome the compatibility problem, Taylor (Taylor 1938) proposed a model that strictly enforces the compatibility by imposing an overall applied strain which will be identical for all grains in the microstructure.

Taylor model: The full-constraints Taylor (FC-Taylor) model, proposed by Taylor [Taylor 1938], is one of the most applicable models of crystal plasticity. In this model, it is assumed that the microscopic plastic strain is equal to the macroscopic plastic strain, while elastic strains are neglected. One of the advantages of this model is that the compatibility equations are satisfied since it deals with a uniform strain field in the entire microstructure; as a result, all grains plastically deform in the same way in accordance with the macroscopic strain. In spite of the satisfactory nature of the compatibility equations and homogeneity of plastic strain throughout the polycrystal in the Taylor model, the stress equilibrium at grain boundaries is neglected.

In the FC-Taylor model, it is assumed that there must be at least five activated slip systems in each grain at the same time. Minimizing the dissipated deformation energy, W, is responsible for selecting the set of appropriate slip systems in each grain. On the other hand, the critical resolved shear stress is independent of the slip system. Regarding the equivalence of internal and external plastic work [Kocks 1970], the dissipated deformation energy is derived as:

$$(W)_{min} = \left(\sum_{s=1}^{s=5} \tau_c^s |\gamma^s|\right)_{min} = \tau_c \left(\sum_{s=1}^{s=5} |\gamma^s|\right)_{min}$$

Here, τ_c^s and γ^s are the critical resolved shear stress and shear stress in a particular slip system, respectively. By equivalence between the internal and external plastic work leads to:

$$\sum_{i,j=1}^{i,j=3} \sigma_{i,j}\, \varepsilon_{i,j} = \sigma.\varepsilon = \tau_c \left(\sum_{s=1}^{s=5} |\gamma^s|\right)_{min}$$

where, σ and ε present the equivalent Von-Mises stress and strain respectively. The Taylor factor for an individual crystal, M, is defined as:

$$M = \frac{\sigma}{\tau_c} = \frac{(\sum_{s=1}^{s=5} |\gamma^s|)_{min}}{\varepsilon}$$

As can be expected the Taylor factor in each crystal depends on its orientation in respect to the applied stress tensor. The average Taylor factor, $\bar{M}$, for a polycrystal is obtained by its volume average weighted by the ODF function:

$$\bar{M} = \int M_g . F_g dg \tag{2.13}$$

thus the macroscopic behaviour of polycrystals is described by:

$$\sigma = \bar{M} . \tau_c \tag{2.14}$$

As was mentioned before, in the literature, the Sachs model is used as a lower bound, and the FC-Taylor model as an upper bound. Both models have some deficiencies and benefits. They can be improved by using intermediate conditions, by relaxing the strict constraints imposed by each model. The Taylor model was modified with assuming that when grains reorient and change their shapes, it is possible to partially relax the strict compatibility requirements imposed in the Taylor model. The modified Taylor model is known as relaxed-constraints (RC-type). Non-uniform deformations that may appear at grain boundaries are excluded in the method. Another RC-type model is the LAMEL model that has been developed by Van Houtte [Houtte 1999 & 2005]. According to this model, the average shape change of a set of two stacked grains is taken to be equivalent to the average shape change of the polycrystal, but in each of the two grains, relaxation is allowed to take place.

Self-Consistent Model: All theories based upon strain uniformity (Taylor-type models) fulfil compatibility conditions but not equilibrium at grain boundaries. In 1987, Molinari proposed a self-consistent approach for the large deformation of polycrystals [Molinari 1987]. In this approach, equilibrium and incompressibility equations are used to arrive at an integral equation for the local velocity gradient. This integral equation can then be solved via different approximate schemes. The principle of the self-consistent scheme is that the interactions between a particular grain and all others are simulated by those between the grain considered and a homogeneous equivalent medium (HEM). In the self-consistent model of Molinari, the equilibrium and the incompressibility conditions were solved using the traditional Green's function method. An important advantage of Molinari's Green's function approach is that it fits naturally with correlation functions. Since the plastic deformation occurs by dislocations sliding which is an inherently rate-dependent process, it is reasonable to extend crystal plasticity theory for time dependent plasticity. Therefore, the self-consistent model is incorporated with a rate-dependent viscoplastic relation such that the viscoplastic compliance tensor of the polycrystal is determined in each strain increment in a self-consistent manner. The viscoplastic self-consistent (VPSC) model is well suited to model large strain behaviour of polycrystals. It accounts for the plastic anisotropy of each grain, as well as that of the polycrystal. It neglects elasticity at large strains. Each grain is modelled as an ellipsoidal inclusion that is embedded into the HEM with the average properties of the whole polycrystal. In this model, with the help of the viscoplastic compliance tensor and by solution of the Eshelby inclusion problem, the stress and strain state of each individual crystal is determined.

Viscoplasticity is achieved by introducing a simple power-law micro-constitutive relation that expresses the shear rate ($\dot{\gamma}^s$) of each slip system (s) as a function of the corresponding resolved shear stress, τ^s:

$$\dot{\gamma}^s = \dot{\gamma}_0 (\frac{\tau^s}{\tau_0^s})^n \tag{2.15}$$

where $\dot{\gamma}_0$ and τ_0^s are the reference shear rate and critical resolved shear stress on the system, respectively, and n is the inverse strain rate sensitivity coefficient of the material. For self-consistency, the macroscopic stress and strain rate of the HEM can be set equal to the average of the stresses and strain rates of all the individual grains. Unlike the FC-Taylor model, the stress and strain rate of each grain can deviate from the corresponding macroscopic quantities, as well as deviate from each other.

One consequence is that each grain changes its form according to its local velocity gradient and deformation history. Another important consequence of the self-consistent formulation is that a grain no longer needs to have five independent slip systems to deform. This feature is especially important for non-cubic crystal structures (e.g. HCP materials), where the number of available slip systems could be less than five on the basal or prismatic slip planes. Most modifications, developments, and implementation of self-consistent models can be found in different works [Molinari 1987, Molinari 1997, Lebensohn 1994 and Lebensohn 1999].

2-3-2-2 dislocation microstructure

The generation and movement of dislocation loops, and the subsequent interaction and recovery of the dislocations are the fundamentals of the evolution of the deformation structure [e.g. Dieter 1988 and Humphreys 1996]. Since in high stacking fault energy materials making the partial dislocations into a dislocation is easy, therefore cross slip and consequently also dynamic recovery are promoted.

The mobile dislocations which are produced through plastic deformation will interact both with each other and also obstacles like solute atoms and particles. Accumulating the dislocations into the materials leads to an increase in the total stored energy. But the system tries to reduce this stored energy by either the dislocation rearrangement which leads to low-energy configurations or through dynamic recovery processes where dislocations annihilate each other [Humphreys 1996].

Regarding rearrangement of dislocation through plastic deformation, there are significant studies describing deformation microstructures in different materials [Bay 1992 and Hughes 2000]. It is presumed that inside a grain the combination and number of simultaneously active slip systems vary from point to point. The number of active slip systems at each location is generally lower than the five predicted by the Taylor model (see the section about Taylor model in § 2-3-2-1-4) which is favourable. So, the grain starts to subdivide into volume elements. Within one element the slip pattern is different from the adjacent one, but collectively they satisfy the Taylor requirement for strain accommodation.

These volume elements are denoted cell block (CB) which consists of a number of neighbouring dislocation cells (DCs) surrounded by long flat dislocation boundaries. These boundaries arise out of geometrical requirement, since the slip systems are different on either side of them. Hence, they are named geometrically necessary boundaries (GNBs). Usually the misorientations of GNBs are too high, so they are famed as high angle boundaries (HAB). Different types of GNBs are described, e.g. dense dislocation walls (DDWs), observed at small strains, and laminar boundaries (LBs), separating flat elongated CBs at large strains. Within the CBs there are cells separated by cell boundaries. These boundaries are formed through mutual trapping of mobile dislocations, and so they are termed incidental dislocation boundaries (IDBs) (Fig. 2.32). Since IDBs possess less misorientation, they are recognized as low angle boundaries (LAB).

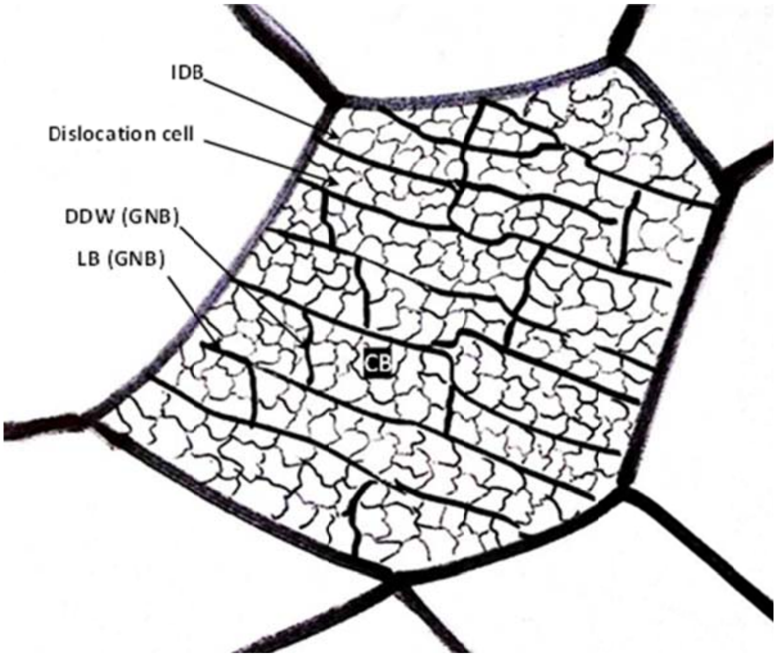

Figure 2.32: schematic representation of grain subdivision through plastic deformation

The spacing of both GNBs and IDBs decrease with increasing deformation. Obviously the GNB spacing is larger than the IDB spacing, but the difference diminishes at large strains as the cell blocks finally contain only one cell across their width. Also in terms of misorientation, the GNB misorientation is higher and increases more rapidly with strain as compared to the IDBs. While the IDB misorientation increases slowly to about 3° at large strains, the GNB misorientation increases up to 15-20°. Eventually, the GNBs turn into high-angle boundaries (>15°), and no saturation in the misorientation is observed for these boundaries.

In addition to the amount of plastic strain, the dislocation microstructure changes with parameters such as the plastic strain mode through the distribution of slip on the active slip systems, the material and also the deformation conditions. It was reported that in the uniaxial tensile test, dislocations aligned with the plane of active slip system in most grains [Fernandes 1938] and the grains tend to be elongated in the load direction. A similar morphology is formed through the rolling process of aluminium and steel. It is worthy to note that IDBs and GNBs are clearly studied in the samples deformed by uniaxial tension or rolling. However, in the SPD methods where shear deformation are imposed through the process the distinction between IDBs and GNBs are lost and the distinction can be simply made between HAB and LAB [Bowen 2004]. Also it was reported that substructure of the specimen deformed by asymmetric rolling as a SPD process appears in an equiaxed organization which is attributed to the imposed shear strain [Kim 2002]. The stacking fault energy of the materials can also control the microstructure, i.e. a higher number of activated slip systems leads to forming more equiaxed cells whereas fewer activated slip systems results in an elongated substructure during the process [Gracio 1989].

2-4 formability of materials

An important concern in forming processes is whether the desired process can proceed without failure of the sample. Therefore, parameter of formability of materials is defined as their ability to undergo plastic deformation through a forming process without failure. The formability of materials is a complicated topic which is strongly influenced by not only a material's properties such as microstructure and texture but also process conditions such as strain path, strain rate and temperature. Regarding the scope of this work, the effect of some of the parameters on the materials formability will be presented in the following section.

2-4-1 effect of texture

Anisotropy of mechanical properties of metallic sheets is a macroscopic behaviour which is introduced by the R-value (Lankford coefficient). The R-value is defined as the ratio of plastic strain in the width direction to that in the thickness direction of the sheet under tensile loading (Eq. 2.16). A high R-value suggests that there is a high resistance to thinning resulting in higher formability of the material.

$$R = \frac{\varepsilon_w}{\varepsilon_t} \tag{2.16}$$

Here, ε_w and ε_t are true plastic strain in the width and thickness of the tensile test sample, respectively (Fig. 2.33). Since the R-value varies with the direction of the tensile load with respect to the rolling direction (RD), macroscopic indicators defined as the normal anisotropy ($\overline{R}$) and the planar anisotropy (ΔR) are usually used and defined as [Hosford 1993] :

$$\overline{R} = \frac{R_0+2R_{45}+R_{90}}{4} \tag{2.17}$$

$$\Delta R = \frac{R_0-2R_{45}+R_{90}}{2} \tag{2.18}$$

where R_0, R_{45} and R_{90} are the R-value in 0, 45 and 90° from the RD respectively.

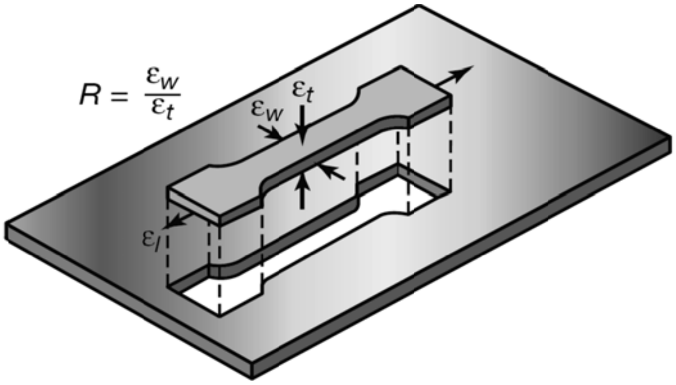

Figure 2.33: tensile test sample of a metallic sheet in the rolling direction

The normal and planar anisotropy are of great importance for a deep drawing process. Higher normal anisotropy leads to increasing deformation before failure, i.e. obtaining greater drawing depth hence higher formability. When a cylindrical cup is deep drawn from a metallic sheet, the rim of this cup will not be level but will appear as a number of distinct peaks and an equal number of valleys, as shown in Fig. 2.34. This phenomenon is known as the earing problem. This problem is very undesirable, as it causes inhomogeneous wall thickness reduction and may interfere with automated deep-drawing operations. This problem is related to the planar anisotropy of the sheet. For materials with ΔR>0 the ears appear in the RD and TD whereas for the materials with ΔR<0 the ears occur in the 45° from the RD. And it is obvious that no earing happens when the planar anisotropy equals 0.

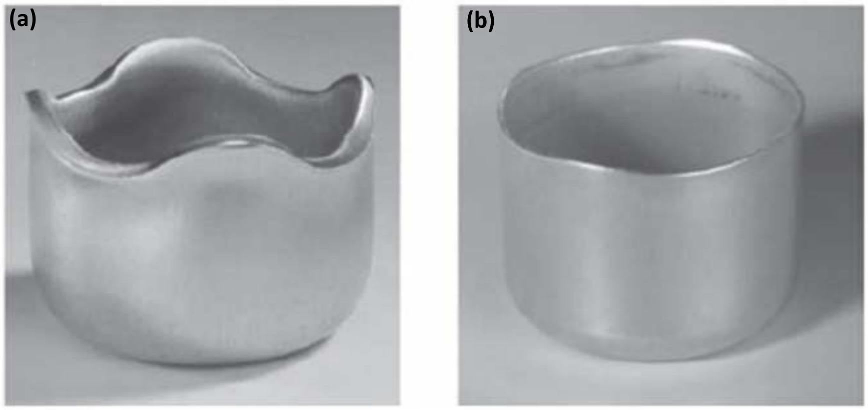

Figure 2.34: deep drawn cups, a) with earing, and b) without earing

The R-value and consequently the earing problem in deep drawing are closely related to crystallographic orientation [Inoue 2007]. For polycrystalline materials, it is possible to increase the normal anisotropy and/or the R-value at specific directions in a sheet plane by controlling crystallographic texture.

Recently, several studies have been conducted to investigate the mechanical responses of each individual component in various directions with respect to the load direction [Lequeu 1988 and Choi 2000]. It was shown that in FCC materials, cube and Goss components possess a low value of normal anisotropy compared to those of the copper and brass components. Similarity, the E and F components present even higher normal anisotropy in metallic sheets. These two components belong to the {111}//ND fibre. For instance, since the major texture in annealed low carbon steel is {111}//ND, this material has a higher normal and lower planar anisotropies. However, improvement of the formability in cold-rolling and annealing of aluminium alloys is challenging since the cube {001} <100> and Goss {011} <100> texture components are the major textures [Liu 2002 and Liu 2006]. The {111}//ND fibre in aluminium alloys can be formed under shear strain throughout the sample [Jazaeri 2004, Jin 2004 and Jin 2007].

2-4-2 effect of microstructure

It is well known that beside crystallographic texture, microstructure also influences mechanical responses, i.e. the grain size, grain shape and dislocation substructure determine the macroscopic behaviour of the material. The presence of grain boundaries has an effect on the deformation behaviour of the material by serving as an effective barrier to the movement of glide dislocations. According to the work of Hall and Petch [Hall 1951 and Petch 1953], the yield strength of a polycrystal material (σ_y), could be given by:

$$\sigma_y = \sigma_i + k_y d^{-1/2} \qquad (2.19)$$

where k_y and d are friction stress, constant parameter related to the material and grain size respectively; here, also the overall resistance of lattice to dislocation movement is presented by σ_i. So, concerning the Hall-Petch relation, higher yield strength can be gained by decreasing the size of grains. However, for very fine -grain materials, yield strength is predicted up to the theoretical shear stress, using the Hall-Petch equation. Therefore, a more general model which deals with the relationship of dislocation density and yield strength is derived as:

$$\sigma_y = \sigma_i + \alpha G b \sqrt{\rho} \qquad (2.20)$$

where σ_y and σ_i have the same meaning as in equation 2.19 and ρ is the dislocation density. It is noted that dislocation was generated at the grain boundaries and experimentally shown that the dislocation density ρ was inversely proportional to the grain size; i.e. equation 2.19 has the same concept as equation 2.20. The produced dislocation rearrange to a more stable state and form LAB and HAB boundaries as discussed before. The low angle boundaries (e.g. IDBs) cause hardening through dislocation effects while the high angle boundaries (e.g. GNBs) cause hardening through size effect; i.e. they act as barriers against further dislocation movements [Kang 2007].

With the goal of improving mechanical behaviours in the engineering application, continuous efforts have been devoted to developing techniques for grain refinement. The SPD methods noted in the previous section have become one of the most promising methods to reach this goal. The mechanical response of the materials is modified through grain refining to a sub-micrometre range using SPD methods.

2-4-3 effect of strain path

There is a number of different complex forming processes to produce an engineering piece. Depending on the final shape, it may involve change of deformation mode. The more complicated the final shape is, the greater the variety of strain paths required. Change in the plastic deformation path through processes influences the formability of the materials.

A number of researches have been carried out to observe the strain path change influences on the stress-strain curves in materials [Wagoner 1983]. In order to study the mechanical properties of materials after change of strain path, it is important to know the behaviour of glide dislocations under these conditions. The effect of pre-strain on dislocation substructure in different engineering materials has been studied. In these materials, the dislocation structure induced by the pre-strain becomes unstable. While the microstructure is going to be disrupted and dissolved, a new dislocation structure typical of the new strain path forms. In addition, a change in strain path leads to activate different slip systems upon the direction of loading which results in the appearance of various textures.

For characterizing the effect of pre-strain on mechanical properties, Schmitt proposed a scalar parameter that provides an estimate of amplitude of the strain path change. This parameter is a unique and non-ambiguous definition for any sequence of two linear strain paths [Schmitt 1994].

$$\alpha = \frac{\varepsilon_{pre} : \varepsilon_p}{|\varepsilon_{pre}| \cdot |\varepsilon_p|} \tag{2.21}$$

where ε_{pre} is the tensor corresponding to the first plastic strain and ε_p the tensor representing the plastic part of the subsequent deformation. The parameter α is cosine of the angle between two vectors which represent first and second strain path. Hence, it can be varied between -1 up to 1 for different strain path changes [e.g. Gracio 2000, Nesterova 2001 and Barlat 2003]. Usually Schmitt factor influence on mechanical properties in the subsequent strain path during a complex plastic deformation. This effect can be characterized in two different categories: (a) lower initial follow stress with increased strain hardening; and (b) an increased initial follow stress accompanied by a lower strain hardening [Wagoner 1983].

As already mentioned change in strain path during plastic deformation leads to change in the mechanical properties of the specimens. In terms of formability, a strain path change has a strong influence on forming limit diagrams (FLD) both for necking and fracture. The FLD does not present a simple fracture criterion, but a function relating ε_1 to ε_2.

Since the strain paths for simple tensile tests are straight lines having the slope -(1+R)/R in the ε_1, ε_2 plane, the load paths will shift to the left by increasing R. A higher value of R also allows for higher values of the final strain ε_1. As long as the initial deformation implies $\varepsilon_2<0$ followed by biaxial expansion, the limit curve II is higher than the FLD I which is a simple, linear load path (Fig. 2.35).

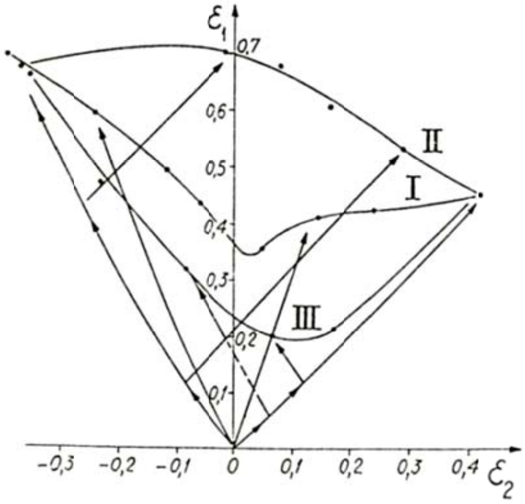

Figure 2.35: influence of strain path on the forming limit diagram

In contrast, if $\varepsilon_2 > 0$ during the first step of loading and subsequently, simple tensile load follows the limit curve III is below the FLD I for linear path. This is the reason that industry engineers always proceed first with a tensile or a compressive deformation, and then eventually apply expansion to have more value of formability in the sheet samples. For these two cases the value of α parameter is the same; however different effects on the FLD curves appear. This case indicates that α parameter alone is not enough to study the effect of pre-strain on the mechanical behaviours of materials.

Generally, it is believed that the stress levels after strain path changes stem from the developments on the micro scales. The dislocation glides in the crystal lattice depends on the deformation and the direction of the applied deformation. Different classes of substructures are recognized, depending on the deformation direction. Research in this field is running to deduce the mechanisms that cause the strain path dependent behaviour on the macro scale.

2-5 microstructure and texture of ASR samples

There are a large number of works which have been carried out to observe the influence of ASR on microstructure and crystallographic texture. Researchers have reported that the microstructure of metallic sheets becomes equiaxed through ASR. Figure 2.36 illustrates TEM images of aluminium sheet deformed with the ASR process after annealing at 150°C for one hour [Jiang 2009]. Similar results were obtained by other researchers [e.g. Kim 2002].

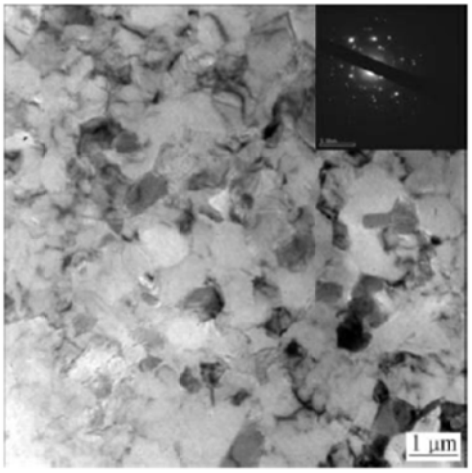

Figure 2.36: TEM image and diffraction pattern of 90% ASR aluminiumafter annealing at 150°C for one hour [Jiang 2009]

Additionally the electron back scattering diffraction (EBSD) observation was carried out to investigate the fine grains obtained through ASR; e.g. figure 2.37 presents an observation of ASR deformed low carbon steel [Ding 2009]. In Fig. 2.37a the equiaxed fine grains are considerably coarser after annealing at higher temperatures (Fig. 2.37b-d).

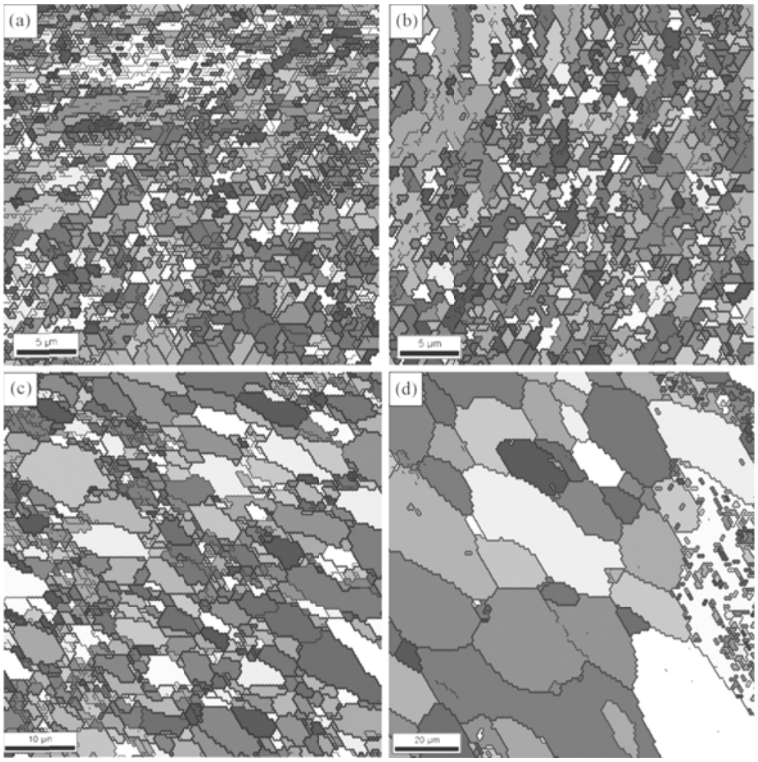

Figure 2.37: grain maps from EBSD of low carbon steel: a) ASR deformed and heat treated at b) 400, c) 500 and d) 600 °C [Ding 2009]

TEM images of a low carbon steel sheet asymmetrically rolled are illustrated in Fig. 2.38. The dislocation walls divide the grains into the dislocation cells. The TEM microstructure of the ASR steel sheet is in a good qualitatively agreement with the EBSD results shown in Fig. 2.38.

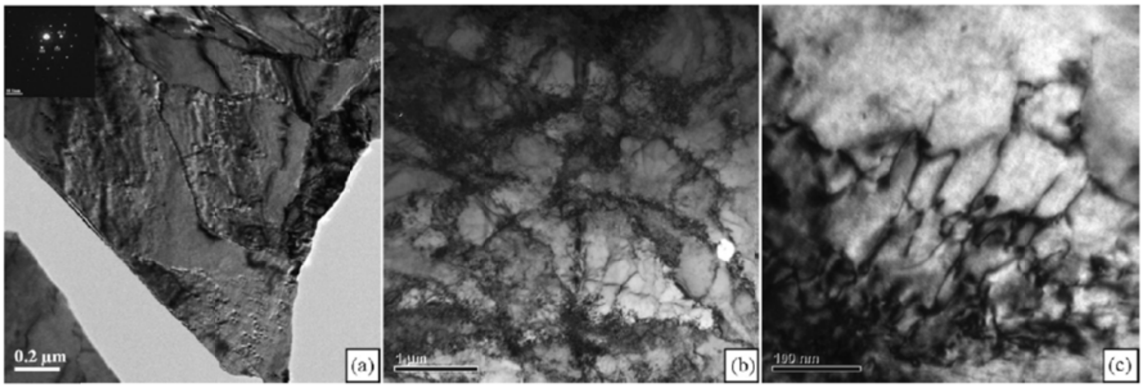

Figure 2.38: TEM images of a ASR steel sheet [Ding 2009]

In addition, Wautheir et al. showed the microstructure of steel sheets deformed by ASR using EBSD cartographies (Fig. 2.39). Some of the grains contain many of dark lines which are known to correspond to local misorientations. This microstructure feature is called fragmentation and is the result of formation of dislocation cells in the deformed material. Fragmentation in the grains increases with higher asymmetry levels [Wautheir 2009].

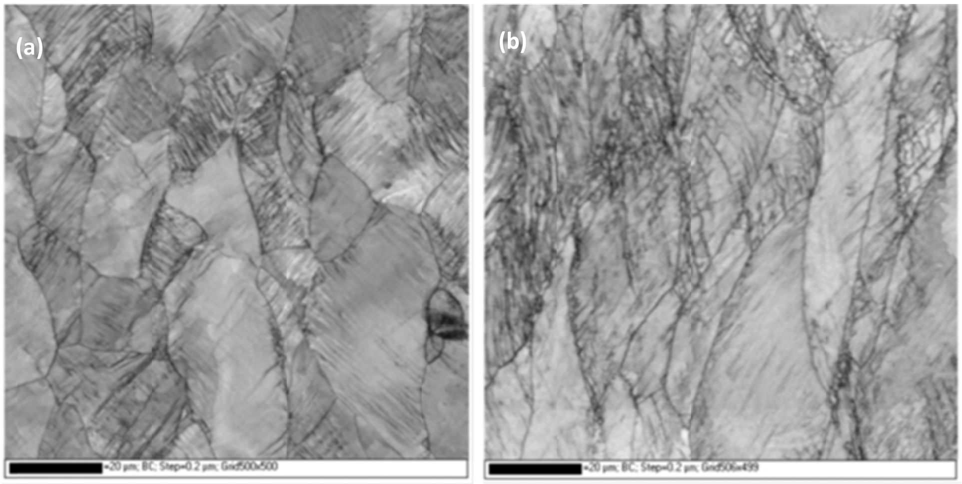

Figure 2.39: EBSD cartographies showing microstructures of TD planes after: a) 32.2% reduction for 1.1 roll speed ratio and b) 36.8% reduction for 1.45 roll speed ratio [Wautheir 2009]

As mentioned in previous sections, shear strain is distributed in thickness of sheet samples in the ASR process. The shear texture is pronounced during the ASR process thanks to the distributed shear strain in the specimen [e.g. Kim 2001b and Jin 2007 and Toth 2012]. The shear texture development in ASR is a significant aspect of the process which distinguishes it from the conventional rolling. Fig. 2.40 presents {111} pole figures of the center region of AA-1050 sheet deformed in ASR with 93% total reduction.

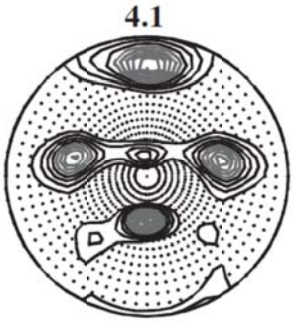

Figure 2.40: {111} pole figure of aluminium after 93% total reduction with ASR [Lee 2002c]

Additionally φ_2=45° ODF section of ASR deformed AA-6xxx is shown in Fig. 2.41 [Sidor 2008]. Figures 2.40 & 2.41 indicate that shear texture components (e.g. E, F and H) in FCC structure appear in the aluminum sheets when asymmetrically rolled.

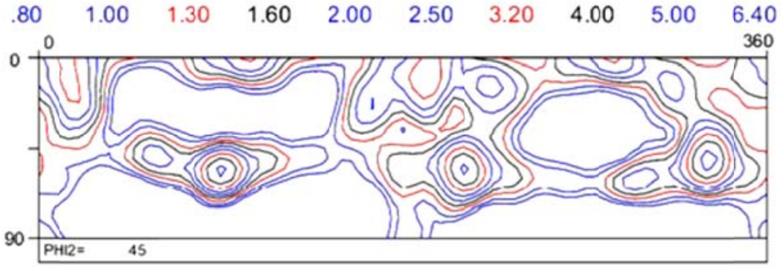

Figure 2.41: φ_2=45° ODF section of asymmetrically rolled aluminum alloy sheet [Sidor 2008]

Furthermore, Toth et al. reported the developed texture of interstitial free steel sheet asymmetrically rolled as shown in Fig. 2.42 [Toth 2012]. As can be seen, a weak but ND-type fiber existed before ASR. After C-ASR, the ND fiber appears shifted down towards larger ϕ values.

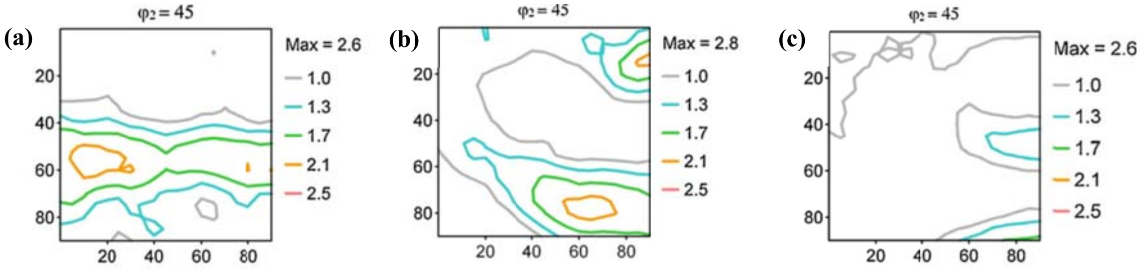

Figure 2.42: φ_2=45° ODF section of IF steel: a) initial, b) C-ASR and c) R-ASR processes [Toth 2012]

As presented in section 2-4-2-1-3, the ideal rolling texture of BCC materials is characterized by α and γ fibres with a strong F component. Sha et al. has shown that a strong F component is formed under the ASR process in two different ways: ASR in all passes and ASR only in the last pass (Fig. 2.43). Since α and γ fibres are rolled texture, the F component of γ fibre also belongs to shear deformation texture, thus the rolling texture can be related to shear deformation texture [Sha 2008].

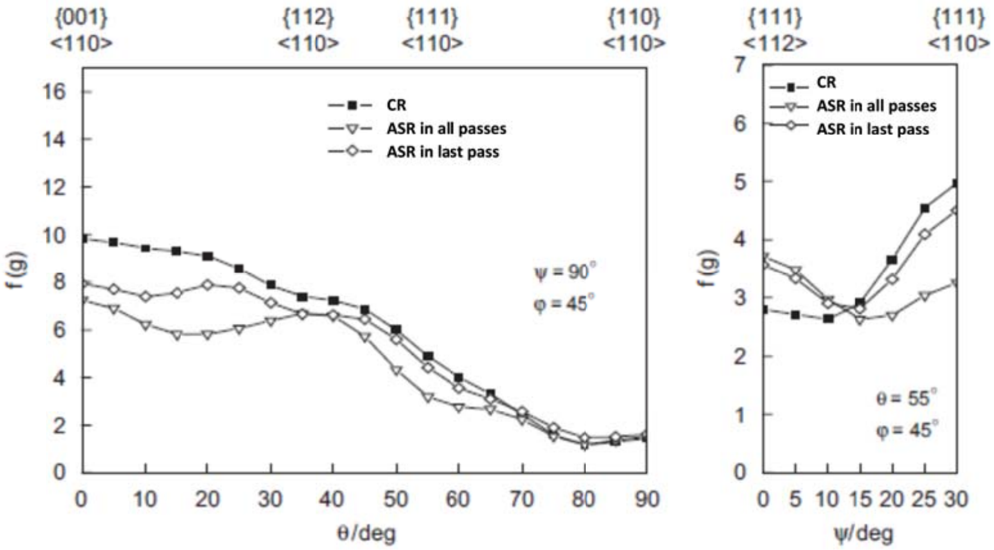

Figure 2.43: orientation density along α and γ fibres in deformed non-orientated silicon steel material with CR, ASR processes [Sha 2008]

Chapter 3

Preliminary tests and experimental procedure

In this chapter the materials and experimental methodologies are introduced. Also preliminary results required for further studies are presented in addition to designed experiments. The strategy for selection of the materials subjected to investigation in this work takes into consideration the influence of the ASR process on two of the most used engineering materials. Among engineering materials, aluminium alloys and steels have been extensively used in industries due to their properties and abundance. In this study an aluminium-magnesium alloy and also interstitial free (IF) steel were chosen to explore the effect of shear strain imposed by the ASR process on their mechanical properties. In following section, the initial properties of each case are given.

3-1 AA-5182

In the recent years, aluminium alloys have been considered to be one of the most often used materials in several industrial applications as they possess a good combination of high ratio of strength to weight and good corrosion resistance. Appropriate properties of aluminium alloys cause them to be used in a wide range of applications; e.g. packaging, marine, aeronautic and automotive industries (Fig. 3.1). Improving the mechanical properties of these materials may lead to reducing the weight of the structure which translates into less fuel consumption and associated environmental advantages. Among aluminium alloys (5xxx series alloy), a non-heat treatable aluminium-magnesium alloy was selected for this work. The presence of magnesium as the main alloying element in the 5xxx series leads to solute hardening of the alloy, and efficient strain hardening, resulting in good strength. This strength, combined with the appropriate formability and also other excellent properties (e.g. corrosion resistance, high quality anodising ability and weldability) of the 5xxx series alloy results in many applications. However, there is a major problem which is the low deep drawability. It makes this alloy an interesting choice for this work since the ASR process has been introduced as a successful process to improve the deep drawability of sheet materials.

Figure 3.1: some examples of deep drawn pieces produced from aluminium alloy sheets

3-1-1 as received material and equipment

The material used in this study was 3mm thick, fully recrystallized AA-5182 sheet supplied by the ALCOA Company. Its chemical composition is listed in table 3.1.

Table 3.1: chemical composition of AA-5182

Mg	Si	Fe	Cu	Mn	Cr	Zn	Ti
4.5%	0.2%	0.35%	0.15%	0.2-0.5%	0.1%	0.25%	0.1%

The uniaxial tensile tests were carried out in order to measure the mechanical responses of the sheet sample. The tests were performed using a universal testing machine Shimadzu Autograph in which a non-contact video extensometer MFA-25 was used to measure the length and width changes of the tensile specimen through tension (Fig. 3.2a). The ASTM tensile test samples were cut from the original sheet in three directions of RD, TD and 45° from the RD. A tensile sample is shown in Fig. 3.2b.

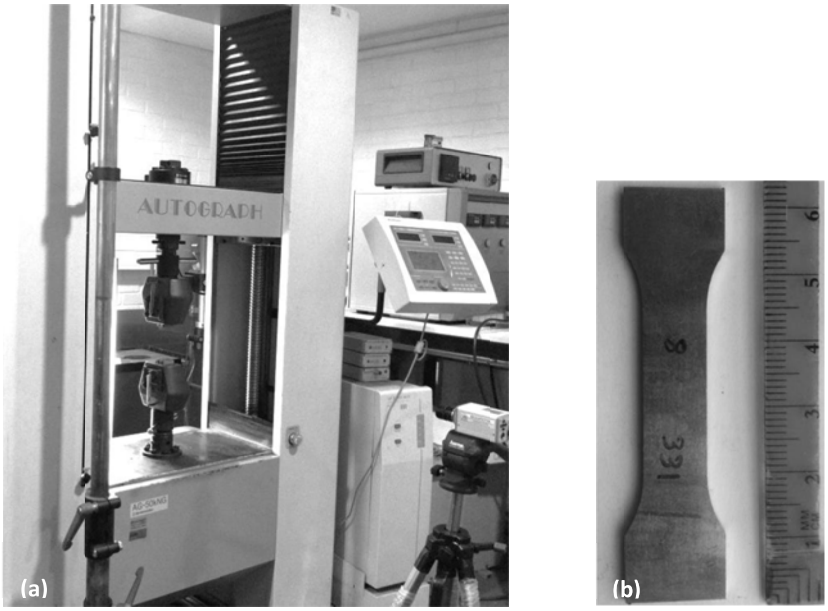

Figure 3.2: tensile test: a) tensile test machine _ University of Aveiro and b) a tensile test sample

The uniaxial tensile tests were carried out at room temperature and a constant engineering strain rate of $10^{-4}s^{-1}$. The mechanical responses are shown in Fig. 3.3.

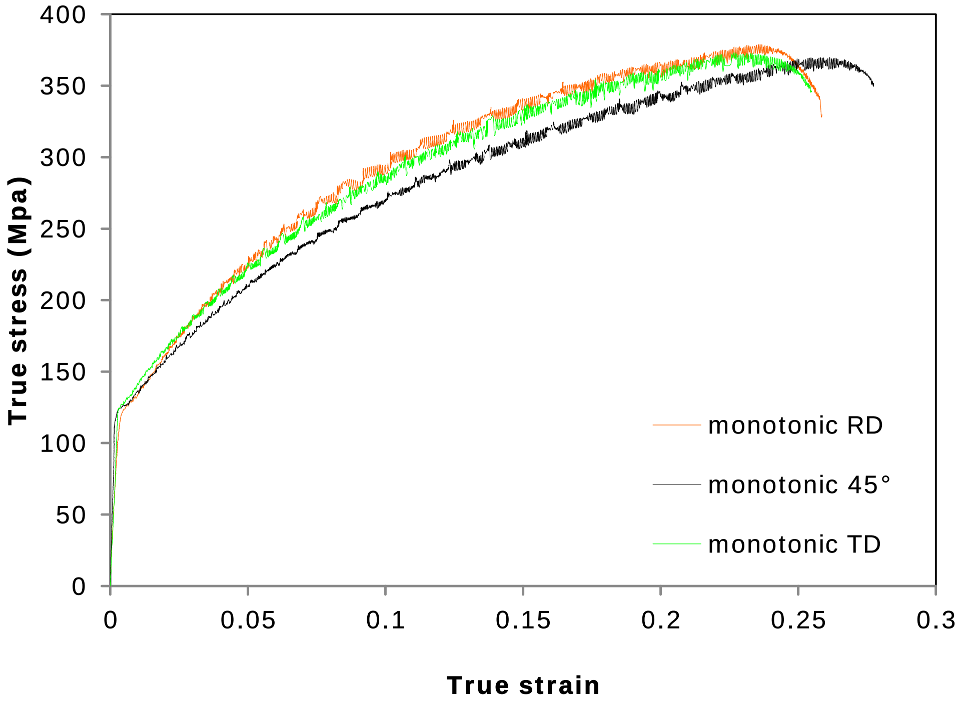

Figure 3.3: uniaxial tensile test results of the AA-5182 in RD, 45° from RD and TD directions

The high strength of this aluminium alloy obtained through tensile tests is due to the interaction of Mg atoms with mobile dislocations. Also the solute Mg atoms in this alloy cause the serration in the strain-stress curve to appear which is called Portevin-Le Chatelier (PLC) effect (Fig. 3.4). The number of mobile dislocations is increased by plastic deformation (here tension). When these dislocations are temporarily arrested at dislocation tangles, the segregated Mg atoms around the tangles diffuse by pipe diffusion to these arrested dislocations. They then form atmospheres around the dislocations which leads to their being locked. When the applied force is raised high enough, the dislocations break away from the atmosphere and move freely toward the next tangles. Repeating the pinning and unpinning process leads the serrations in the stress-strain curve to appear [Wen 2004].

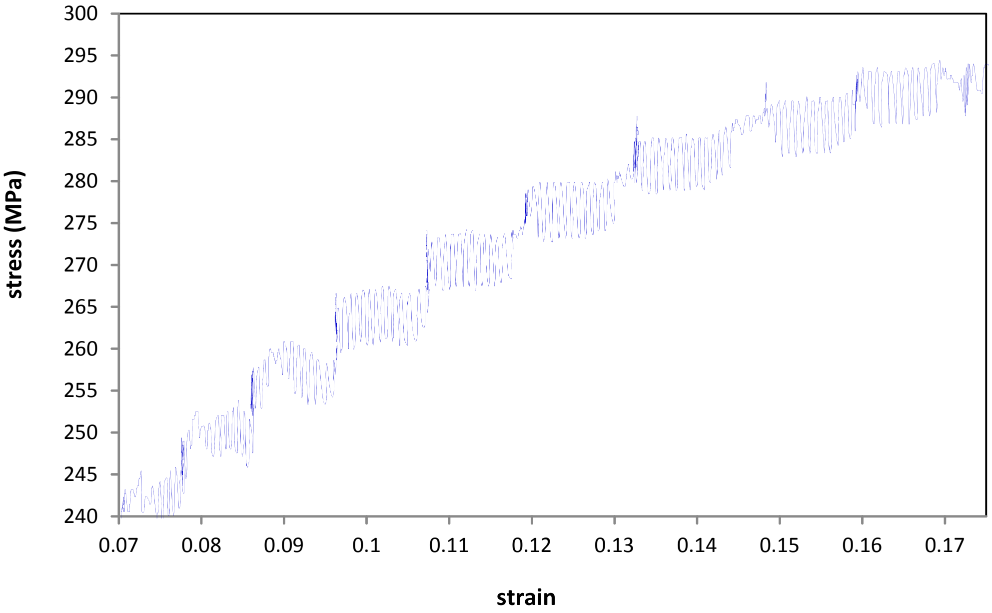

Figure 3.4: the serration appeared during uniaxial tension in AA-5182

Figure 3.5 presents the variance of R-value of initial sample by the angle from RD. This figure indicates that the R-value of as received sheet sample in the RD is 0.58, which decreases slightly to 45° from the RD and then rises up to 1.1 in the TD. Hence regarding eq. 2-17 & 2-18, the normal and planar anisotropy of this material are 0.59 and 0.48 respectively.

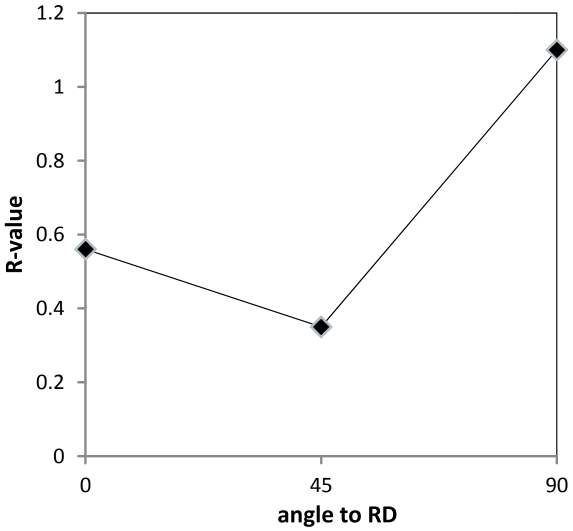

Figure 3.5: R-value in various directions from RD

Texture measurements were performed using a Philips X'pert diffractometer with an X-Ray texture goniometer in back reflection mode at the mid-thickness locations of the sheets (Fig. 3.6). The principal of texture measurement was mentioned in section 2-3.

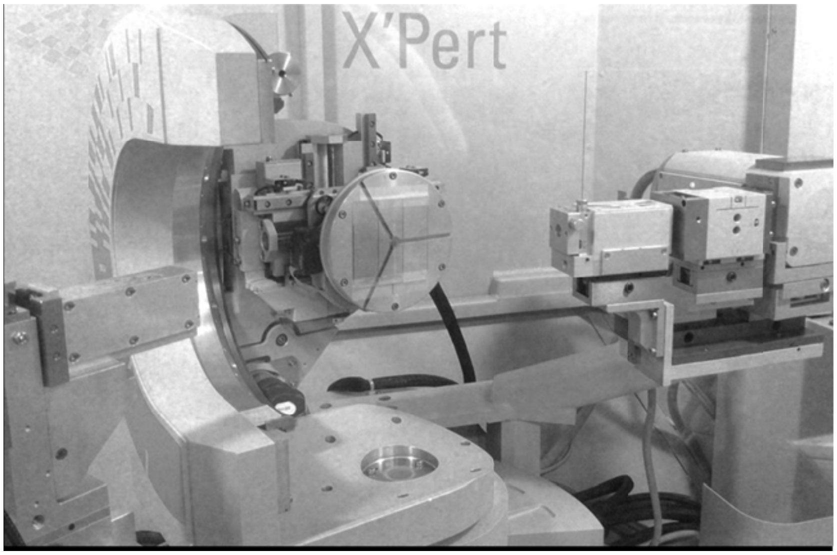

Figure 3.6: X-ray diffraction device and a texture goniometer _ University of Aveiro

The crystallographic texture of as received sample is illustrated in figure 3.7. The cube component which is pronounced in the pole figures confirms that as-received sheet sample is fully annealed.

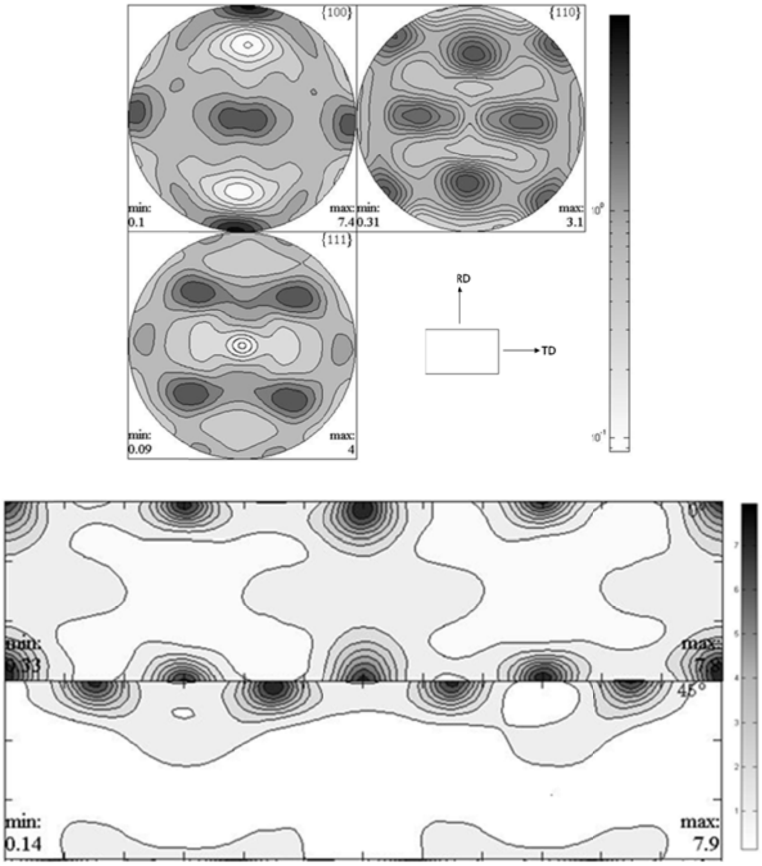

Figure 3.7: X-ray polefigures and ODF (φ_2=0 and 45°) of as received AA-5182 sample

3-1-2 experiments

Since the final products of the aluminium sheet factories are in rolled form, the experiments here were designed to develop crystallographic texture from the starting point of rolling texture to that of shear. Therefore, the sheet samples were first conventionally rolled and recovered and then ASR was applied to change the texture.

3-1-2-1 preliminary rolling process and annealing

As received samples were conventionally rolled by 60% reduction of thickness down to 1.2mm and subsequently heat treated for recovery at 300°C for 45 minutes. The designed rolling machine at the University of Aveiro contains two working-rolls of equal diameter of 180mm, each one rotate by an independent motor. The rotation speed and also the rotation direction of each working-roll are controlled by a computer using specific software (Fig. 3.8).

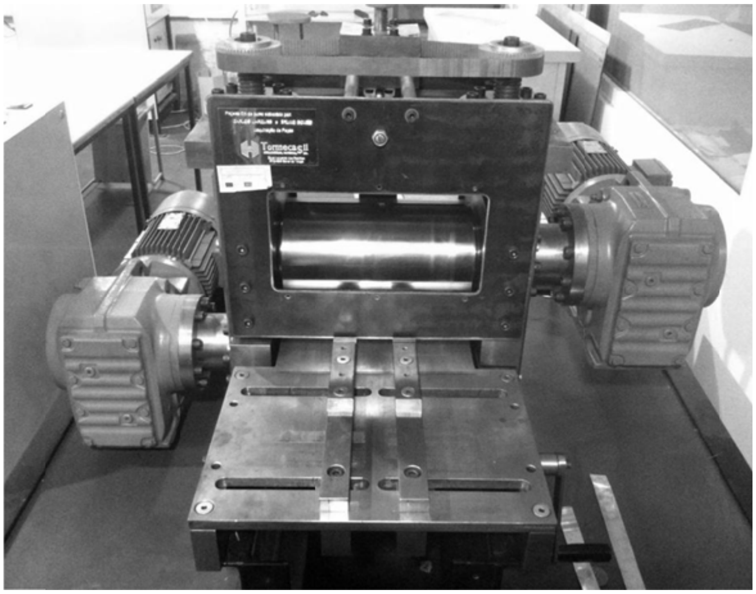

Figure 3.8: rolling machine _ University of Aveiro

The crystallographic texture of these specimens after rolling and annealing is presented in Figure 3.9. This figure shows that the texture of the as received recrystallized sheets changed from cube (Fig. 3.7) to rolling texture components by the imposed 60% rolling and heat treatment. In the following, these samples (Fig. 3.9) will be called the initial samples.

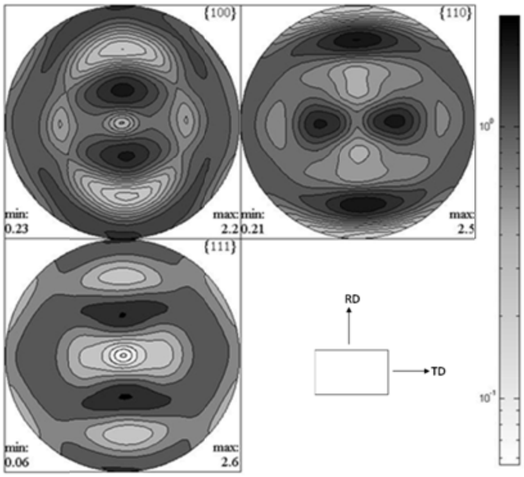

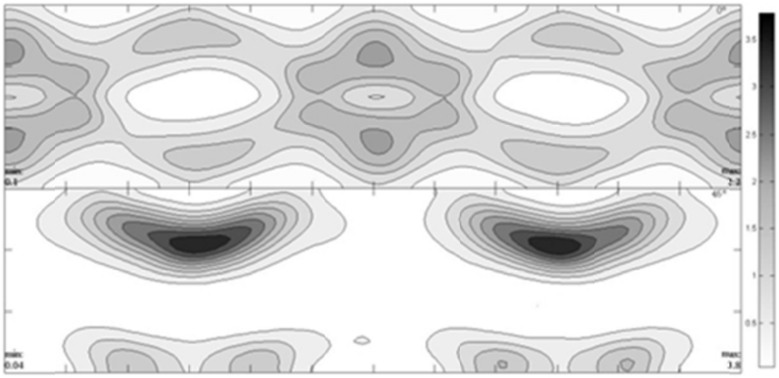

Figure 3.9: X-ray pole figures and ODF (φ_2=0 and 45°) of the rolled and annealed AA-5182

3-1-2-2 ASR rolling

The initial samples (Fig. 3.9) were subjected to two passes of asymmetric rolling as well as conventional rolling. These processes were carried out to reduce the thickness of the specimens from 1.2 to 0.6mm. The ASR process was designated into two different types: reversed asymmetric rolling (R-ASR) where the rolling direction was reversed after the first pass and continuous asymmetric rolling (C-ASR) where the rolling direction was not reversed. R-ASR and C-ASR processes were performed with a velocity ratio of 3 and also no lubrication was introduced to the rolls. The principal of the process and also its parameters were described in the last chapter. In order to measure the value of the shear strain in the thickness, perpendicular lines were scratched with a steel pen on the side face of the sheets.

3-1-2-3 thermal stability

With the purpose of studying the effect of texture evolution on mechanical response, an appropriate heat treatment temperature should be promoted on the rolled samples to annihilate the dislocations inside the grains but keeping the modified texture. Hence the rolled samples (CR, R-ASR and C-ASR) were kept in the furnace for 45 minutes within a temperature range of 200-320°C to evaluate the effect of annealing temperature on their stress-strain curves.

The yield strength and uniform elongation obtained by uniaxial tension in RD are briefly shown in Fig. 3.10. The specimens present approximately 20% uniform elongation and the same value of yield stress after annealing at 280°C for 45 minutes. As can be seen in the figure, C-ASR and R-ASR are more sensitive to temperature in heat treatment compared to the same sample rolled by CR. Regarding these results the heat treatment at 280°C for 45 minutes was chosen as an appropriate annealing condition for the rest of the experiments.

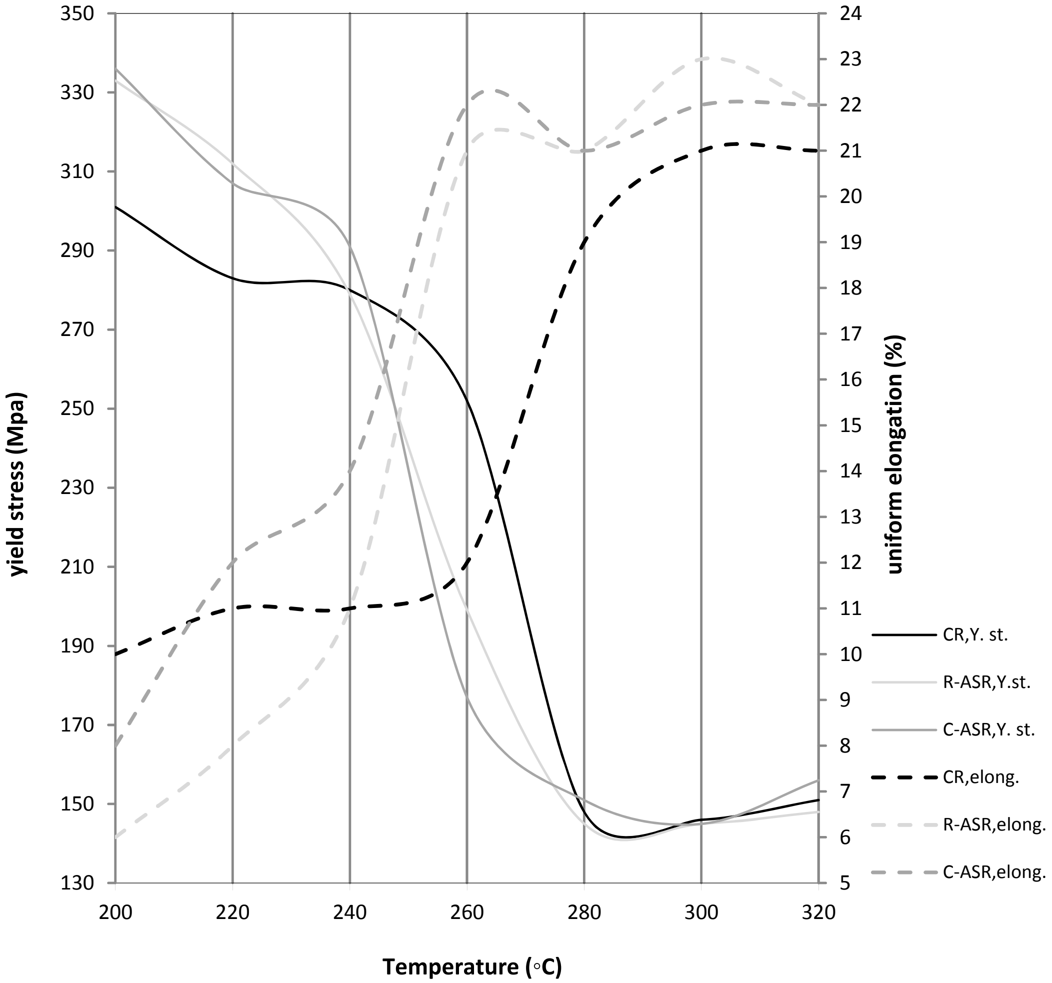

Figure 3.10: influence of annealing temperature (for 45 minutes) on the yield strength and uniform elongation obtained by uniaxial tensile tests in RD of CR, C-ASR and R-ASR deformed samples

3-1-2-4 tensile tests

Regarding the appropriate heat treatment condition obtained in the previous section, the specimens rolled by CR, C-ASR and R-ASR processes were annealed at 280°C for 45 minutes. Subsequently, tensile tests were performed at room temperature along 0°, 45° and 90° with respect to the RD. These tests were performed at a strain rate of $10^{-4}s^{-1}$. The change of the width and length of each samples were measured to obtain R-values.

3-1-3 modelling

For the modelling, we use the viscoplastic self-consistent (VPSC) model of Molinari et al. [Molinari 1987] which was further developed by Lebensohn and Tome [Lebensohn *1992*]. In this, plasticity occurs by crystallographic slip on {111} <110> slip systems. The initial critical resolved shear stress is assumed the same for all systems.

3-1-3-1 prediction of texture evolution through rolling

The X-ray data of the initial samples (Fig. 3.9) were used as input files for the VPSC model. The macroscopically imposed velocity gradient for the sheets under CR and ASR processes is approximated by plane strain compression for CR and combined plane strain compression and shear for ASR:

$$L_{CR} = \begin{bmatrix} \dot{e}_{11} & 0 & 0 \\ 0 & 0 & 0 \\ 0 & 0 & \dot{e}_{33} \end{bmatrix}, \; L_{ASR} = \begin{bmatrix} \dot{e}_{11} & 0 & \dot{e}_{13} \\ 0 & 0 & 0 \\ 0 & 0 & \dot{e}_{33} \end{bmatrix} \qquad (3.1)$$

Here $\dot{e}_{11}$, $\dot{e}_{33}$ and $\frac{1}{2}\dot{e}_{13}$ are strain rate components with indices 1, 2 and 3 representing the normal, transverse and rolling directions, respectively. The tensor L presents the macroscopic velocity gradient.

3-1-3-2 prediction of mechanical behaviours

For the mechanical behaviour of the rolled samples under tensile tests, the VPSC model was used to simulate the tensile stress-strain curves of different samples. Furthermore, in order to predict the macroscopic anisotropy (R-value) of the polycrystalline aggregates, both the VPSC polycrystalline model and the Taylor model were used and the predicted results were compared to the experimental ones.

In the above mentioned plasticity models, we used Voce law for strain hardening which is characterized by an evolution of the threshold resolved shear stress, τ, with accumulated shear strain, Γ, in each grain of the form [Tome 1984]:

$$\tau = \tau_0 + (\tau_1 + \theta_1 \Gamma)\left(1 - exp\left(-\Gamma \left|\frac{\theta_0}{\tau_1}\right|\right)\right) \tag{3.2}$$

Here, τ_0, θ_0, θ_1 and $(\tau_0+\tau_1)$ are the initial critical resolved shear stress (CRSS), the initial strain hardening rate, the second strain hardening rate and back extrapolated CRSS, respectively. To determine these parameters, we used tensile stress-strain response of a conventional rolled sample as a reference (Fig. 3.11). The following parameter values are therefore determined by fitting:

τ_0= 55, θ_0= 455, θ_1= 22 and τ_1= 72 MPa

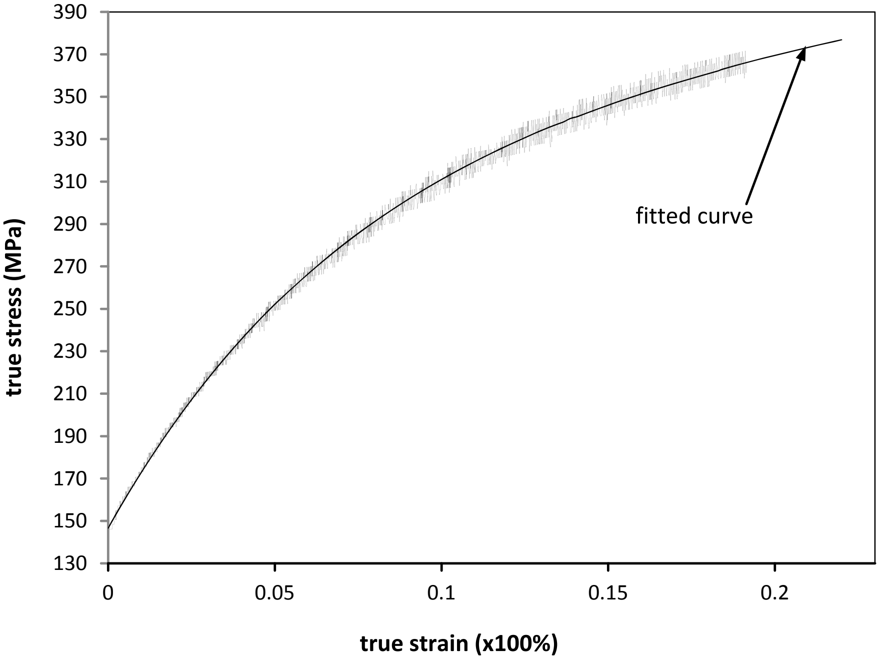

Figure 3.11: stress-strain curve of CR and annealed sample and also the fitted curve using Voce law parameters

3-2 IF steel

Steel is an alloy of iron and up to 2% carbon and other elements. Carbon is small enough to locate into the interstices of a primarily iron crystal, making it an "interstitial element" in steel. If the amount of carbon in the steel is reduced to less than 0.005%, most of these interstitial spaces will not be occupied and, as such, can be called interstitial-free (IF) steel. Achieving this low carbon level does not occur when using conventional steel processing. Instead, the molten steel must be put under a vacuum that decarburizes it by removing carbon monoxide, as well as other gases like hydrogen and nitrogen which are capable of locating in interstitial places. Moreover the residual carbon and nitrogen are combined with niobium, titanium, vanadium or some similar element with a strong affinity for carbon and nitrogen. Over the past few decades IF steel has become increasingly popular in the automotive industry where large deformations and excellent surface finishing are required such as fenders or door lining, find no alternative to the IF steel grade (Fig. 3.12).

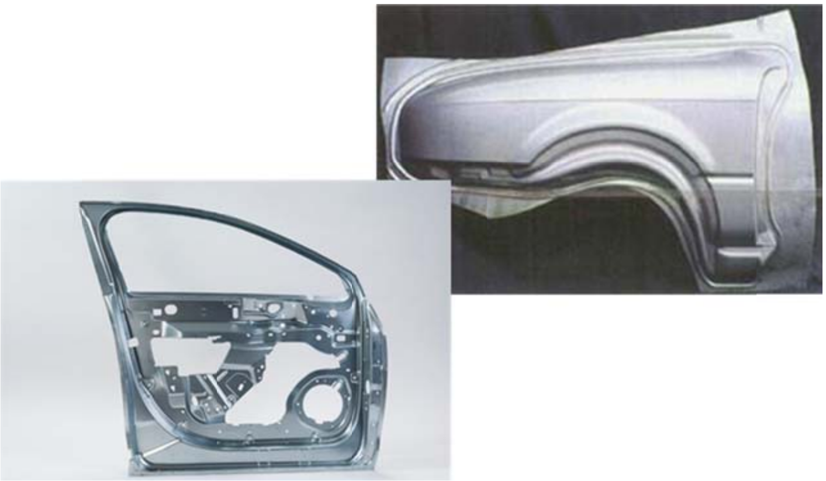

Figure 3.12: some examples of IF steel applications in automotive industries

3-2-1 as received material

The material used in the present investigation was 1.18mm thick interstitial free steel sheet supplied from ArcelorMittal Company. Its chemical composition is given in table 3.2.

Table 3.2: chemical composition of as received IF steel

C	Ti	V	Ni	Mn	Co	Mo
0.004%	0.040%	0.001%	0.017%	0.061%	0.002%	0.002%

Mechanical properties of as received sheet samples were measured using the uniaxial tensile tests. The tensile test samples were prepared from the original sheet in three directions of RD, TD and 45° from the RD. The tests were performed at room temperature and a constant engineering strain rate of $10^{-4}s^{-1}$. The stress-strain curves of different directions from RD are shown in Fig. 3.13.

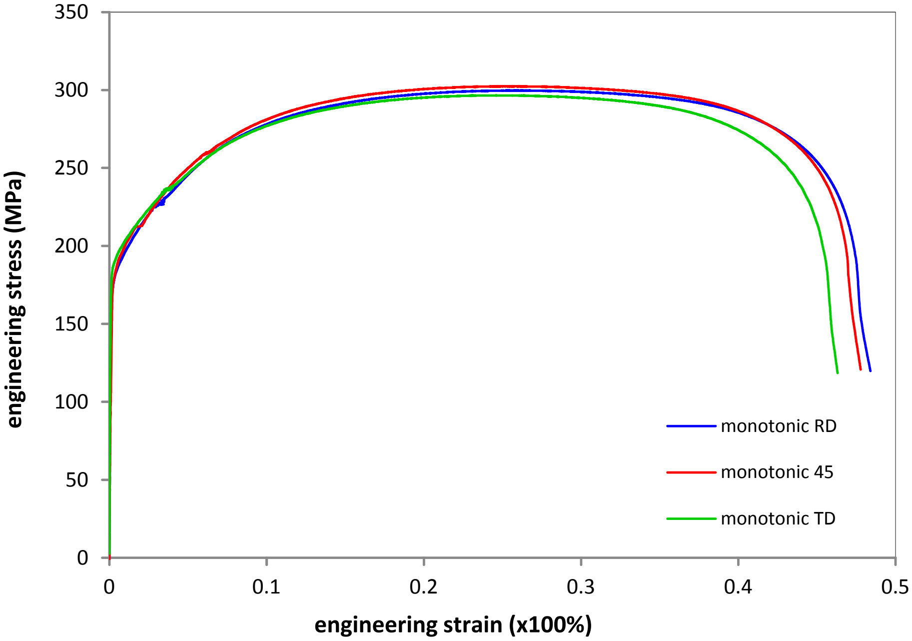

Figure 3.13: stress-strain curves of initial sample in various directions from RD

R-value of sheet IF steel in three different directions from RD is shown in figure 3.14. This figure indicates that the R-value of the as received sheet sample is higher than those in an Al-5182 sheet which is desirable for deep drawing applications.

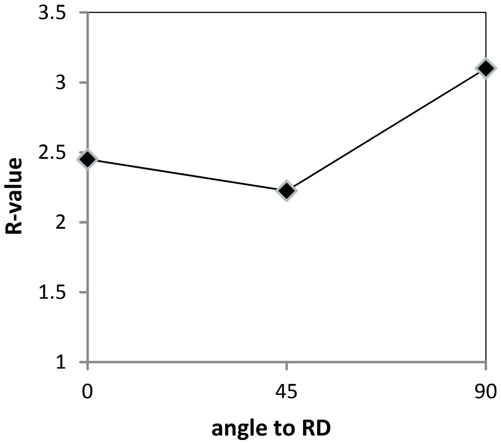

Figure 3.14: R-value in various directions from RD

An optical microscopy was carried out to study the microstructure of as received IF steel sheet and is presented in figure 3.15. The equiaxed grains with an average grain size of around 25µm indicate that the as received material was recrystallized.

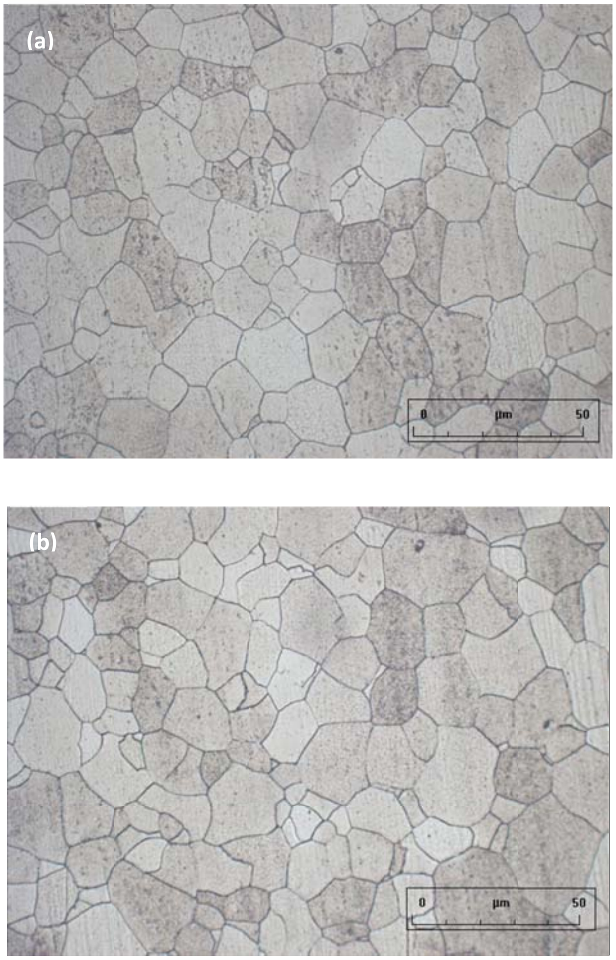

Figure 3.15: optical microstructure of as received IF stee1 sheet from a) TD and b) ND planes

3-2-2 ASR process

As received sample was subjected to four ASR and CR passes which lead to different amounts of strain from 18% to 60%. The ASR process was carried out using a velocity ratio of 1.5 of upper and lower working-rolls and without lubrication. C-ASR and R-ASR processes were applied in the same manner as explained in § 3-1; i.e. in the C-ASR the sheet direction was kept in all passes while in R-ASR the sample direction was changed with respect to RD.

In the next round of tests we investigated, the effect of the total reduction by imposing, respectively, thickness reductions of 5, 10 and 20% in each of the 4 passes. Subsequently, the tensile specimens were prepared along the RD from CR, R-ASR and C-ASR samples and annealed at 550°C for one hour. The tensile tests were applied at ambient condition and an engineering strain rate of $10^{-4}s^{-1}$.

3-2-3 microstructure observation

An optical observation and also an atomic force microscopy were carried out to study the microstructure change on the TD planes resulting from CR and ASR processes. Also with the goal of investigation of substructure of rolled samples, a 300kV Hitachi H-9000 transmission electron microscope (TEM) was used. TEM specimens were prepared from the mid thickness of the sheet sample and parallel to the ND plane. Initially the samples were mechanically polished and then electropolished with a jet thinner machine.

3-2-4 thermal stability

With the purpose of studying the thermal stability of rolled specimens, the rolled samples underwent different annealing treatments at 500-700°C for 1 hour in an electrical furnace. Tensile test have been carried out at a strain rate of $10\text{-}4s^{-1}$.

Figure 3.16 indicates the variation of yield strength and uniform elongation of 60% R-ASR and CR sheet samples after different temperatures of annealing. It can be seen that increasing the temperature from 550 to 625°C does not show any significant change in the yield strength; however, increasing the temperature from 650 up to 700°C leads to a slump of stress level and increases the uniform elongation in the stress-strain curves.

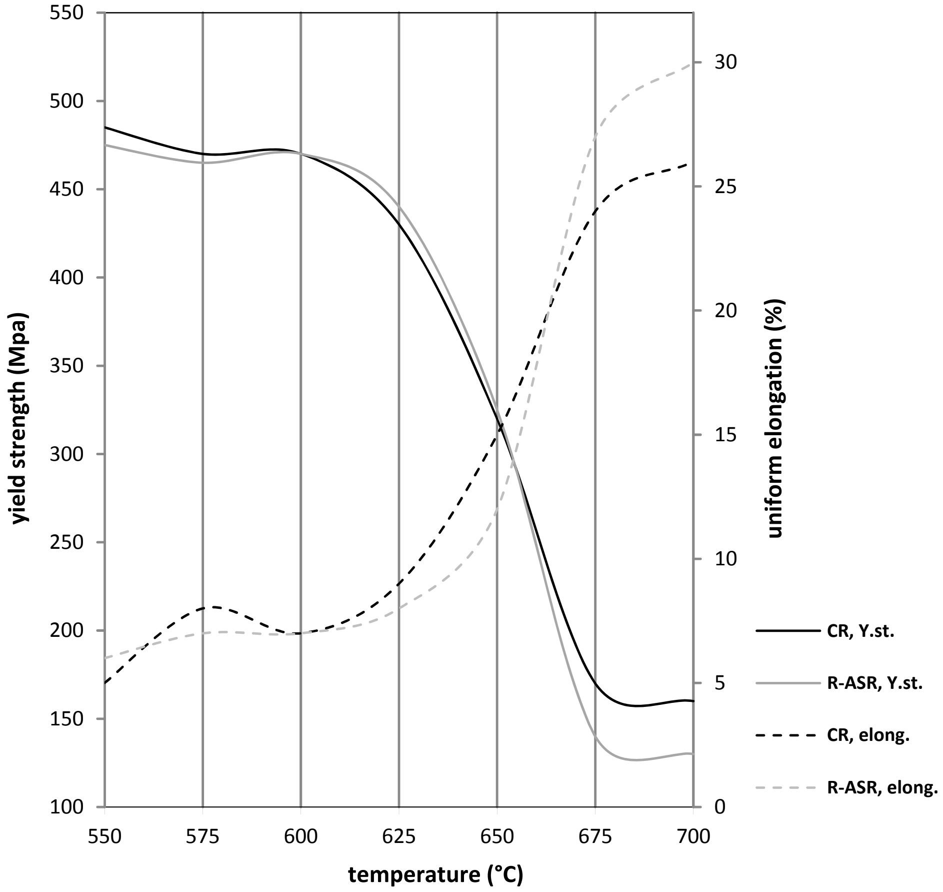

Figure 3.16: thermal stability of ASR sample: influence of annealing temperature on the yield stress and uniform elongation of the IF steel sheets

Figure 3.17 presents the microstructure of the asymmetrically rolled and heat treated samples at various temperatures. Heat treatment up to 650°C does not lead to a change in the microstructure whereas annealing at 700°C results in equiaxed recrystallized grains; i.e. annealing at lower temperatures may only cause recovery.

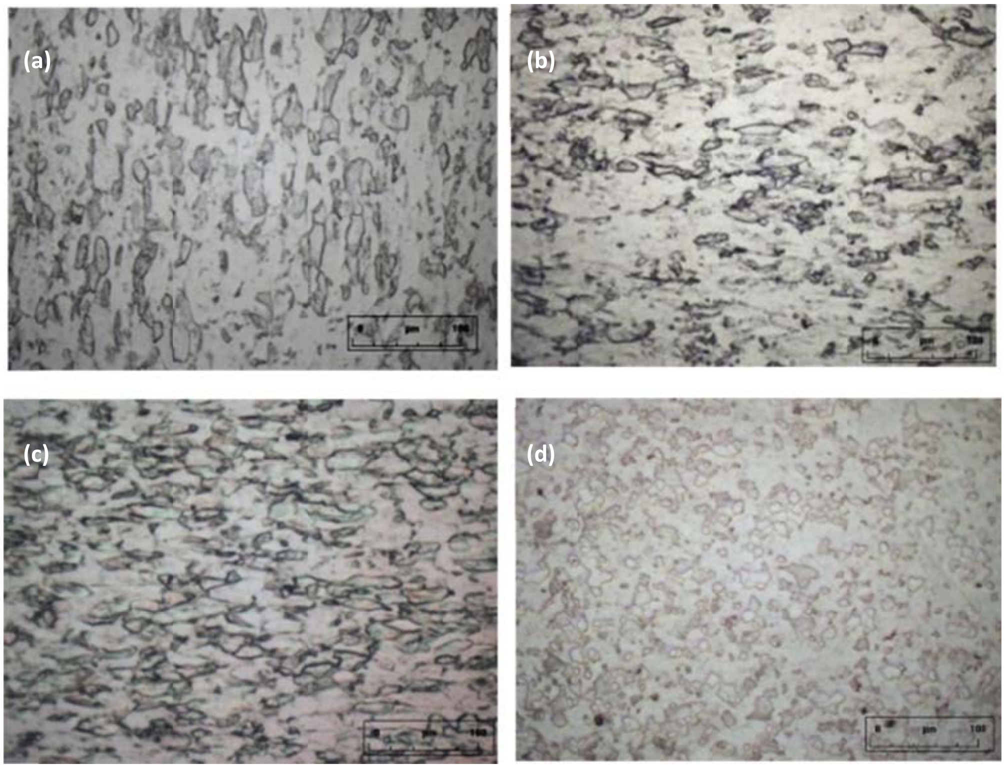

Figure 3.17: influence of annealing temperature on microstructure of IF steel sheets: a)550, b)600, c) 650 and d) 700°C for one hour

3-3 Strain path effect: C-ASR vs. R-ASR

In the current work, three different strain paths of C-ASR, R-ASR and CR are investigated. With the purpose of understanding the materials' behaviour through strain path change in the second pass of each strain route, the α parameter [Schmitt 1994] was calculated. α parameter is cosine of the angle between two vectors representing first and second strain route and provides an estimate of amplitude of the impact of strain path change on the activity of different slip systems through the plastic deformations as discussed in § 2-4-3.

Here, two passes of CR, as well as two passes of R-ASR and C-ASR are supposed to reduce the sheet thickness. As mentioned in the previous section, the sample direction is changed in the second pass of R-ASR, whereas it is kept un-changed for the C-ASR process (Fig. 3.18). Hence, the first pass and the second pass of each process are subjected as pre- and subsequent strain paths.

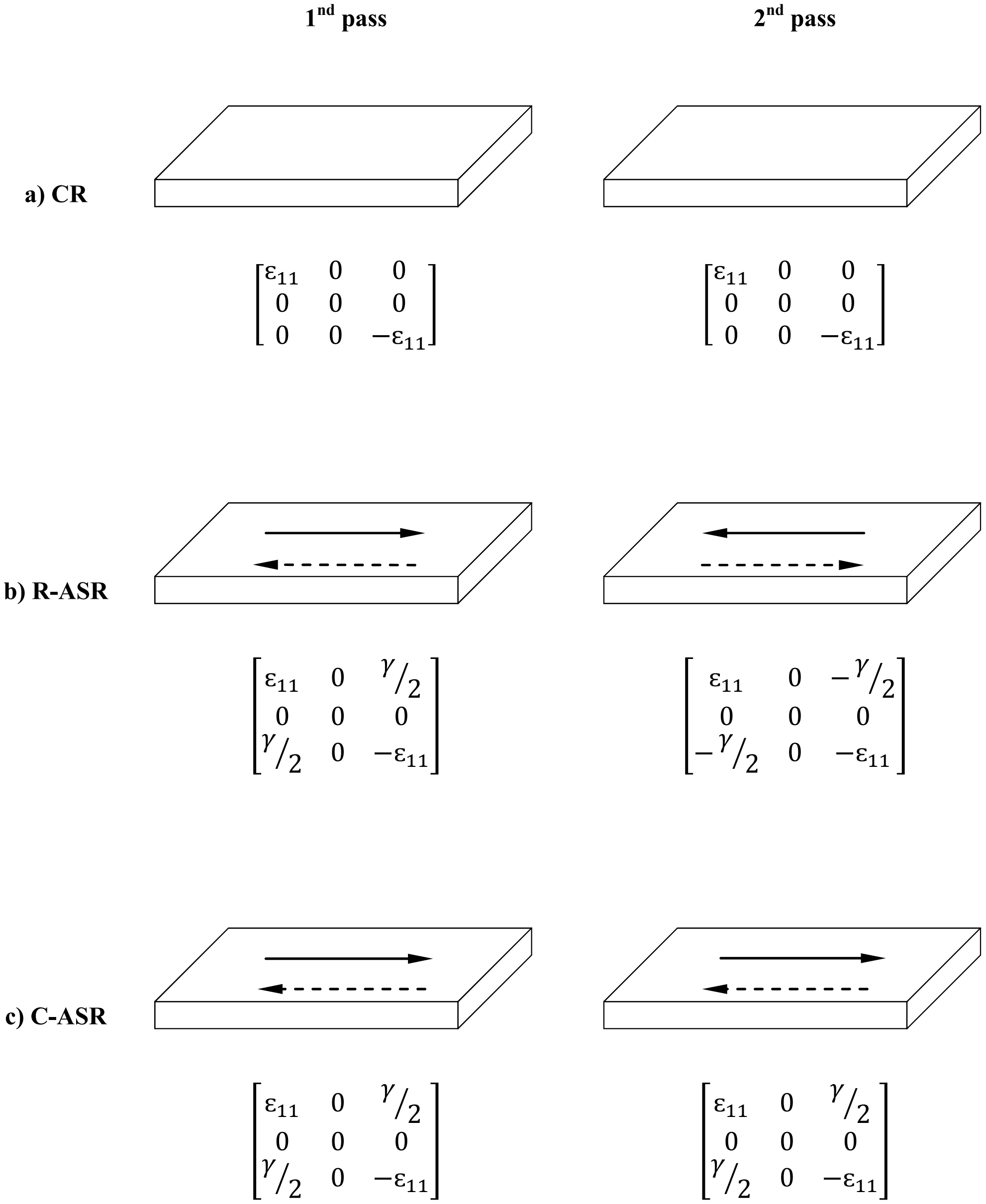

a) CR

$$\begin{bmatrix} \varepsilon_{11} & 0 & 0 \\ 0 & 0 & 0 \\ 0 & 0 & -\varepsilon_{11} \end{bmatrix} \qquad \begin{bmatrix} \varepsilon_{11} & 0 & 0 \\ 0 & 0 & 0 \\ 0 & 0 & -\varepsilon_{11} \end{bmatrix}$$

b) R-ASR

$$\begin{bmatrix} \varepsilon_{11} & 0 & {}^{\gamma}/_{2} \\ 0 & 0 & 0 \\ {}^{\gamma}/_{2} & 0 & -\varepsilon_{11} \end{bmatrix} \qquad \begin{bmatrix} \varepsilon_{11} & 0 & -{}^{\gamma}/_{2} \\ 0 & 0 & 0 \\ -{}^{\gamma}/_{2} & 0 & -\varepsilon_{11} \end{bmatrix}$$

c) C-ASR

$$\begin{bmatrix} \varepsilon_{11} & 0 & {}^{\gamma}/_{2} \\ 0 & 0 & 0 \\ {}^{\gamma}/_{2} & 0 & -\varepsilon_{11} \end{bmatrix} \qquad \begin{bmatrix} \varepsilon_{11} & 0 & {}^{\gamma}/_{2} \\ 0 & 0 & 0 \\ {}^{\gamma}/_{2} & 0 & -\varepsilon_{11} \end{bmatrix}$$

Figure 3.18: the first and second pass of various strain routes: a) CR, b) R-ASR and c) C-ASR processes

Here, γ is the shear strain imposed through the ASR processes and also ε_{11} is the compressive strain in deformation routes. According eq. 2-21 α parameters for two passes of each process are given as:

a) $$\alpha_{CR} = \frac{\varepsilon_{11}.\varepsilon_{11}+(-\varepsilon_{11}).(-\varepsilon_{11})}{\sqrt{\varepsilon_{11}{}^{2}+(-\varepsilon_{11})^{2}}\,.\,\sqrt{\varepsilon_{11}{}^{2}+(-\varepsilon_{11})^{2}}} = 1$$

b) $$\alpha_{R-ASR} = \frac{\varepsilon_{11}.\varepsilon_{11}+(-\varepsilon_{11}).(-\varepsilon_{11})+(\gamma/_2).(-\gamma/_2)+(-\gamma/_2).(\gamma/_2)}{\sqrt{\varepsilon_{11}{}^2+(-\varepsilon_{11})^2+(\gamma/_2)^2+(-\gamma/_2)^2}.\ \sqrt{\varepsilon_{11}{}^2+(-\varepsilon_{11})^2+(-\gamma/_2)^2+(\gamma/_2)^2}} = \frac{\varepsilon_{11}{}^2-(\gamma/_2)^2}{\varepsilon_{11}{}^2+(\gamma/_2)^2} < 1$$

c) $$\alpha_{C-ASR} = \frac{\varepsilon_{11}.\varepsilon_{11}+(-\varepsilon_{11}).(-\varepsilon_{11})+(\gamma/_2).(\gamma/_2)+(\gamma/_2).(\gamma/_2)}{\sqrt{\varepsilon_{11}{}^2+(-\varepsilon_{11})^2+(\gamma/_2)^2+(\gamma/_2)^2}.\ \sqrt{\varepsilon_{11}{}^2+(-\varepsilon_{11})^2+(\gamma/_2)^2+(\gamma/_2)^2}} = \frac{\varepsilon_{11}{}^2+(\gamma/_2)^2}{\varepsilon_{11}{}^2+(\gamma/_2)^2} = 1$$

The calculated α parameters for two passes of CR and C-ASR equal 1, which means the strain path did not change between the passes whereas in R-ASR process the α parameter is less than 1 which depends on the magnitude of γ relatively to ε_{11}; e.g. the α parameter of two passes of R-ASR process equals 0 for value of $\varepsilon_{11} = \frac{\gamma}{2}$. For α parameters close to 0 the new slip systems become active which were latent in the first pass. On the contrary, through the second pass of CR and C-ASR dislocations glide on the same slip systems used in the previous pass.

It should be noted that in the calculations, it was assumed that the ratio of $\frac{\varepsilon_{11}}{\gamma}$ is the same for both passes of C-ASR processes. The change of $\frac{\varepsilon_{11}}{\gamma}$ ratio may lead to having a different strain path in the second pass of C-ASR, also.

Chapter 4

Results and discussion

4-1 AA-5182

4-1-1 macroscopic shear strain

After rolling, the lines scratched on the side face of the sheets can be clearly observed as shown in Fig. 4.1. Figure 1a shows that during the first pass of ASR, the line which was initially perpendicular to the rolling plane tends to incline towards the rolling direction. Through the second pass under C-ASR process, the angle increases as shown in figure 4.1b. However, for the second pass under R-ASR, the line rose from the first pass position (Fig. 4.1a) to the vertical direction as shown in figure 4.1c. The measured inclination of the line represents the additional shear deformation of ASR in each pass. Since there is no shear deformation in the CR process, at the centre of the specimen, no inclination of the scratched line is observed after the first and the second pass. However, the friction between the working rolls and the sheet causes a small amount of shear strain away from the centre which is negligible.

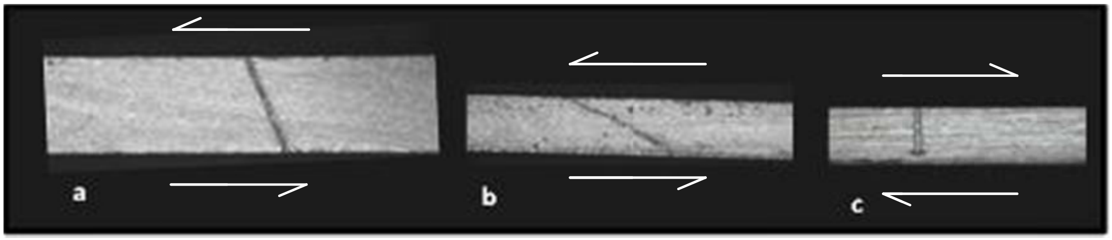

Figure 4.1: scratched line on the side face of the samples after: a) first pass ASR, b) second pass of C-ASR and c) second pass of R-ASR

4-1-2 texture development under rolling

In this section, the textures are represented by pole figures and ODFs in the Euler space represented by φ_1, ϕ and φ_2 angles [Bunge 1982]. We show the sections of the Euler space at φ_2=0° and φ_2 = 45°. In chapter 2, the ideal texture components for rolling, shear and recrystallization are listed along with their corresponding Euler angles. We also compare the predicted texture of the VPSC model to our experimental results.

Figure 4.2 shows texture developed by CR after two passes where Figure 4.2a illustrates the experimental results for pole figures and φ_2 =0° and φ_2 =45° sections and Figure 4.2b represents the corresponding texture as predicted by the VPSC model. In the simulation, the CR is approximated by plane strain compression deformation. In Figure 4.2a, the Copper, Dillamore and the Brass texture components are the major components. These components generally belong to the so-called β-fibre. In addition to β-fibre, a few remaining cube textures can be detected as well. The Copper and the Brass texture components can also be seen in the predicted results in Figure 4.2b.

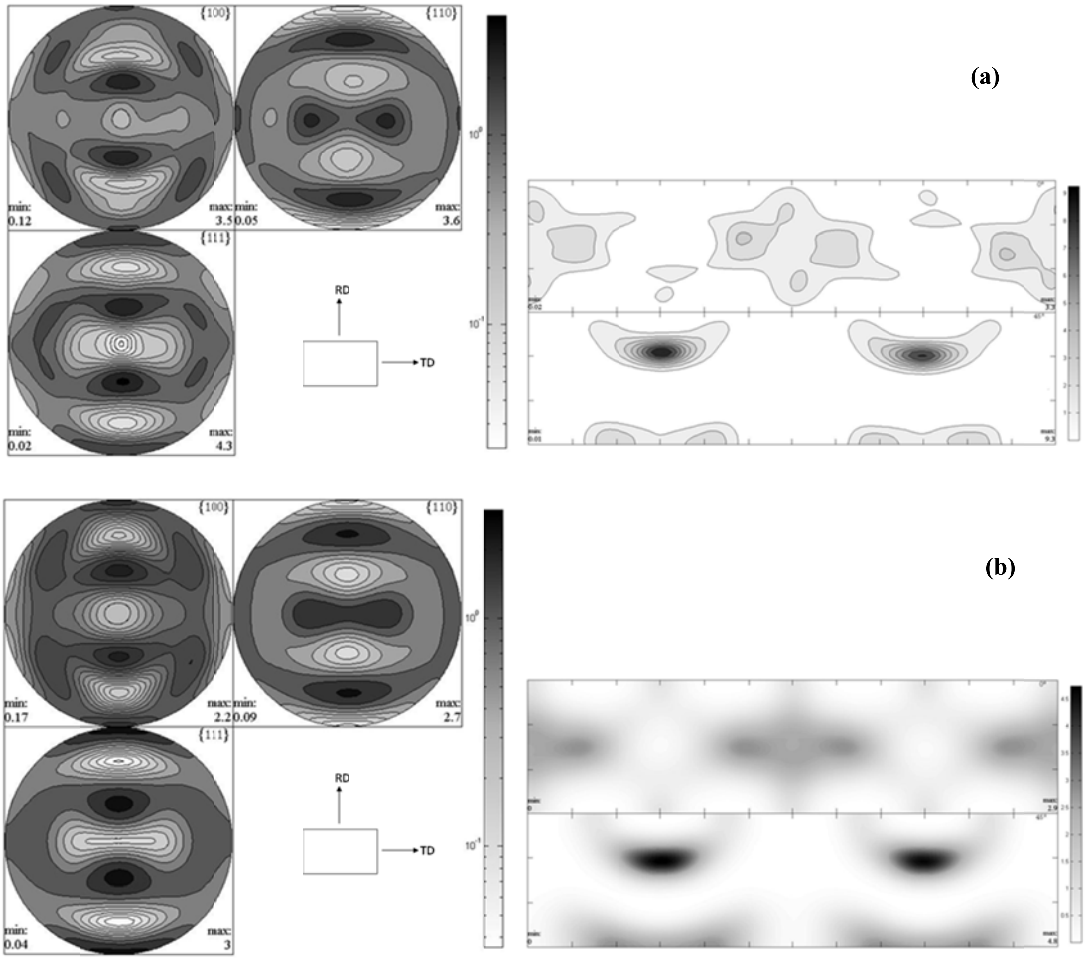

Figure 4.2: texture of CR (50% reduction); a) experimental and b) predicted by VPSC model

Figure 4.3 shows the influence of shear strain on the texture after a single pass of asymmetric rolling, which is the same for both C-ASR and R-ASR. As revealed by texture measurement in Figure 3a, shear plastic deformation in asymmetric rolling process leads to a disturbance in the symmetry which exists in the CR texture. We note that the H ({001}<110>), the E ({111}<110>) and the F ({111}<112>) components as the shear components can be detected at section φ_2 =45°. Figure 3b represents the texture simulated by the VPSC model. As these ODFs indicate, the simulated results are qualitatively in agreement with the experimental ones but with higher predicted intensities.

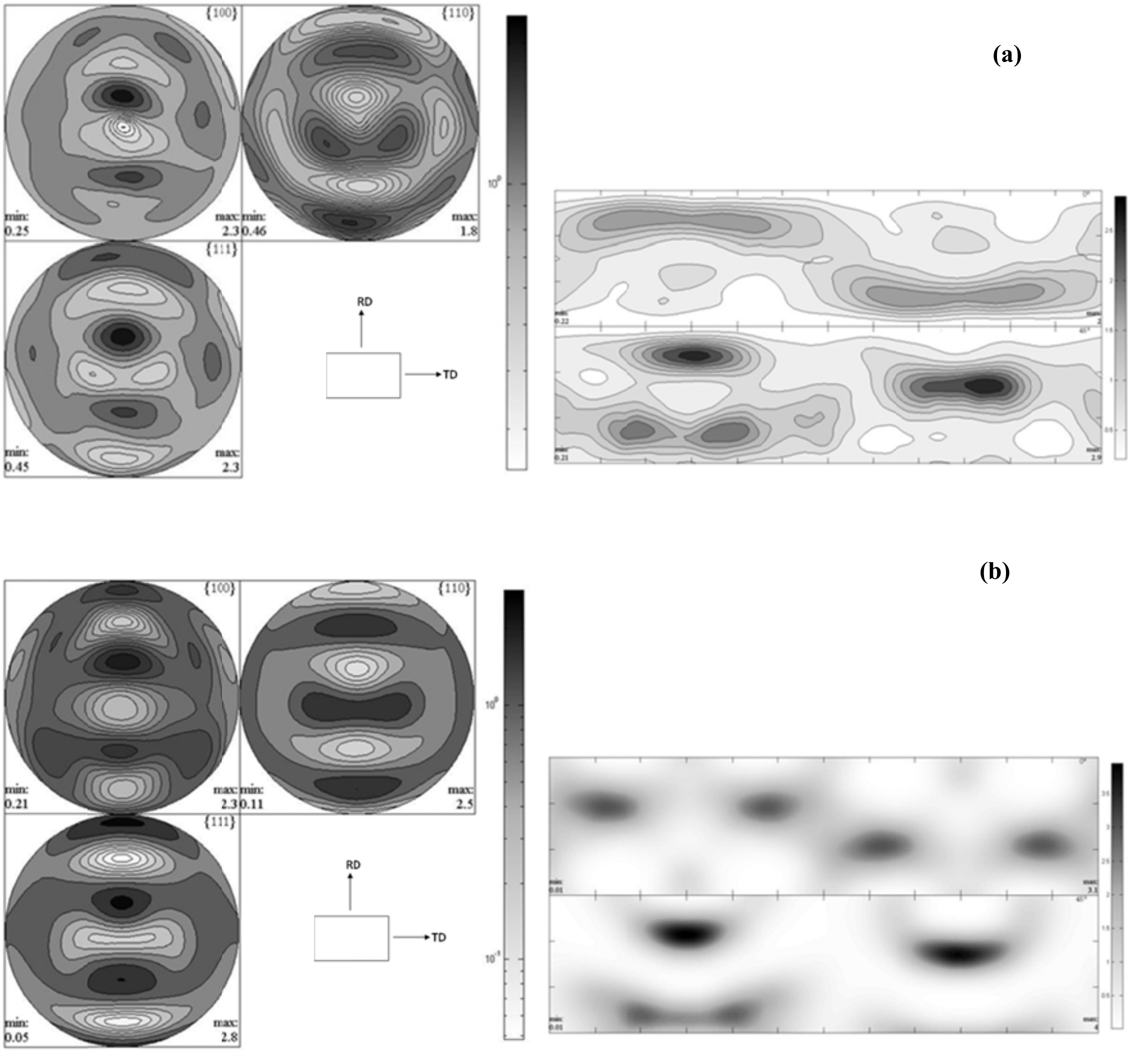

Figure 4.3: crystallographic texture of one pass of ASR (28% reduction): a) experimental, b) predicted by VPSC model

The developed textures of the samples by C-ASR and R-ASR after the second pass are shown SR processes possess the H texture as a shear texture. Also, the φ_2 =45° section of both ODFs indicates that the texture of samples produced by R-ASR or C-ASR processes are dominated mostly by the H, E and F (see chapter 2). We note that the E and F components belong to {111}//ND fibre.

Since the strain path of C-ASR in the second pass has not changed, the same texture components can be seen as in the first pass, but with different intensities (see Fig. 4.3a and Fig. 4.4a). However, in the second pass of R-ASR the shear components appear to shift 180° in φ_1 axis after the first pass (see Fig. 4.3a and Fig. 4.5a).

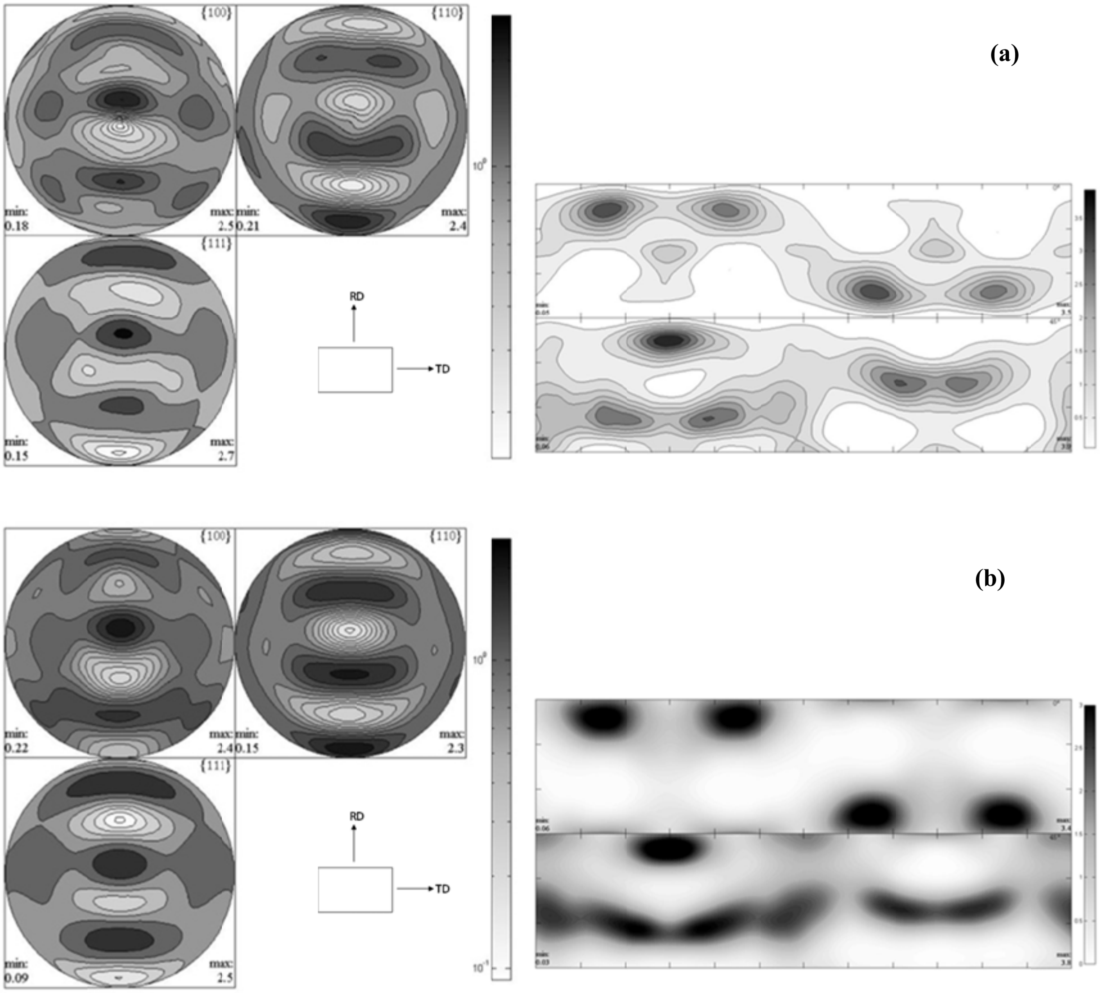

Figure 4.4: C-ASR: a) experiment and b) simulation

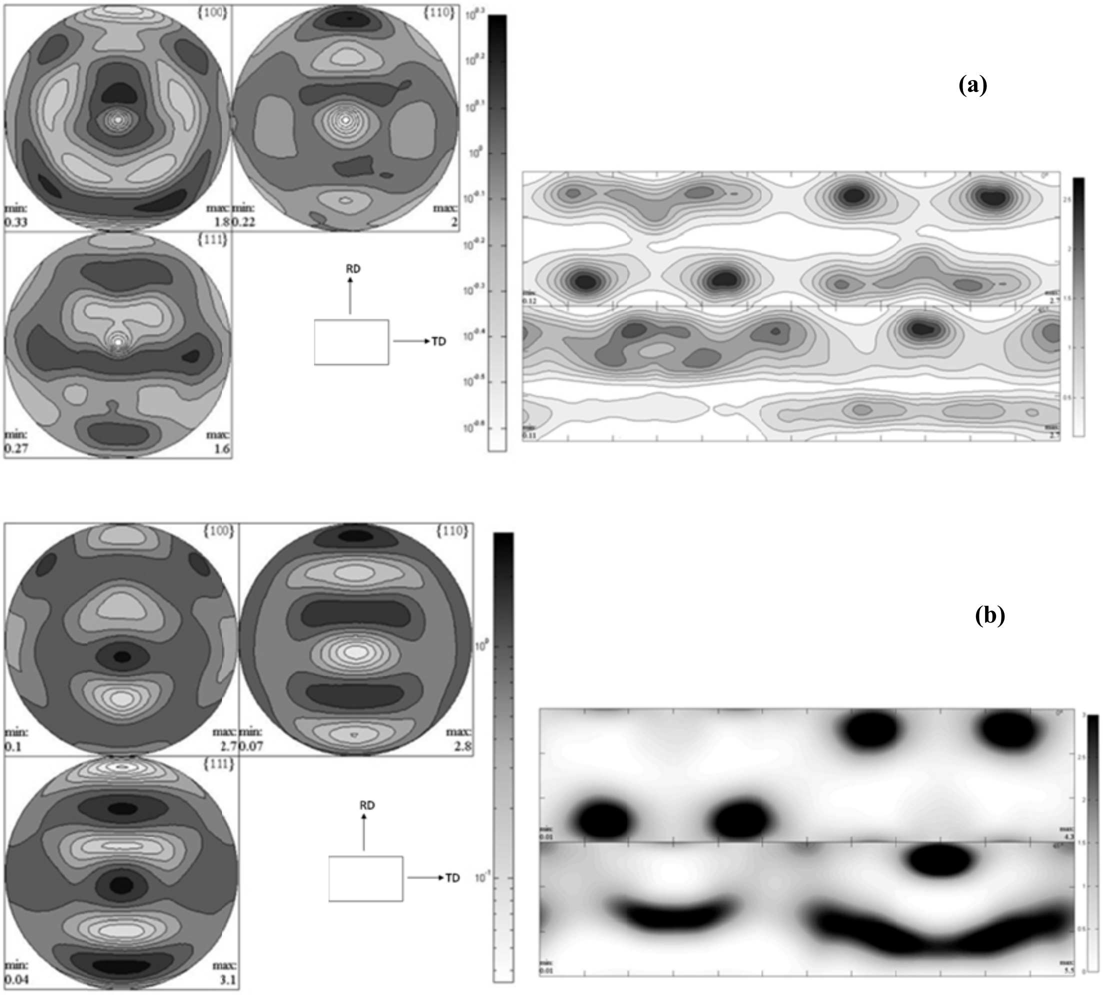

Figure 4.5: R-ASR: a) experiment and b) simulation

The predicted textures, obtained from the VPSC model for both processes, are presented in Figures 4.4b & 4.5b. The simulated results for the sample produced by C-ASR show qualitatively similar texture to the experimental ones (see Fig. 4.4a,b). However, as Figures 5a,b indicate, there are important differences in the relative intensities of the texture components between the experimental results and predicted ones for the sheet subjected to R-ASR (see Fig. 4.5a,b). The main difference appears for φ_2 = 45° where the predicted results overestimate the intensities and deviate from the developed texture components, except for the H component.

4-1-3 mechanical behaviour

4-1-3-1 stress-strain curves

For the macroscopic stress-strain response of the rolled sheets, figure 4.6 shows the tensile stress-strain curve response of the AA-5182 samples rolled by CR, R-ASR and C-ASR after heat treatment. We note that the samples produced by R-ASR and C-ASR processes possess less strain hardening than the sample rolled by CR process. In figure 6 we also plotted the predicted stress-strain curves using the VPSC model. As can be seen, the agreement is fairly good for both ASR processes. We note that the tensile stress-strain response of the conventionally rolled sample was used to determine the hardening parameters as explained in chapter 3.

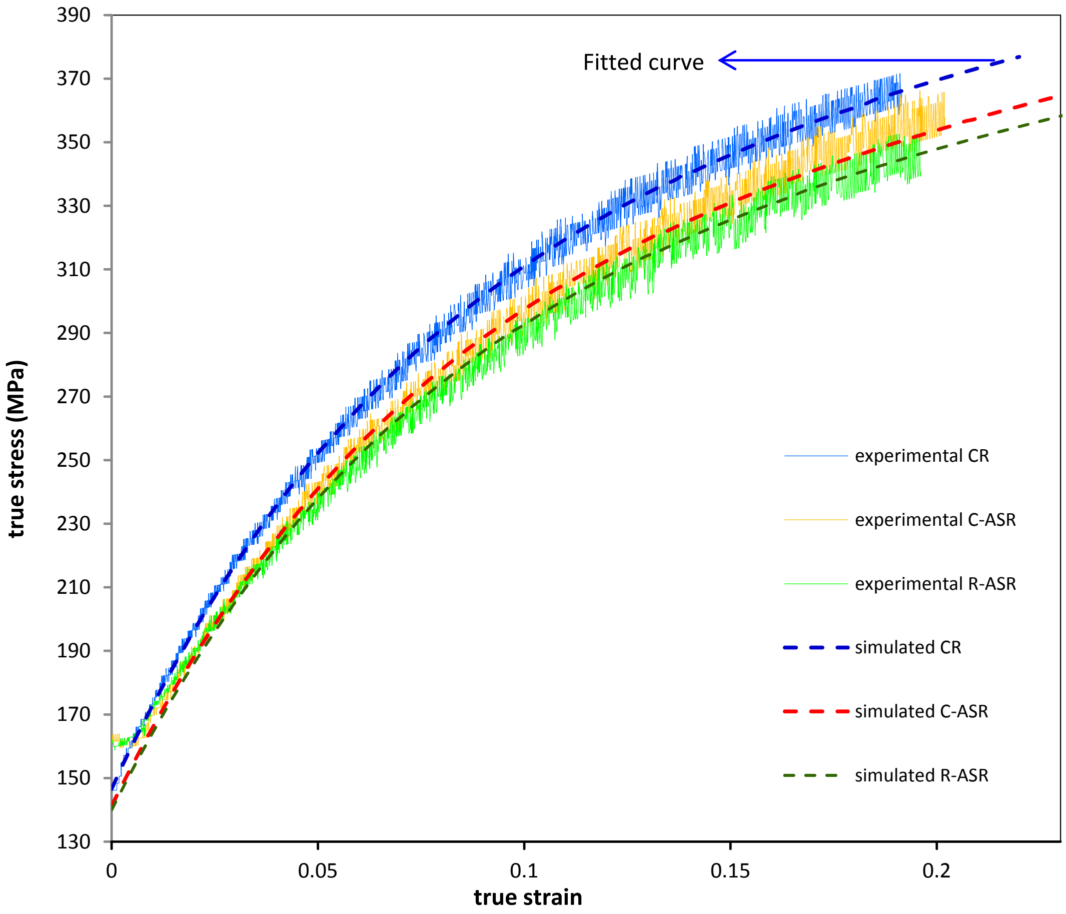

Figure 4.6: the experimental and simulated (VPSC approach) stress-strain curves of R-ASR, C-ASR and CR samples in RD

4-1-3-2 plastic anisotropy of mechanical behaviours

Figure 4.7 shows the experimentally measured R-value of different samples. In this figure, we also show the R-values for the as received recrystallized sheets (Fig. 4.7a). This figure shows that the R-value of the recrystallized sample in the RD is 0.58 which decreases slightly to 45° from the RD and then rises to 1.1 in the TD. The variation of R-value of the conventionally rolled sample with respect to the tensile load direction is shown in Figure 4.7b. In contrast to the recrystallized sample, there is a steady increase from 0° to 45° from the RD. However, the R-value decreases in the TD. Figure 4.7c represents the variation of R-value of the samples deformed by the C-ASR process which is 0.97, 1.17 and 0.73 in the RD, at 45° from the RD and in the TD, respectively. This translates into an increase from 0° to 45° then a decrease from 45° to 90° (TD). A similar trend can be seen in the sample rolled by R-ASR in Figure 4.7d, but with lower values.

Figure 4.7 also represents the R-value variation with the angle from the RD of the samples obtained by the VPSC model. In this figure, the variation of the R-value with the tensile direction predicted by the VPSC model, exhibits a similar trend. However, Figure 4.7a shows that the VPSC prediction overestimates the experimental data in various directions. In addition, Figure 4.7b indicates that the VPSC model prediction for the conventionally rolled sample overestimates the experimental results at 45 and 90° directions from the RD, but predicts well the R-value in the RD. Furthermore, the predicted R-values of the sample deformed by the C-ASR, in the RD and at 45° from the RD are higher than the experimentally measured ones (Fig. 4.7c). However, for the sample subjected to R-ASR, the prediction of R-value in these two directions is in good agreement with the experimental results (see Fig. 4.7d). In the TD direction, the predicted R-value slightly overestimates the experimental value for both C-ASR and R-ASR.

Since the Taylor model is one of the most used approaches, we have also used this model to predict the R-value. The predicted results are shown in Figure 4.7 in comparison to the experimental ones and to the VPSC predictions. The obtained results show that the Taylor predictions follow similar trends as the VPSC predictions but with lower estimated R-values (Fig. 4.7acd), except for the conventionally rolled samples for low angles from the RD (Fig. 4.7b).

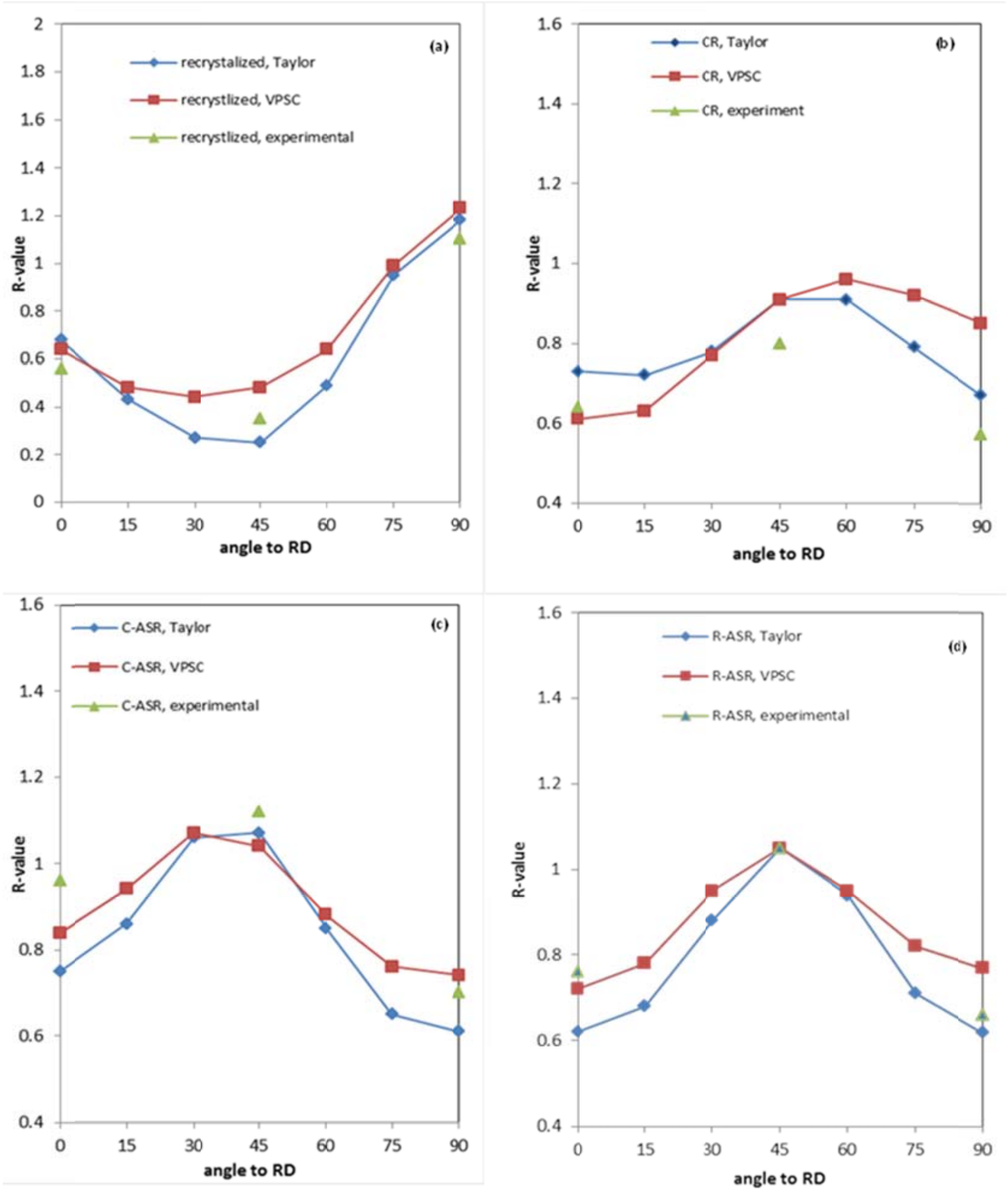

Figure 4.7: the variation of R-value in different directions from the RD, a) recrystallized, b) CR, c) C-ASR and d) R-ASR samples

Table 4.1 gives the normal and planar anisotropy in the recrystallized sample and three rolled specimen under uniaxial tensile tests according to the equation 2.17 & 2.18 given in § 2-4-1. As a result, $\overline{R}$ is higher in the specimen produced by C-ASR and R-ASR in comparison with CR and recrystallized samples. However, the absolute value of ΔR increased slightly by applying ASR processes in comparison with CR process, but it is still smaller than that in the recrystallized sample. The high $\overline{R}$ may lead to increase the resistance to thinning. In addition the low planar anisotropy (small $|\Delta R|$) may result in increasing the resistance to earing in deep drawing applications. Therefore, these parameters are important for the practical applications, particularly deep drawing, to avoid earing and thinning problems as discussed in chapter 2.

Table 4.1: normal and planar anisotropy of CR, C-ASR and R-ASR samples

anisotropy / sample	**Normal anisotropy: $\overline{R}$**	**Planar anisotropy: $|\Delta R|$**
recrystallized state	0.59	0.48
CR	0.70	0.19
C-ASR	0.98	0.28
R-ASR	0.89	0.34

4-1-4 discussion- simulation of individual texture components

The study focuses on producing the desirable texture in aluminium alloy sheets to improve its drawability. Figures 4.3-4.5 show the effect of shear strain on the crystallographic texture development during ASR processes. As mentioned before, the prominent texture components in these figures are dominated by the E, the F and the H components. The mechanical properties of these shear components have been investigated in previous works [Lequeu 1988, Bacroix 1999 and Sidor 2008] where it has been shown that they possess good anisotropic properties, appropriate for deep drawing applications.

4-1-4-1 Texture

The texture produced by a single pass of ASR contains these shear components which become more pronounced after the second pass in C-ASR. However, reversing the sheet sample in the second pass of R-ASR leads to shifting these components by 180° in φ_1 axis which are still shear texture components. The results indicate that both types of ASR processes (C-ASR and R-ASR) are capable of producing shear textures. According to Figures 4.2-4.5, it is obvious that the polycrystal simulations of the texture evolution in CR and C-ASR strain modes are successfully predicted but with different intensities. However, discrepancy between the predicted and the experimental textures is obtained for the sample subjected to R-ASR. These texture components produced by ASR processes are also reported in the results of Kim et al. [Kim 2002].

4-1-4-2 Tension

This work also provides a correlation between the experimental mechanical responses and polycrystal modelling predictions. From figure 4.6, the tensile stress-strain curves of the samples produced by CR, C-ASR and R-ASR for both experimental and simulation are in good agreement. With the purpose of understanding the role of different texture components on the macroscopic behaviour, VPSC modelling was carried out to simulate the behaviour of each individual component through a uniaxial tensile test as shown in Fig. 4.8. In spite of higher value of E and F (shear components) than copper and brass (rolling components) in the lower strain, rolling components present more strain hardening than shear ones. Hence the existence of Copper and Brass texture components is responsible for more strain hardening of the sample produced by CR compared to the samples rolled by ASR processes observed in Fig. 4.6.

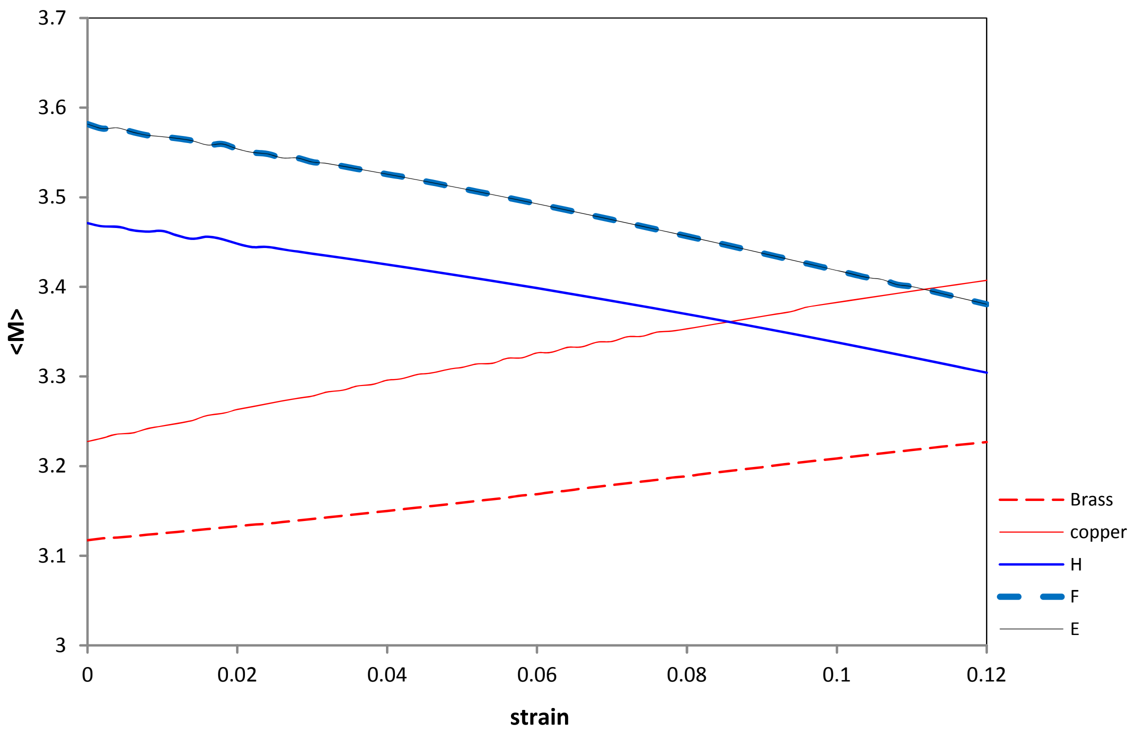

Figure 4.8: VPSC simulation of uniaxial tension in RD of individual texture components

4-1-4-3 plastic anisotropy

Figure 4.7 shows the mechanical plastic anisotropy of the recrystallized sample and the specimen deformed by CR and ASR processes. In these results we observed that the texture of the recrystallized sample leads to a low value of normal anisotropy (Fig. 4.7a) compared to that of CR (Fig. 4.7.b). By comparing these curves to the ones simulated for each individual texture components of the recrystallization texture provided in figure 4.9, it can be shown that the relatively low R-value with the V-shaped profile found in the recrystallized sample is due to the cube component, whereas the larger R-value obtained in TD is attributed to the Goss texture component.

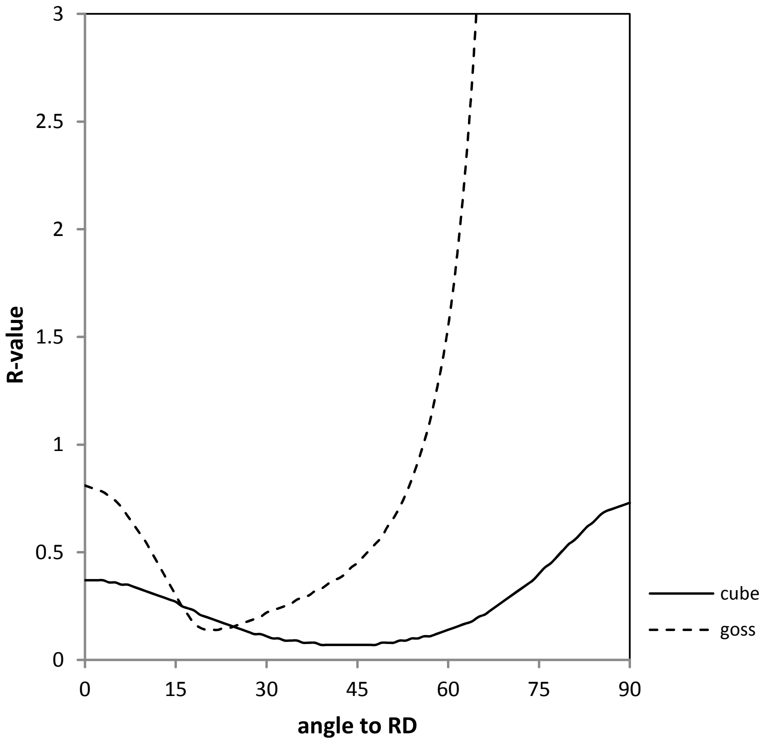

Figure 4.9: R-value simulation (VPSC) of recrystallization components in different direction from the RD

As already mentioned in the previous part of § 4-1-3-2, the results of anisotropy properties of the deformed samples indicate that the R-value of ASR samples possess a higher R-value while presenting higher planar anisotropy as well.

By comparing the results in Fig.7bcd and the curves simulated by VPSC of rolling and shear components, shown in Fig. 4.10, this raises the idea that the presence of shear texture components results in a relatively high R-value. The VPSC simulated R-value trends of individual components in figures 4.9 & 4.10 are in qualitative agreement with the previous works [e.g. Lequeu 1988 and Inoue 2007].

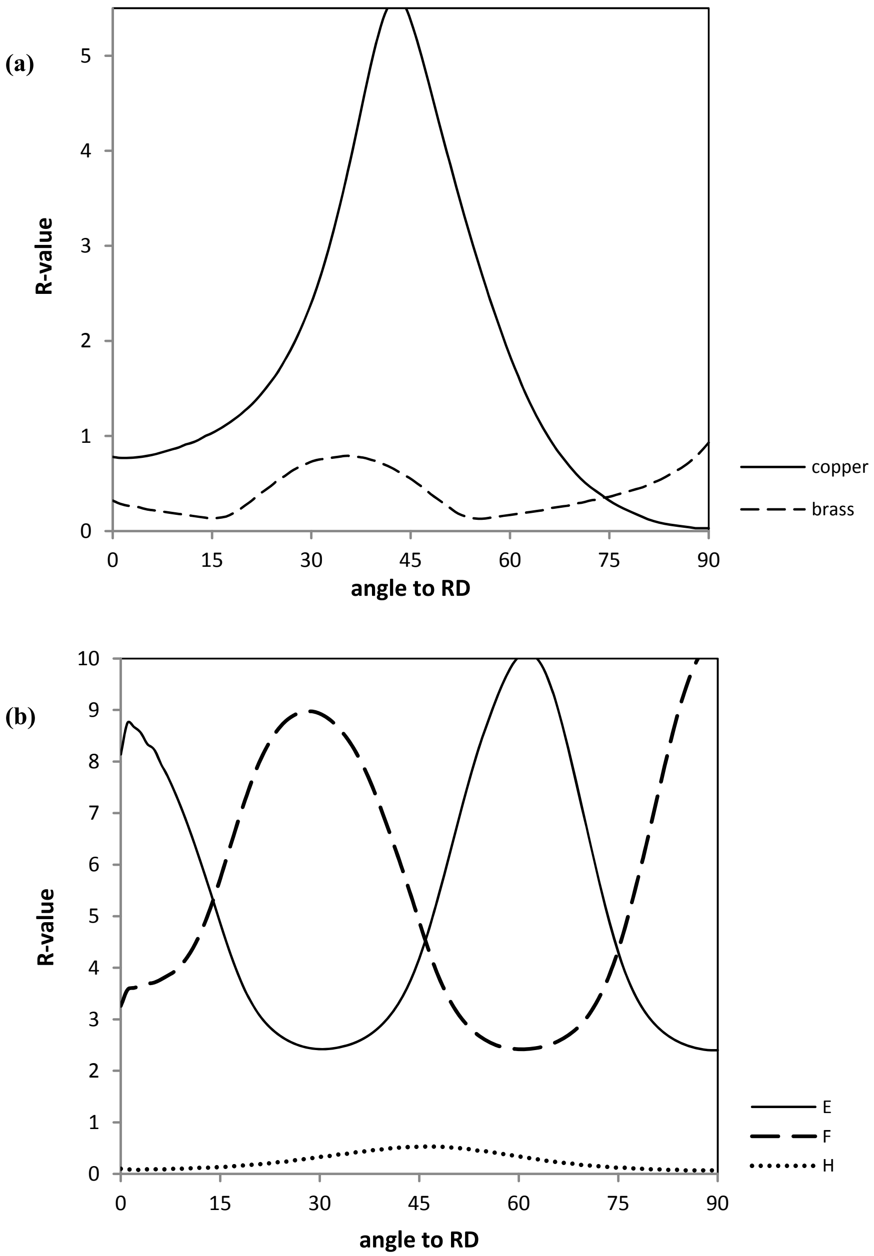

Figure 4.10: R-value simulation (VPSC) of a) rolling and b) shear texture components in different direction from the RD

Figure 4.10 indicates that copper and brass which are the main components in the sample rolled by CR are generally associated with higher normal anisotropy and maximum at 45°from RD. On the other hand, the E and the F texture components developed in ASR processes lead to increase the normal anisotropy under the uniaxial tension (see Fig. 4.7cd and Fig. 4.10b). However, developing these textures leads to increasing planar anisotropy in comparison with the conventionally rolled sample. This can be a limitation of these processes which should be investigated in future works.

Consequently, regardless of the exact value of the simulations in figures 4.8-4.10 offering a relative comparison of mechanical responses of various crystallographic texture components, one may conclude that crystallographic texture may control the macroscopic behaviours of this material. Generally, the difference between experimental results and predicted ones by the models in figures 4.6 & 4.7 could be due to texture gradient effect in the thickness or due to microstructural effects such as grain size, grain shape and dislocation structure.

4-2 IF steel

4-2-1 texture development under rolling

Figure 4.11 shows the φ_2=45° section of ODF presentation of the sheets deformed through CR and C-ASR. In both specimen γ and α fibres are pronounced. However, the γ fibre in the C-ASR sample is more uniform and weaker in comparison with the γ fibre of the CR sample. The E_1 and the i texture components appeared in the sheet conventionally rolled as illustrated in Fig. 4.11a.

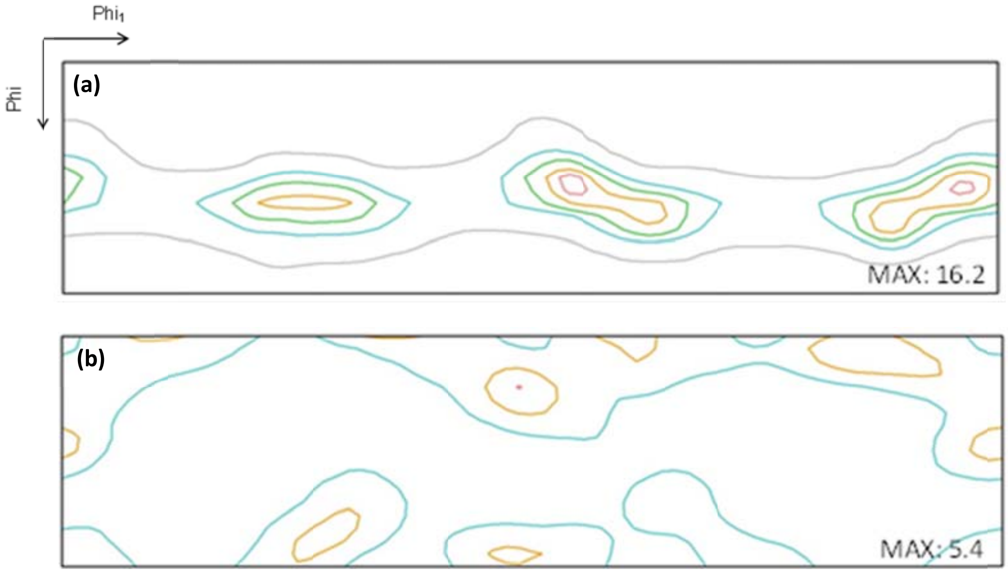

Figure 4.11: φ_2=45° section of ODF of the samples deformed 60% with a) CR and b) C-ASR

4-2-2 microstructure observation

Figures 4.12 & 4.13 illustrate the microstructure of C-ASR and CR samples in two total reductions taken with optical microscopy (OM) and atomic force microscopy (AFM). After C-ASR and CR the grains appear slightly elongated in the rolling direction. According to the results, no significant difference between the investigated samples can be detected. However, in Fig. 4.12c the darker regions appear with a wrinkled skin covering the elongated grains in the C-ASR sample. This feature of microstructure which is called fragmentation can also be seen in the result of AFM observation of C-ASR sample in Fig. 4.13c. The observed fragmentation may be associated with a different dislocation organization of the C-ASR sample, which may be due to the role of shear strain. The shear strain imposed through C-ASR causes the activation of different slip systems than those activated through CR. Different routes of dislocation movement result in a different dislocation organization.

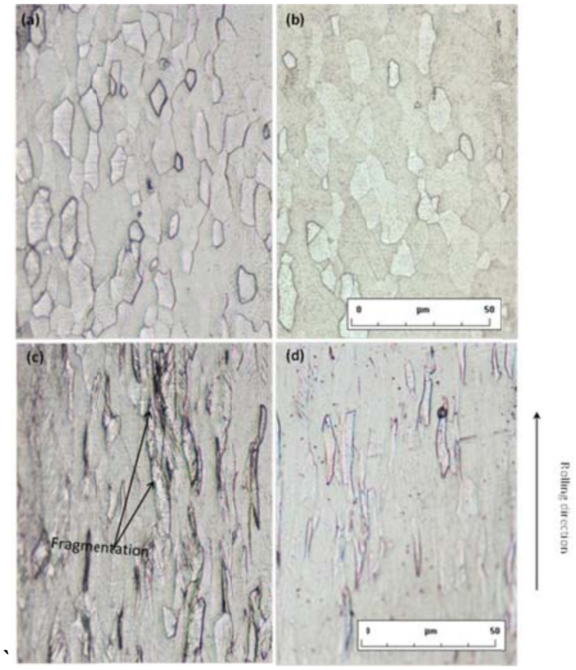

Figure 4.12: optical microscopical observation of TD plane of the samples rolled for 18% reduction with a) C-ASR, b) CR, and 60% reduction with c) C-ASR and d) CR

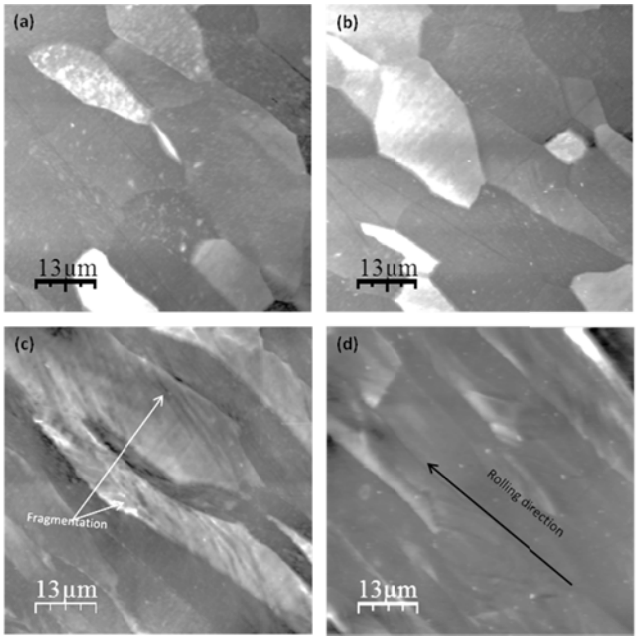

Figure 4.13: AFM observation of TD plane of the samples rolled for 18% reduction with a) C-ASR, b) CR, and 60% reduction with c) C-ASR and d) CR

The TEM observation of substructure of the sheets deformed by 18% total reduction using C-ASR and CR are shown in Fig. 4.14 & 4.15. The dislocation cells starts to form in both

C-ASR and CR samples aligned with the rolling direction. Since the level of plastic deformation is small, the grains are devided into large dislocation cells using un-well defined dislocation walls. The grain boundary indicated in Fig. 4.14b, shows that the substructure on the other side of the grain boundary are quite different; i.e. dislocation density and also their organization arenot the same. This is due to the large difference between the orienations of two adjacent grains, and consequently different active slip sytems activated through the plastic deformation.

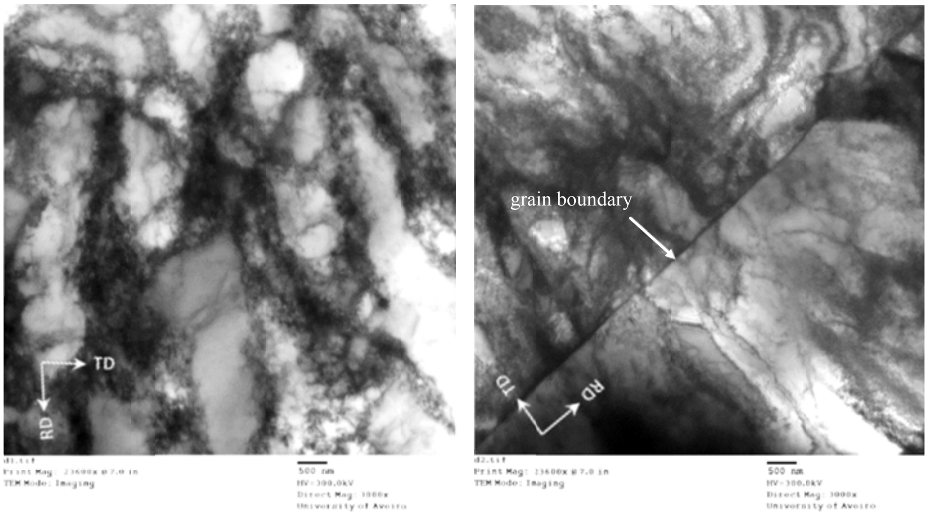

Figure 4.14: TEM observation of ND plane of the sample rolled for 18% reduction with C-ASR process

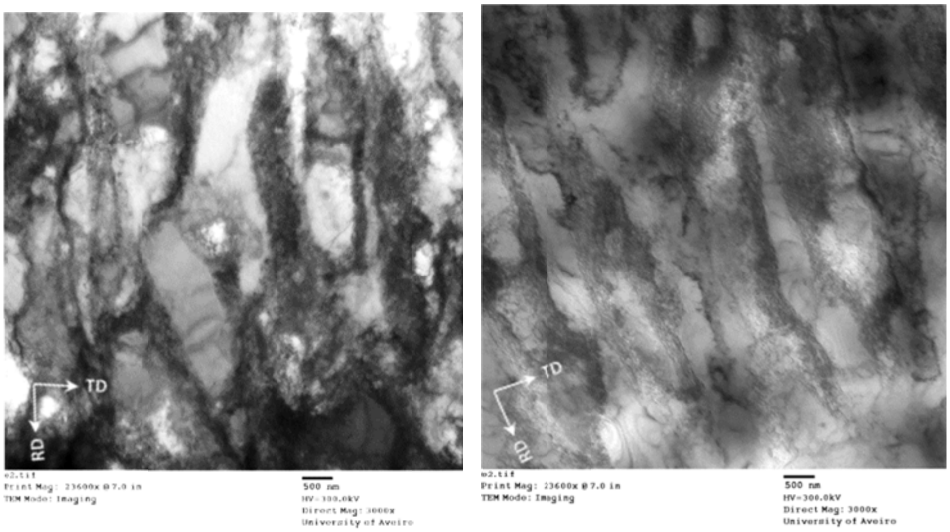

Figure 4.15: TEM observation of ND plane of the sample rolled for 18% reduction with CR process

Figures 4.16 & 4.17 show the TEM observation of the 60% reduction rolled samples using C-ASR and CR, respectively. The substructure of C-ASR sample is characterized by dislocation walls which form rough, equiaxed dislocation cells whereas the dislocation cells of CR sample are elongated along the rolling direction. In addition, the dislocation cells produced during C-ASR are relatively smaller than those produced during CR. The dislocation walls which are characterized as darker regions originate from accumulation and rearrangement in the plastic deformations (Fig. 4.16 & 4.17). This feature of dislocation structure of asymmetric rolled sheets was also reported in previous works [e.g. works of Ding 2009 and Jiang 2009].

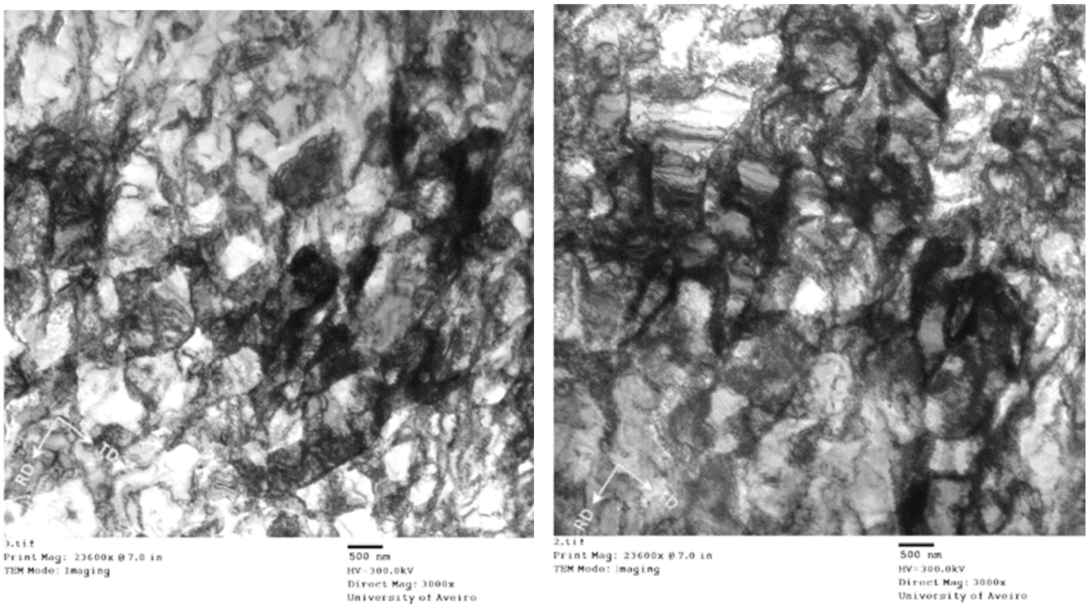

Figure 4.16: TEM observation of ND plane of the sample rolled for 60% reduction with C-ASR process

The equiaxed dislocation cells presented in Fig. 4.16 are due to the shear strain imposed through the C-ASR process. The shear strain allows the formation of equiaxed cells, because of the large rotation rates which are involved during C-ASR process. It should be noted that in some parts of surface regions of the CR sheet sample the equiaxed substructure can also be detected which is associated with the shear deformation imposed by friction between sheet and working-roll surfaces. However as only small parts of sheet thickness of CR sample experienced the shear deformation induced by friction, the majority part of sheet thickness are characterized by elongated substructure as shown in Fig. 4.17.

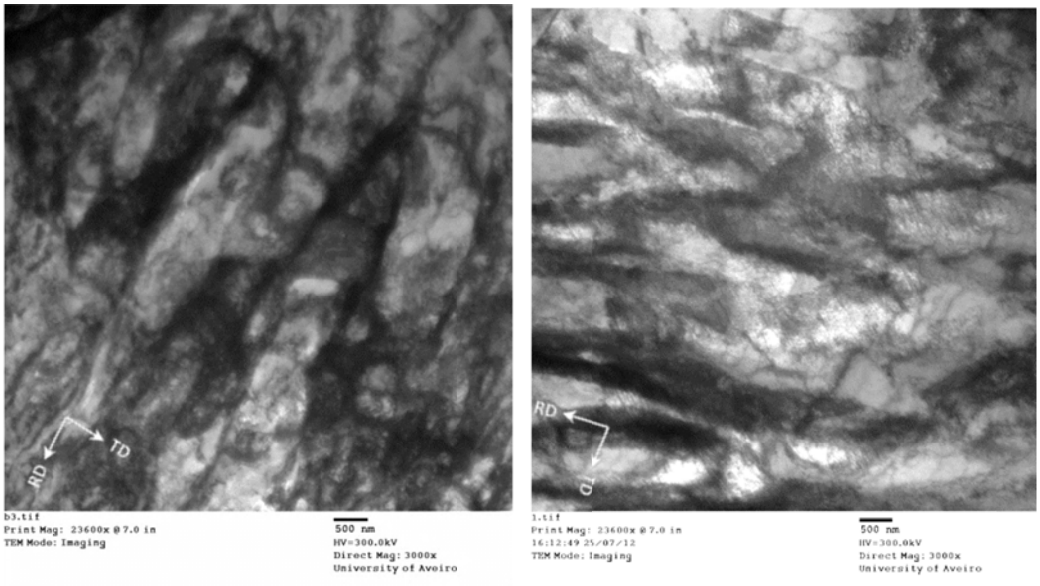

Figure 4.17: TEM observation of ND plane of the sample rolled for 60% reduction with CR process

Figure 4.18 illustrates the influence of reversing the sample between the ASR pass (i.e. R-ASR process) on the substructure of the sample. A significant number of dislocations cover the observed surface which have not yet organized. However, there are some evident in this figure showing newly formed dislocation walls which rearrange the dislocations and form imprecise equiaxed cells. The new dislocation cells are larger in comparison with those observed in the C-ASR sample (Fig. 4.16). At first sight, these results are in contradiction with the previous studies showing that changes in strain path should give rise to increasing misorientation between dislocation cells and promoting fined substructure [Iwahashi 1997 and 1998]. However, this approach is not generally accepted. In fact, Gholinia et al. has shown that a constant strain path is the most effective way to form fine grained structures for aluminium alloys [Gholinia 2000].

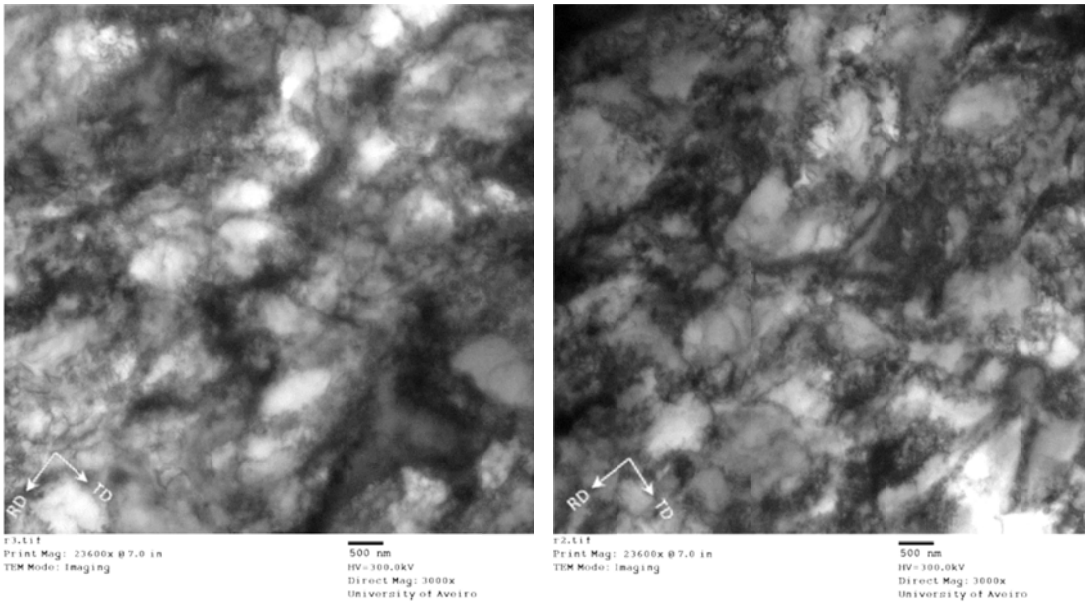

Figure 4.18: TEM observation of ND plane of the sample rolled for 60% reduction with R-ASR process

Fig. 4.16-4.18 presented the TEM substructure induced by various plastic deformation processes where the important characteristic feature is the various strain routes. Regarding α parameters for each process obtained in § 3-3, it can be inferred that slip systems activities of the CR and the C-ASR processes do not change between the passes; i.e. the dislocations slide on the same crystallographic plane and direction in all passes. Nevertheless, changing the sample direction between R-ASR passes leads to the activation of new slip systems or/and previous slip systems moving in the opposite directions. This may result in a not-very-well organized substructure in R-ASR sheets (Fig. 4.18) compared to that in C-ASR one (Fig. 4.16).

4-2-3 mechanical behaviours

Figure 4.19 shows the stress-strain curves resulted from tensile test in RD of 18% rolled IF steels obtained from the various experiments (CR, R-ASR and C-ASR). It can be seen that ASR samples show higher yield strength in comparison to CR samples. However, the CR sample plastically deformed with hardening where ASR samples tended to soften in the tensile test. The trends observed of both C-ASR and R-ASR experiments are similar and only small differences have been detected.

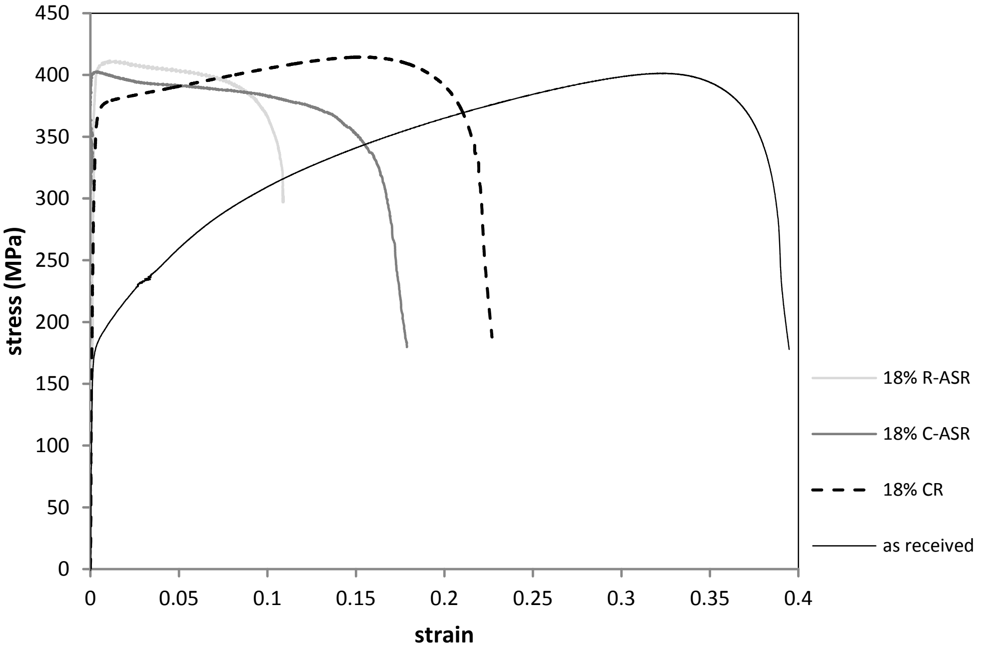

Figure 4.19: true stress-strain curves of asymmetric rolled samples under different strain paths

The difference in the stress-strain curves of the CR and ASR samples in tension shown in Fig. 4.19 may be attributed to the micro-features formed through pre-strain. In order to understand the materials' behaviour through strain path change, the α parameter was calculated regarding § 2-4-3; i.e. the C-ASR and uniaxial tension are subjected as pre- and subsequent strain paths respectively in Eq. 2.21. The macroscopically imposed plastic strain for the sheets under these two plastic deformation routes in an isotropic case ($R_\theta = 1$) is approximated by $\varepsilon_{\text{C-ASR}}$ and ε_{ten}:

$$\varepsilon_{C-ASR} = \begin{bmatrix} \varepsilon_{11} & 0 & \gamma/2 \\ 0 & 0 & 0 \\ \gamma/2 & 0 & \varepsilon_{33} \end{bmatrix},$$

$$\varepsilon_{ten} = \begin{bmatrix} \cos^2\theta + \frac{1}{2}\sin^2\theta & 0 & 0 \\ 0 & \cos^2\theta + \frac{1}{2}\sin^2\theta & 0 \\ 0 & 0 & -\frac{1}{2} \end{bmatrix} \tag{4.2}$$

where ε_{11} and γ are compression and shear strains imposed in C-ASR, respectively; and θ is the angle between tensile test direction and rolling direction. Different relative ratios of shear on compressive strain ($\frac{d\gamma}{d\varepsilon_{11}}$) are applied in order to evaluate the influence of the amount of shear strain imposed in C-ASR on the α parameter of in the sequence of C-ASR and tension strains. Figure 4.20 presents the variation of the α parameter of different ratios of ($\frac{d\gamma}{d\varepsilon_{11}}$) in various directions from RD. It is obvious that the ($\frac{d\gamma}{d\varepsilon_{11}}$) = 0 is related to the CR where no shear strain were imposed in the metallic sheet during the process. Consequently, according to the plotted curves in Fig. 4.20, increasing shear strain and/or keeping ε_{11} low (lower reduction) through C-ASR may lead to a decrease in the α parameter. The extreme slump of α parameter induced by a shear strain occurs in RD (i.e. C-ASR and tension were carried out in RD).

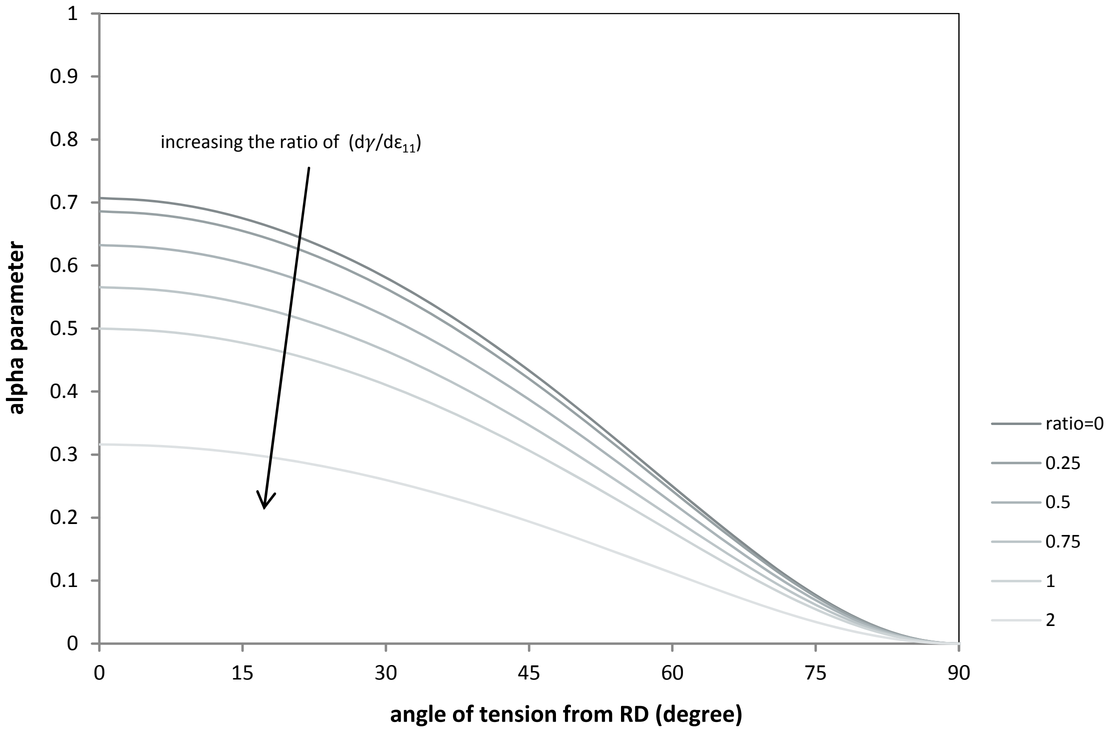

Figure 4.20: α parameter of sequence of strain paths: C-ASR (different $\frac{d\gamma}{d\varepsilon_{11}}$) and uniaxial tension

In a real condition of experiments where the rolled sheets are anisotropic and with the measured ratio of $\frac{d\gamma}{d\varepsilon_{11}}$, the α parameters were calculated as 0.93 and 0.81 for the sequences of CR and C-ASR respectively, followed by a uniaxial tension in RD. The details of the anisotropic case and calculations are given in appendix A.

As a matter of fact, the calculations of both cases (one plotted in Fig. 4.20 and the case measured experimentally) show that the α parameter of CR is higher than that for C-ASR when followed by a uniaxial tensile test in RD. It is true that the difference of the calculated α parameters between CR and C-ASR is not very significant. But the study indicates that some new slip systems of C-ASR sample were activated in tension which had been latent during C-ASR process; but in the CR sheet, the previously activated slip systems of pre-strain (CR process) are involved in the plastic deformation through the tensile test. Hence, different behaviour of CR and C-ASR samples in the tensile test (Fig. 4.19) can be due to activity of different slip systems in these specimens.

Figure 4.21 shows the stress-strain curves (tensile test) of the samples deformed under CR, C-ASR and R-ASR for 60% reduction. The result indicates that there is no difference between C-ASR and R-ASR curves, while the ultimate strength (UTS) of CR curve reaches 10 MPa higher than those of ASR samples. The small difference between the curves may be attributed to large amount of imposed plastic deformation through rolling processes translating high dislocation density. This means that the fined equiaxed substructure of ASR samples (observed in Fig. 4.12-4.18) and strong rolling texture of CR sheet (observed in Fig. 4.11) becomes ineffective on the stress-strain curves shown in Fig. 4.21.

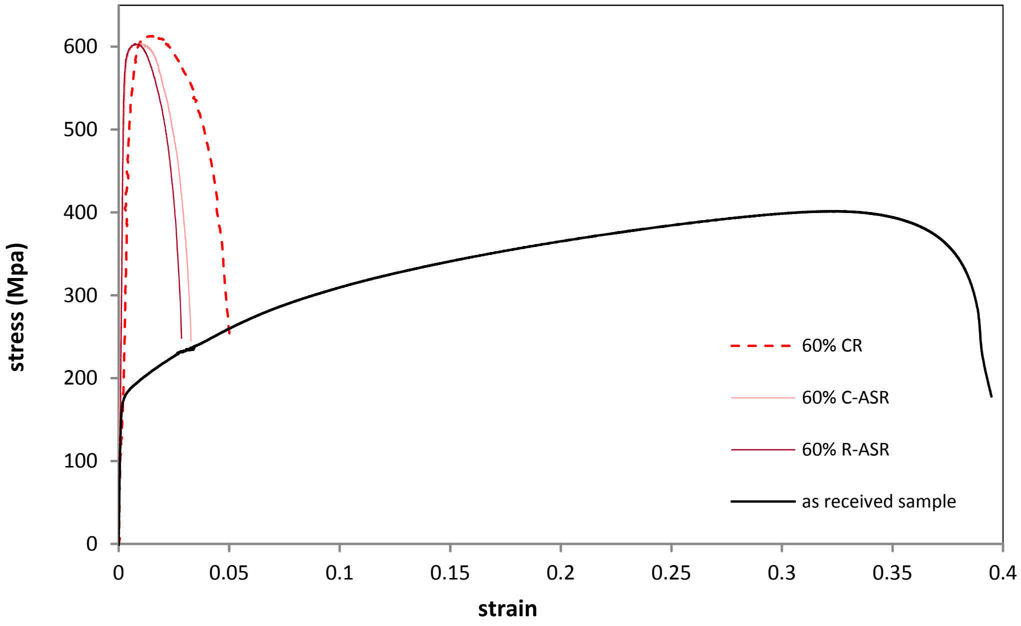

Figure 4.21: true stress-strain curves of uniaxial tensile test in RD

In order to avoid sample fracture through the tensile test and observe the impact of microstructure and texture on the mechanical behaviours, heat treatment was carried out, with the results obtained in § 3-2-4. Figure 4.22 shows the stress-strain curves (tensile test) of the samples deformed under CR and C-ASR with different reductions per pass followed by annealing at 550°C for one hour. Each sample was subjected to 4 passes giving rise to total deformations ranging approximately from 18% to 60%. It can be noticed that for low reductions (18%) the stress curve for the C-ASR sample presents the highest stress and for 60% reduction the highest stress level was detected for the CR sheet. Such a phenomenon leads to the appearance of a transient behaviour for reduction ratios around 36%. However, the uniform elongations through tensile test for each group of deformation are similar (see Fig. 4.22).

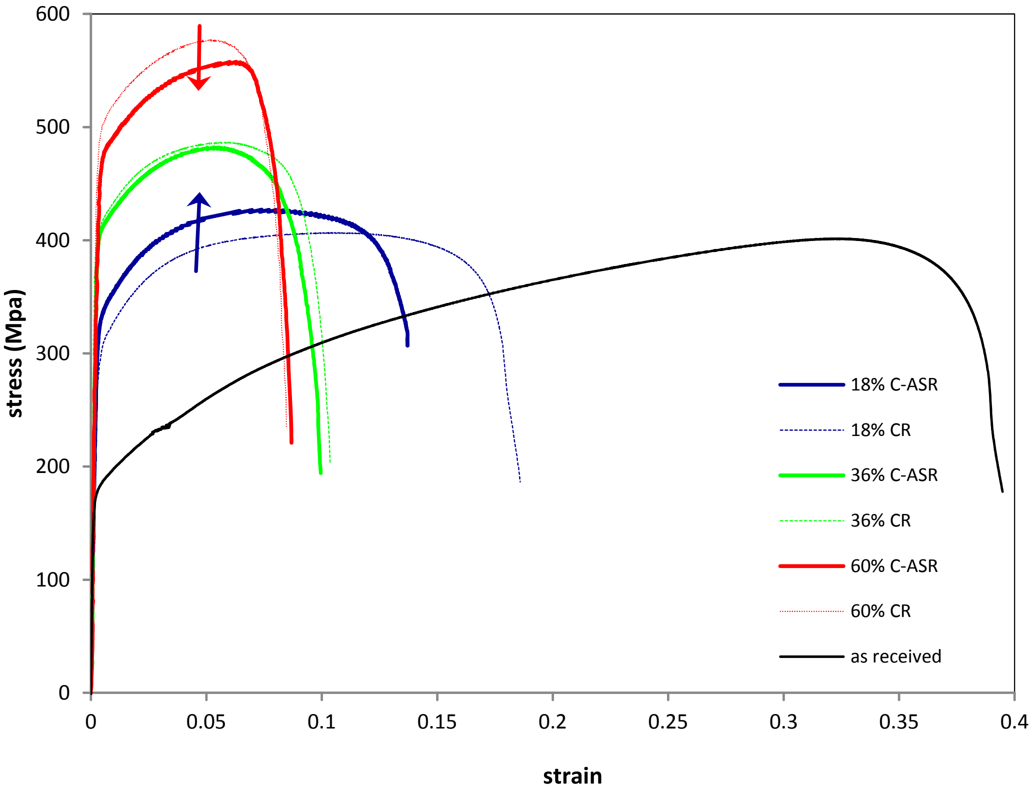

Figure 4.22: true stress- strain curves of CR and C-ASR samples after annealing

Furthermore, the Lankford coefficient of deformed samples in the rolling direction given in table 4.2 shows that imposing shear strain in addition to compression strain may lead to a slightly increase in the R-value of the deformed sheets. However, at 36% reduction, the R-values of both samples are approximately the same.

Table 4.2: R-value in RD of different reductions of CR and C-ASR

reduction process	**18%**	**36%**	**60%**
C-ASR	0.75	0.80	0.78
CR	0.65	0.81	0.62

As already explained in chapter 2, factors of microstructure and crystallographic texture determine the mechanical properties. An annealing at 550°C for one hour (a recovery heat treatment) may result in a rearrangement of substructure induced by plastic deformation processes (shown in Fig. 4.16 & 4.17) which causes misorientation angles of dislocation cell walls to increase. Additionally, crystallographic orientations of the deformed sheets remained unchanged through the recovery annealing. The texture of C-ASR and CR samples presented in figure 4.11 indicated that both samples possess the same components but with the different intensities; i.e. the i and E_1 components in the CR sample appeared with higher intensities. Consequently, the resulting feature after low temperature annealing of C-ASR samples in comparison with the CR ones, is a fine and equiaxed substructure and a relatively lower intense rolling texture.

In order to evaluate the impact of produced texture in the mechanical response, VPSC approach was carried out to simulate the behaviour of each individual texture component through tensile test in RD as plotted in Fig. 4.23. The variation of <M> of rolling texture components of the i, E_1 and E_2 present a similar trend and higher than those of F_1 and F_2 components in each amount of strain, whereas the recrystallization texture components (e.g. cube and goss) behave with the lowest ones.

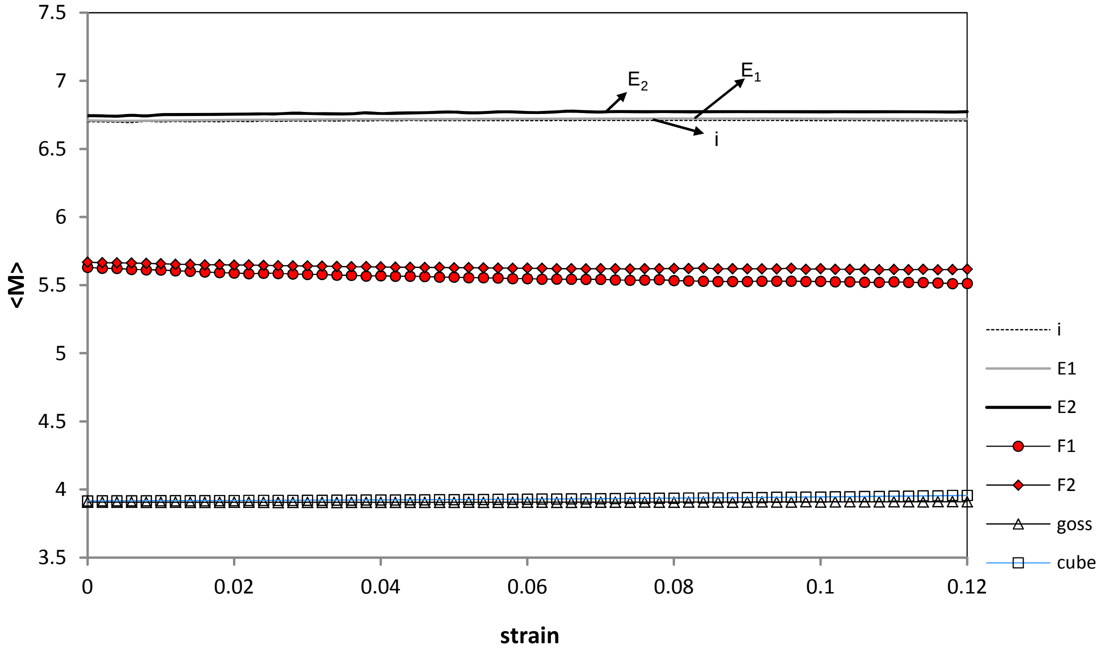

Figure 4.23: simulation (VPSC approach) of the mechancial behaviour through tension in RD of individual texture components (BCC)

The simulated curves reveal that the relatively strong rolling texture of the CR sheet (particularly i and E_1 components) may lead to increase the stress through tension in RD. On the contrary, concerning the Hall-Petch relationship given in § 2-4-2, a fine microstructure of C-ASR sheets may raise their stress levels higher than CR sample with a coarse microstructure.

In various reductions of pre-strain, the factor of fine microstructure of the C-ASR specimen leads to increase the strength; but in the higher reduction (60% total reduction in thickness) where the CR sheet has higher UTS point, the impact of crystallographic texture gets more effective. In the other words, due to the small pre-strain of 18% total reduction, the new textures have not completely developed while in 60% total reduction sheets the fully developed texture affects the mechanical response and increases the stress levels through tension in RD (see Fig. 4.22).

Chapter 5

General conclusions

In this thesis, asymmetric rolling as a new method to produce the metallic sheets with enhanced properties regarding industrial requirements was studied. In order to achieve this goal a comprehensive view of the process in metallic sheets is needed. Since aluminium alloys and steels are two significant metals used in industries, this work was dedicated to studying the ASR process on the micro and macro behaviours of these two important metallic materials. In this chapter, conclusions from the research are drawn and recommendations are given for further research.

5.1 general conclusions

5.1.1 AA-5182

Due to the appropriate properties of aluminium alloys, particularly their high strength-to-weight ratio, they are getting more interest from industry. However, their anisotropic mechanical responses limit their applications. Part of the work focused on the influence of shear strain in ASR on texture development in the AA-5182 alloy. Furthermore, the mechanical responses of the induced texture were studied. Additionally, the self-consistent model was carried out to simulate texture developing and also the induced mechanical properties. In order to understand the contribution of each individual texture components in mechanical behaviours, the behaviours were observed using polycrystal approaches. The conclusions obtained around the ASR process of AA-5182 sheets are listed in brief below:

- The results revealed that the asymmetric rolling process can be interpreted as the combination of shear and plane strain compression. The optimization of its parameters led to impose a uniform shear strain on the sheet thickness. The shear deformation could be formed through CR process too, but only in the regions close to the sheet surface, which is negligible. The shear strain near the sheet's surface is due to the friction between the working-rolls and the specimen.

- The results indicate that the shear strain imposed by the ASR process developed shear texture components in the sheet thickness. The E, F and H components pronounced through the first pass of ASR became more intense through the second pass of C-ASR. Whereas the second pass of R-ASR resulted in shifting the components along the φ_1 axis.
- The VPSC simulation results of texture evolution show that the prediction results are in qualitative agreement with the experimental ones; i.e. the shear components appeared in the ASR sheets and rolling components were formed through the CR process.
- In order to evaluate the impact of strain path change through the ASR (and the CR) processes, the α parameters of each process were calculated. An α parameter of less than 1 for two passes of R-ASR where the sample direction changes between the passes was obtained, and of 1 for two passes of C-ASR (and also CR). The calculated α parameters indicate that the same slip systems are activated in the same direction in the first and second pass of C-ASR (and CR); while the activity of slip systems and/or the directions differs in the second pass of the R-ASR process.
- The uniaxial tensile test of the samples deformed by CR, C-ASR and R-ASR processes was carried out. The results indicate that the strain hardening rate in the CR specimen is higher than those of C-ASR and R-ASR samples; and also the C-ASR and R-ASR samples behaved in a similar way. Furthermore, the simulated stress-strain curves of the corresponding textures induced by each process showed similar behaviours (i.e. higher strain hardening rate of CR sample relatively to the ASR samples). The simulation of each individual texture component shows that the E, F and H components (shear texture) yield with lower strain hardening rates compared to those of copper, and brass components (rolling texture).
- The results of R-value obtained through the tensile test in different directions indicate that ASR sheets possess higher normal anisotropy (desirable) and also slightly higher planar anisotropy compared with the CR sample results. This means that ASR processes of aluminium alloys may aid designers to solve low

normal anisotropy of rolled aluminium sheets; but they still have the earing problem in deep-drawn cups.

- The predicted R-value variations with the angle from RD for recrystallized, CR and two types of ASR samples by the Taylor and VPSC model indicate similar trends. The comparison of R-value of each case with the simulated R-value of each individual texture component reveals that anisotropic mechanical behaviour of each specimen is due to its particular texture developed in the plastic deformation process.

5.1.2 IF steel

Two types of ASR process were carried out on the interstitial free steel to study the impact of shear strain on the macro and micro properties of this important material. The influence of shear strain on crystallographic texture development as well as microstructure change was taken into consideration. The induced mechanical responses of the ASR samples were evaluated, and the effect of level of shear strain in ASR on the activity of slip systems in the subsequent strain mode (i.e. uniaxial tensile test) was also investigated. From the results obtained the following conclusions can be drawn:

- Texture analyses indicate that the developed texture of ASR samples is more uniform and weaker than the texture measured from the CR sample.
- The microstructural analysis using optical and atomic force microscopies indicate no great difference in the morphology of two rolled samples by ASR and CR processes. However, dark regions inside grains detected in 60% reduction of the ASR sheet that did not appear in the CR sample. This could be due to the various dislocation organizations in the ASR sheet.
- The substructure analyses of the ASR and CR samples observed by transmission electron microscopy reveal different features in terms of their morphology and size. The dislocation organization formed during the C-ARS is equiaxed and fine compared to that formed during the CR process; i.e. the relatively larger dislocation cells in the CR specimen are elongated along the rolling direction. This observation was mostly seen in higher deformed samples. Since the sample direction had been changed in the R-ASR process (i.e. lower α parameter than C-

ASR), the substructure of R-ASR sample was detected with a small discrepancy from C-ASR sample especially in its size. But it also showed an equiaxed substructure which may be attributed to the imposed shear strain through the R-ASR passes.

- The tensile test results indicate that the mechanical properties of 18% C-ASR and R-ASR are similar; but the CR specimen yielded at a relatively lower stress level.
- The calculated α parameter in the sequence of C-ASR and uniaxial tension shows that a higher level of ASR (i.e. an increase in the ratio of $\frac{d\gamma}{d\varepsilon_{11}}$) through the pre-strain results in a lower α parameter; i.e. the higher ASR levels causes new slip systems to be active and/or dislocations to glide in opposite directions in tension. This observation also indicated that for the sequence of CR process (i.e. $\frac{d\gamma}{d\varepsilon_{11}} = 0$) followed by tension, the α parameter reached its maximum value. The extreme variation of the α parameter with the $\frac{d\gamma}{d\varepsilon_{11}}$ ratio occurred when rolling direction and tensile test direction were parallel (i.e. θ=0).
- The effect of reduction on the stress-strain curves of the rolled and annealed samples were studied: for low reductions, the stress-strain curve of the ASR sample reveals the highest stress while for 60% reduction the highest ultimate strength was recorded for the CR sample; i.e. it presented this transient phenomenon at around 36% reduction of rolling. The experimental results indicated that generally the fine structure induced by ASR process may lead to increase the sheet's strength in various amount of reductions; however, the impact of strong rolling texture developed through the CR process has reverse effect and increase the stress level through tension in RD. In 18% reduction where the ASR sheet presented higher stress, due to a small amount of plastic deformation, the rolling texture have not developed completely in the CR sample and fine structure of ASR sheet caused to increase the stress in tensile test. But, in 60% reduction the higher stress of the CR sheet may be attributed to its strong rolling texture compared to the ASR specimen.

5.2 future researches

Based on the observations obtained, the following proposals are suggested for future work:

- ✓ In order to fully understand the role of shear deformation imposed by the asymmetric rolling process in dislocation organization and substructure analysis particularly in TD and RD planes, additional microstructural analyses are recommended such as the electron back-scattering diffraction (EBSD) technique.
- ✓ With the goal of increasing shear strain through the asymmetric rolling process, optimizing parameters is require, for which finite element methods (FEM) may be useful.
- ✓ Further study can be conducted on different materials with various crystallographic structures such as magnesium alloys. This gives us a more comprehensive understanding of the process.

References

[Bacroix 1999] B.Bacroix, T.Chauveau, J.F.Duarte, A.B.Rocha and J.Gracio; The respective influences of grain size and texture on the formability of a 1050 aluminium alloy; Int. J. Eng. Sci., 37 (1999) 509±526.

[Barlat 2003] F.Barlat, J.M.F.Duarte, J.J.Gracio, A.B.Lopes, E.F.Rauch; Plastic flow for non-monotonic loading conditions of an aluminum alloy sheet sample; Int. J. Plasticity, 19 (2003) 1215–1244.

[Bay 1992] B.Bay, N.Hansn, D.K.Wilsdorf; Microstructural evolution in rolled aluminium; Mater. Sci. Eng. A, 158 (1992) 139-146.

[Bowena 2004] J.R.Bowen, P.B.Prangnell, D.J.Jensen, N.Hansen; Microstructural parameters and flow stress in Al–0.13% Mg deformed by ECAE processing; Mater. Sci. Eng. A, 387–389 (2004) 235–239.

[Bunge 1982] H.J.Bunge; Texture analysis in materials science; Butterworth and Company, ISBN 0-408 166 (1982) 42-5.

[Callister 1999] W.D.Callister; Materials science and Engineering; John Wiley & Sons, Inc.

[Choi 2000] S.H.Choi, J.C.Brem, F.Barlat, K.H.Oh; Macroscopic anisotropy in AA5019A sheets; Acta Mater., 48, (1999) 1853-1863.

[Costa 2005] A.L.M.Costa, A.C.C.Reis, L.Kestens, M.S.Andrade; Ultra grain refinement and hardening of IF-steel during accumulative roll bonding; Mater. Sci. Eng. A, 406 (2005) 279–285.

[Dieter 1988] G.E.Dieter; Mechanical metallurgy; McGraw-Hill Book Company publisher, 1988, ISBN 0-07-100406-8.

[Ding 2009] Y.Ding, J.Jiang, A.Shan; Microstructures and mechanical properties of commercial purity iron processed by asymmetric rolling; Mater. Sci. Eng. A, 509 (2009) 76–80.

[Fernandes 1938] J.V.Fernandes, J.H.Schmitt; Dislocation microstructures in steel during deep drawing; Phil. Mag. A, 48 (1938) 841.

[Gambian 1997] W.Gambin, F.Barlat; Modeling of deformation texture development based on rate independent crystal plasticity; Inetr.J.Plasticity, PII: S0749-16419(1997)1-6

[Gao 2002] H.Gao, S.C.Ramalingam, G.C.Barber, G.Chen; Analysis of asymmetrical cold rolling with varying coefficients of friction; JMPT, 124 (2002) 178–182

[Gholinia 2000] A.Gholinia, P.B.Prangnell, M.V.Markushev; The effect of strain path on the development of deformation structures in severely deformed aluminium alloys processed by ECAE; Acta mater. 48 (2000) 1115±1130

[Gracio 1989] J.J.Gracio, J.V.Fernandes, J.H.Schmitt; Effect of grain size on substructural evolution and plastic behaviour of copper; Mater. Sci. Eng., A, 118 (1989) 97.

[Gracio 2000] J.J.Gracio, A.B.Lopes, E.F.Rauch; Analysis of plastic instability in commercially pure Al alloys; J. Mater. Pro. Tech., 103 (2000) 160-164.

[Hall 1951] E.O.Hall; The deformation and ageing of mild steel: III discussion of results; Proc. Phys. Soc. B, 64 (1951) 747.

[Humphreys 1996] F.J.Humphreys, M.Hatherly; Recrystallization and related annealing phenomena; ELSEVIER Ltd, 1996 ISBN: 0 08 044164 5.

[Hertzberg 1937] R.W.Hertzberg; Deformation and fracture mechanics of engineering materials; JOHN WIELY&SONS, INS., ISBN 0-471-01214-9.

[Holscher 1991] M.Holscher, D.Raabe, K.Lucke; Rolling and recrystallization textures of bcc steels; Steel research 62 (1991) 12.

[Hosford 1993] W.F.Hosford, R.M.Caddell; Metal forming-Mechanics and Metallurgy; Cambridge University Press, ISBN 13 978-0-521-88121-0.

[Houtte 1999] P.V.Houtte, L.Delannay, I.Samajdar; Quantitative prediction of cold rolling textures in low-carbon steel by means of the LAMEL model; Textures and Microstructures 31 (1999) 109-149.

[Houtte 2005] P.V.Houtte, S.Li, M.Seefeldt, L.Delannay; Deformation texture prediction: from the Taylor model to the advanced LAMEL model; Int. J. Plasticity, 21 (2005) 589–624.

[Huang 2001] J.Y.Huang, Y.T.Zhu, H.Jiang, T.C.Lowe; Microstructures and dislocation configurations in nanostructured cu processed by repetitive corrugation and straightening; Acta Mater., 49 (2001) 1497–1505.

[Huang 2003] X.Huang, N.Tsuji, N.Hansen, Y.Minamino; Microstructural evolution during accumulative roll-bonding of commercial purity aluminum; Mater. Sci. Eng. A, 340 (2003) 265-271.

[Hughes 2000] D.A.Hughes, N.Hansen;Microstructure and strength of nickel at large strains; Acta Mater., 48 (2000) 2985±3004.

[Inoue 2007] H.Inoue, T.Takasugi; Texture control for improving deep drawability in rolled and annealed aluminum alloy sheets; Mater.Trans. 48 (2007) 2014-2022.

[Iwahashi 1998] Y.Iwahashi, Z.Horita, M.Nemoto, T.G.Langdon; The process of grain refinement in equal-channel angular pressing; Acta Mater., 46 (1998) 3317±3331.

[Jazaeri 2004] H.Jazaeri, F.J.Humphreys; The transition from discontinuous to continuous recrystallization in some aluminium alloys II – annealing behaviour; Acta Mater., 52 (2004) 3251–3262.

[Ji 2009] Y.H.Ji, J.J.Park; Development of severe plastic deformation by various asymmetric rolling processes; Mater. Sci. Eng. A, 499 (2009) 14-17.

[Jiang 2009] J.Jiang, Y.Ding, F.Zuo, A.Shan; Mechanical properties and microstructures of ultrafine-grained pure aluminum by asymmetric rolling; Scripta Materialia 60 (2009) 905–908.

[Jin 2004] H.Jin, D.J.Lloyd; The tensile response of a fine-grained AA5754 alloy produced by asymmetric rolling and annealing; Metal. Mater. Trans. A, 35(2004) 997-1006.

[Jin 2005]	H.Jin, D.J.Lloyd; The reduction of planar anisotropy by texture modification through asymmetric rolling and annealing in AA5754; Mater. Sci. Eng. A, 399 (2005) 358–367.
[Jin 2007]	H.Jin, D.J.Lloyd; Evolution of texture in AA6111 aluminum alloy after asymmetric rolling with various velocity ratios between top and bottom rolls; Mater. Sci. Eng. A, 465 (2007) 267–273.
[Jining 2004]	Q.Jining, J.H.Han, Z.Guoding, J.C.Lee; Characteristic of textures evolution induced by equal channel angular pressing in 6061 aluminum sheets; Scripta Mater., 51 (2004) 185–189.
[Kamikawa 2007]	N.Kamikawa, T.Sakai, N.Tsuji; Effect of redundant shear strain on microstructure and texture evolution during accumulative roll-bonding in ultralow carbon IF steel; Acta Mater., 55 (2007) 5873–5888.
[Kang 2007]	J.Y.Kang, B.Bacroix, H.Regle, K.H.Oh, H.C.Lee; Effect of deformation mode and grain orientation on misorientation development in a body-centered cubic steel; Acta Mater., 55 (2007) 4935–4946.
[Kim 2001a]	K.H.Kim, D.N.Lee; Analysis of Deformation Textures of Asymmetrically Rolled Aluminum Sheets; Acta Mater., 49, (2001) 2583–2595.
[Kim 2001b]	H.S.Kim, M.H.Seo, S.I.Hong; Plastic deformation analysis of metals during ECAP; J. Mater. Pro. Tech., 113 (2001) 622-626.
[Kim 2002]	S.K.Kim, J.H.Ryu, K.H.Kim, D.N.Lee; The evolution of shear deformation texture and grain refinement in asymmetrically rolled aluminium sheets; Mater. Sci. Res. Int. 8 (2002) 20-25.
[Kocks 1970]	U.F.Kocks; The relation between polycrystal deformation and single-crystal deformation; Metal.Trans., 1 (1970) 1121.
[Kocks 1998]	U.F.Kocks, C.N.Tome, H.R.Wenk; Texture and anisotropy; Cambridge University Press, 1998, ISBN 0 521 46516 8.

[Lebensohn 1994] R.A.Lebensohn, C.N.Toms; A self-consistent viscoplastic model: prediction of rolling textures of anisotropic polycrystals; Mater. Sci. Eng. A, 175 (1994) 71-82.

[Lebensohn 1999] R.A.Lebensohn, T.Leffers; The rules for the lattice rotation accompanying slip as derived from a self-consistent model; Tex.Microstr. 31 (1999) 217–230.

[Lee 2001] S.H.Lee, D.N.Lee; Analysis of deformation textures of asymmetrically rolled steel sheets; Int. J. Mech. Sci., 43 (2001) 1997–2015.

[Lee 2002a] J.C.Lee, H.K.Seok, J.Y.Suh; Microstructural evolutions of the Al strip prepared by cold rolling and continuous equal channel angular pressing, Acta Mater., 50 (2002) 4005–4019.

[Lee 2002b] S.H.Lee, Y.Saito, N.Tsuji, H.Utsunomiya, T.Sakai; Role of shear strain in ultragrain refinement by accumulative roll-bonding (ARB) process; Scripta Mater., 46 (2002) 281–285.

[Lee 2002c] J.K.Lee, D.N.Lee; Shear texture development and grain refinement in asymmetrically rolled aluminum alloy sheets by varied reduction per pass; Materials Science Forum, 408–412 (2002) 1419–24.

[Lequeu 1988] P.Lequeu, J.J.Jonas; Modeling of the Plastic Anisotropy of Textured Sheet; Metal. Trans. A, 19A (1988) 105-120.

[Liu 2002] W.C.Liu, J.G.Morris; Texture evolution of polycrystalline AA 5182 aluminum alloy with an initial {001} <110> texture during rolling; Scripta Mater. 47 (2002) 487–492.

[Liu 2006] W.C.Liu, Z.Lib, C.S.Man, D.Raabe, J.G.Morris; Effect of precipitation on rolling texture evolution in continuous cast AA 3105 aluminum alloy; Mater. Sci. Eng. A, 434 (2006) 105–113.

[Molianari 1987] A.Molinari, G.R.Canova, S.Ahzi; A self consistent approach of the large deformation polycrystal viscoplasticity; Acta Mater. 35 (1987) 2983-2994.

[Molianari 1997] A.Molinari, S.Ahzi, R.Kouddane; On the self-consistent modeling of elastic-plastic behavior of polycrystals; Mech. Mater., 26 (1997) 43-62.

[Nesterova 2001] E.V.Nesterova, B.Bacroix, C.Teodosiu; Microstructure and texture evolution under strain-path changes in low-carbon interstitial-free steel; Metallurgical and Mater. Trans. A, 32A (2001) 2527.

[Park 2005] J.J.Park, N.J.Park; Influence of orthogonal shear on texture and R value in aluminum sheet; J. Mater. Pro. Tech., 169 (2005) 299–307.

[Petch 1953] N.J.Petch; The cleavage strength of polycrystals; J. Iron Steel Inst., 174 (1953) 25.

[Saito 1998] Y.Saito, N.Tsuji, H.Utsunomiya, T.Sakai, R.G.Hong; Ultra-fine grained bulk aluminum produced by accumulative roll-bonding (ARB) process; Scripta Mater., 39 (1998) 1221-1227.

[Saito 2000] Y.Saito, H.Utsunomiya, H.Suzuki, T.Sakai; Improvement in the R-value of aluminum strip by a continuous shear deformation process; Scripta Mater., 42 (2000) 1139–1144.

[Salimi 2002] M.Salimi, F.Sassani; Modified slab analysis of asymmetrical plate rolling; Int. J. Mech. Sci., 44 (2002) 1999–2023.

[Schmitt 1994] J.H.Schmitt, E.L.Shen, J.L.Raphanel; A parameter for measuring the magnitude of a change of strain path: validation and comparison with experiments on low carbon steel; Inter. J. Plasticity, 10 (1994) 535-551.

[Segal 1981] V.M.Segal, V.I.Reznikov, A.E.Drobyshevskiy, V.I.Kopylov, Russian Metal. (Englsih version), 1 (1981) 99.

[Sha 2008] Y.H.Sha, F.Zhang, S.C.Zhou, W.Pei, L.Zu; Improvement of recrystallization texture and magnetic property in non-oriented silicon steel by asymmetric rolling; J. Magnetism and Magnetic Mater., 320 (2008) 393–396.

[Sidor 2008] J.Sidor, A.Miroux, R.Petrov, L.Kestens; Microstructural and crystallographic aspects of conventional and asymmetric rolling processes; Acta Mater., 56 (2008) 2495–2507.

[Simoes 2008] F.J.P.Simoes, R.J.A.Sousa, J.J.Gracio, F.Barlat, J.W.Yoon; Mechanical behavior of an asymmetrically rolled and annealed 1050-O sheet; Int. J. Mech. Sci., 50 (2008) 1372–1380.

[Skrotzki 2008] W.Skrotzki, L.S.Toth, B.Kloden, H.G.Brokmeier, R.A.Massion; Texture after ECAP of a cube-oriented Ni single crystal; Acta Mater., 56 (2008) 3439-3449.

[Tome 1984] C.Tome, G.R.Canova, U.F.Kocks, N.Christodoulou, J.J.Jonas; The relation between macroscopic and microscopic strain hardening in FCC polycrystal; Acta Metall., 32 (1984) 1637–1653.

[Toth 2004] L.S.Toth ,R.A.Massion, L.Germain, S.C.Baik, S.Suwas; Analysis of texture evolution in equal channel angular extrusion of copper using a new flow field; Acta Mater. 52 (2004) 1885–1898.

[Toth 2012] L.S.Toth, B.Beausir, D.Orlov, R.Lapovok, A.Haldar; Analysis of texture and R value variations in asymmetric rolling of IF steel; J. Mater. Pro. Tech., 212 (2012) 509– 515.

[Utsunomiy 2007] H.Utsunomiya, T.Ueno, T.Sakai; Improvement in the r-value of aluminum sheets by differential-friction rolling; Scripta Mater., 57 (2007) 1109–1112.

[www] http://aluminium.matter.org.uk

[Wagoner 1983] R.H.Wagoner, J.V.Laukonis; Plastic Behavior of Aluminum-Killed Steel Following Plane-Strain Deformation; Metal. Trans. A, 14A (1983) 1487.

[Wauthier 2009] A.Wauthier, H.Regle, J.Formigoni, G.Herman; The effects of asymmetrical cold rolling on kinetics, grain size and texture in IF steels; Mater. Character., 60 (2009) 90-95.

[Wen 2004] W.Wen, Y.Zhao, J.G.Morris; The effect of Mg precipitation on the mechanical properties of 5xxx aluminum alloys; Mater. Sci. Eng. A, 392 (2005) 136–144.

[Werenskiold 2005] J.C.Werenskiold, H.J.Roven; Microstructure and texture evolution during ECAP of an AlMgSi alloy: Observations, mechanisms and modeling; Mater. Sci. Eng. A, 410–411 (2005) 174–177.

[Yan 2011]	Z.M.yan, Z.W.Wen, Z.D.Tong; Production of Mg-Al-Zn magnesium alloy sheets with ultrafine-grain microstructure by accumulative roll-bonding; Trans. Nonferrous Met. Soc. China, 21 (2011) 991-997.
[Yong 2009]	T.Yong, G.Y.Hui. W.Z.Dong, W.G.Dong; Analysis of rolling pressure in asymmetrical rolling process by slab method; J. Iron Steel RES. INT., 16 (2009) 22-26.

Appendix A

α parameter

The materials' behaviours after change in strain path in a complex strain mode was taken into consideration in § 2-4-3. The activity of different slip systems and their corresponding in the plastic deformation after strain path change were discussed. Additionally, the specific case of a tension of the C-ASR sheet were studied and the α parameter regarding this strain routes change for an isotropic condition were calculated in § 3-3. In "Appendix A", the α parameter of the tensile test of the C-ASR sample for anisotropic condition are studied and the α parameter regarding this strain routes change are calculated. Generally, the α parameter of two sequence strain paths of $\varepsilon_{\text{C-ASR}}$ and ε_{ten} are given as:

$$\alpha = \frac{\varepsilon_{C-ASR} : \varepsilon_{ten}}{|\varepsilon_{C-ASR}| \cdot |\varepsilon_{ten}|} \tag{A.1}$$

where $\varepsilon_{\text{C-ASR}}$ and ε_{ten} are strain tensors of the C-ASR (pre-strain) and tensile test, respectively. The $\varepsilon_{\text{C-ASR}}$ is obtained as:

$$\varepsilon_{\mathrm{C-ASR}} = \begin{bmatrix} \varepsilon_{\mathrm{p}} & 0 & \gamma/_2 \\ 0 & 0 & 0 \\ \gamma/_2 & 0 & -\varepsilon_{\mathrm{p}} \end{bmatrix} \tag{A.2}$$

Here, ε_{p} is the compressive plane strain and γ is the shear strain imposed in the C-ASR process throughout the thickness of the sample. The tensile test tensor, ε_{ten} is determined as:

$$\varepsilon_{ten} = \begin{bmatrix} \varepsilon'_{11}cos^2\theta + \varepsilon'_{22}sin^2\theta & (\varepsilon'_{22} - \varepsilon'_{11})cos\theta.sin\theta & \varepsilon'_{13} \\ (\varepsilon'_{22} - \varepsilon'_{11})cos\theta.sin\theta & \varepsilon'_{11}sin^2\theta + \varepsilon'_{22}cos^2\theta & \varepsilon'_{23} \\ \varepsilon'_{31} & \varepsilon'_{32} & \varepsilon'_{33} \end{bmatrix} \tag{A.3}$$

where θ is the angle between tensile test and rolling directions. Additionally, ε′ depending on the Lankford coefficient of the angle θ is obtained as:

$$\varepsilon' = \begin{bmatrix} 1 & 0 & 0 \\ 0 & -\frac{R_\theta}{1+R_\theta} & 0 \\ 0 & 0 & -\frac{1}{1+R_\theta} \end{bmatrix} \tag{A.4}$$

Hence, we have:

$$\varepsilon_{ten} = \begin{bmatrix} cos^2\theta - (\frac{R_\theta}{1+R_\theta})sin^2\theta & (\frac{-2R_\theta-1}{1+R_\theta})cos\theta.sin\theta & 0 \\ (\frac{-2R_\theta-1}{1+R_\theta})cos\theta.sin\theta & sin^2\theta + (-\frac{R_\theta}{1+R_\theta})cos^2\theta & 0 \\ 0 & 0 & -\frac{1}{1+R_\theta} \end{bmatrix} \tag{A.5}$$

Consequently, the α parameter for the sequence of C-ASR and tension is obtained using relations of A.1, A.2 & A.5:

$$\alpha_{\ C-ASR\ ,\ ten} =$$

$$\frac{\varepsilon_p.\left(\cos^2\theta - \left(\frac{R_\theta}{1+R_\theta}\right)\sin^2\theta\right) + \varepsilon_p.\left(\frac{1}{1+R_\theta}\right)}{\sqrt{2.\varepsilon_p^2 + \frac{\gamma^2}{2}}.\sqrt{\left(\cos^2\theta - \left(\frac{R_\theta}{1+R_\theta}\right)\sin^2\theta\right)^2 + (\sin^2\theta + -\frac{R_\theta}{1+R_\theta}\cos^2\theta)^2 + 2.(\frac{-2R_\theta - 1}{1+R_\theta}\cos\theta.\sin\theta)^2}}$$

$$\tag{A.6}$$

The α parameter of the sequence of C-ASR followed by tension, regarding samples' anisotropy and experimental parameters is obtained as 0.81 in rolling direction (i.e. θ=0). In the case of CR process where no shear strain were imposed through the thickness of the sample (i.e. γ=0), this parameter calculated as 0.93 for the rolling direction.